# Development of the Rolling Wheel Deflectometer (RWD)

**FHWA-DTFH-61-14-H00019**

U.S. Department of Transportation

**Federal Highway Administration**

## FOREWORD

The Federal Highway Agency (FHWA) has been involved with the development of a Rolling Wheel Deflectometer (RWD) for several decades. The RWD has potential to benefit State highway agencies by making pavement structural evaluation feasible at the network level. One of the barriers to this technology has been a lack of analysis tools developed around moving wheel loads, as opposed to the current technology, falling weight deflectometers (FWDs). This report provides a comprehensive analysis of RWD vs. FWD deflection basins and presents potential tools for implementing the RWD in practice.

Thomas Van
Office of Infrastructure

# TECHNICAL REPORT DOCUMENTATION PAGE

| | | |
|---|---|---|
| 1. Report No.<br>FHWA-DTFH-61-14-H00019 | 2. Government Accession No. | 3. Recipient's Catalog No. |
| 4. Title and Subtitle<br>Development of the Rolling Wheel Deflectometer (RWD) | | 5. Report Date<br>March 17, 2020 |
| | | 6. Performing Organization Code |
| 7. Author(s)<br>Mr. Douglas A. Steele, P.E.; Dr. Hyung Lee, P.E.; and Mr. Curt A. Beckemeyer, P.E. | | 8. Performing Organization Report No. |
| 9. Performing Organization Name and Address<br>Applied Research Associates, Inc.<br>100 Trade Centre Boulevard, Suite #200<br>Champaign, IL 61820 | | 10. Work Unit No. (TRAIS)<br><br>11. Contract or Grant No.<br>DTFH61-14-H00019 |
| 12. Sponsoring Agency Name and Address<br>U.S. Department of Transportation<br>Federal Highway Administration<br>1200 New Jersey Ave., SE<br>Washington, DC 20590 | | 13. Type of Report and Period Covered<br>Draft Final Report; September 2015–March 2020<br><br>14. Sponsoring Agency Code |
| 15. Supplementary Notes<br>The Contracting Officer's Representative was Mr. Thomas Van, FHWA. | | |


16. Abstract

Nondestructive deflection testing has played an important role in pavement evaluation, design, and management for several decades. During this period, the tool of choice for structural evaluation has been the falling weight deflectometer (FWD), due to its ability to accurately measure very small pavement deflections by means of a nondestructive load generating impact and measurement with various types of deflection transducers. In terms of application, the FWD is overwhelmingly used for project-level evaluation and design.

Over the last two decades, moving wheel deflectometers have been developed and tested to collect nondestructive deflection data from instrumented truck-trailer combinations traveling at normal highway speeds. Researchers have used various techniques to measure the surface deflections produced by the trailer's loaded axle, with the purpose of measuring data with sufficient accuracy for network-level evaluation, such as pavement management activities.

The Federal Highway Administration began funding Rolling Wheel Deflectometer (RWD) development in the late 1990s. This device consists of a 53-ft semi trailer with a dual-tire, 18-kip single axle that has been instrumented with several generations of deflection measuring systems, including a scanning laser, spot lasers, and most recently, machine vision cameras and custom-designed flashing strobe lights. The system has been developed and tested over the years to improve data accuracy, measurement of the full deflection basin, and applicability to pavement management. It has been demonstrated to over 20 State highway agencies as part of its deployment.

One barrier to RWD data implementation has been its inherent differences from the current standard, as commonly used FWD data analysis techniques are not directly transferable to RWD data. This report discusses the differences in loading characteristics between devices, presents theoretical and field data comparisons, and provides strain correlations for use of both FWD and RWD data in network-level management. The field study included side-by-side FWD and RWD testing on 23 test sites in Mississippi.


| | |
|---|---|
| 17. Key Words<br>Rolling wheel deflectometer, Falling weight deflectometer, ViscoWave, network-level evaluation, pavement management systems, dynamic pavement modeling, curvature indices, asphalt strain, deflection basin parameters, basin shape factors | 18. Distribution Statement<br>No restrictions. This document is available to the public through the National Technical Information Service, Springfield, VA 22161.<br>http://www.ntis.gov |

| | | | |
|---|---|---|---|
| 19. Security Classif. (of this report)<br>Unclassified | 20. Security Classif. (of this page)<br>Unclassified | 21. No. of Pages<br>87 | 22. Price |

**Form DOT F 1700.7 (8-72)** Reproduction of completed page authorized.

# SI* (MODERN METRIC) CONVERSION FACTORS

## APPROXIMATE CONVERSIONS TO SI UNITS

| Symbol | When You Know | Multiply By | To Find | Symbol |
|---|---|---|---|---|
| | | **LENGTH** | | |
| in | inches | 25.4 | millimeters | mm |
| ft | feet | 0.305 | meters | m |
| yd | yards | 0.914 | meters | m |
| mi | miles | 1.61 | kilometers | km |
| | | **AREA** | | |
| $in^2$ | square inches | 645.2 | square millimeters | $mm^2$ |
| $ft^2$ | square feet | 0.093 | square meters | $m^2$ |
| $yd^2$ | square yard | 0.836 | square meters | $m^2$ |
| ac | acres | 0.405 | hectares | ha |
| $mi^2$ | square miles | 2.59 | square kilometers | $km^2$ |
| | | **VOLUME** | | |
| fl oz | fluid ounces | 29.57 | milliliters | mL |
| gal | gallons | 3.785 | liters | L |
| $ft^3$ | cubic feet | 0.028 | cubic meters | $m^3$ |
| $yd^3$ | cubic yards | 0.765 | cubic meters | $m^3$ |
| | | NOTE: volumes greater than 1000 L shall be shown in $m^3$ | | |
| | | **MASS** | | |
| oz | ounces | 28.35 | grams | g |
| lb | pounds | 0.454 | kilograms | kg |
| T | short tons (2000 lb) | 0.907 | megagrams (or "metric ton") | Mg (or "t") |
| | | **TEMPERATURE (exact degrees)** | | |
| $^oF$ | Fahrenheit | 5 (F-32)/9<br>or (F-32)/1.8 | Celsius | $^oC$ |
| | | **ILLUMINATION** | | |
| fc | foot-candles | 10.76 | lux | lx |
| fl | foot-Lamberts | 3.426 | candela/$m^2$ | $cd/m^2$ |
| | | **FORCE and PRESSURE or STRESS** | | |
| lbf | poundforce | 4.45 | newtons | N |
| $lbf/in^2$ | poundforce per square inch | 6.89 | kilopascals | kPa |

## APPROXIMATE CONVERSIONS FROM SI UNITS

| Symbol | When You Know | Multiply By | To Find | Symbol |
|---|---|---|---|---|
| | | **LENGTH** | | |
| mm | millimeters | 0.039 | inches | in |
| m | meters | 3.28 | feet | ft |
| m | meters | 1.09 | yards | yd |
| km | kilometers | 0.621 | miles | mi |
| | | **AREA** | | |
| $mm^2$ | square millimeters | 0.0016 | square inches | $in^2$ |
| $m^2$ | square meters | 10.764 | square feet | $ft^2$ |
| $m^2$ | square meters | 1.195 | square yards | $yd^2$ |
| ha | hectares | 2.47 | acres | ac |
| $km^2$ | square kilometers | 0.386 | square miles | $mi^2$ |
| | | **VOLUME** | | |
| mL | milliliters | 0.034 | fluid ounces | fl oz |
| L | liters | 0.264 | gallons | gal |
| $m^3$ | cubic meters | 35.314 | cubic feet | $ft^3$ |
| $m^3$ | cubic meters | 1.307 | cubic yards | $yd^3$ |
| | | **MASS** | | |
| g | grams | 0.035 | ounces | oz |
| kg | kilograms | 2.202 | pounds | lb |
| Mg (or "t") | megagrams (or "metric ton") | 1.103 | short tons (2000 lb) | T |
| | | **TEMPERATURE (exact degrees)** | | |
| $^oC$ | Celsius | 1.8C+32 | Fahrenheit | $^oF$ |
| | | **ILLUMINATION** | | |
| lx | lux | 0.0929 | foot-candles | fc |
| $cd/m^2$ | candela/$m^2$ | 0.2919 | foot-Lamberts | fl |
| | | **FORCE and PRESSURE or STRESS** | | |
| N | newtons | 0.225 | poundforce | lbf |
| kPa | kilopascals | 0.145 | poundforce per square inch | $lbf/in^2$ |

*SI is the symbol for the International System of Units. Appropriate rounding should be made to comply with Section 4 of ASTM E380.
(Revised March 2003)

## TABLE OF CONTENTS

## LIST OF FIGURES

## LIST OF TABLES

## LIST OF ABBREVIATIONS AND SYMBOLS

**Abbreviation**

| | |
|---|---|
| AASHTO | American Association of State Highway and Transportation Officials |
| AC | asphalt concrete |
| AI | Asphalt Institute |
| ATB | asphalt-treated base |
| AUPP | area under pavement profile |
| BC | binder course |
| BELLS | Baltzer, Ertman-Larson, Lukanen, Stubstad |
| BELLS2 | second generation BELLS equation |
| BELLS3 | third generation BELLS equation |
| CI | Curvature Index |
| CLS | crushed limestone |
| COV | coefficient of variation |
| CRADA | cooperative research and development agreement |
| CSA | concrete sand |
| CSDC | crushed stone drainage course |
| CSM | crushed stone material |
| CTM | cement-treated material |
| DBP | deflection basin parameter |
| DMI | distance measuring instrument |
| DOT | Department of Transportation |
| DSI | Deflection Slope Index |
| ESAL | equivalent single axle load |
| FHWA | Federal Highway Administration |

| | |
|---|---|
| FWD | falling weight deflectometer |
| GB | granular base |
| GPS | global positioning system |
| JULEA | Jacob Uzan Layered Elastic Analysis |
| LA | lime ash |
| LFA | lime fly ash |
| LED | light emitting diode |
| LTM | lime-treated material |
| LTPP | Long-Term Pavement Performance |
| LTRC | Louisiana Transportation Research Center |
| MAP-21 | Moving Ahead for Progress in the 21st Century Act |
| M&R | maintenance and rehabilitation |
| MS-17 | Manual Series No. 17 |
| MEPDG | *Mechanistic-Empirical Pavement Design Guide* |
| NHS | National Highway System |
| PCI | Pavement Condition Index |
| PQI | Pavement Quality Index |
| PMS | pavement management system |
| RI | RWD Index |
| RoC | radius of curvature |
| RSL | remaining service life |
| RWD | Rolling Wheel Deflectometer |
| SBC | stabilized base course |
| SC | surface course |
| SCI | Surface Curvature Index |

| | |
|---|---|
| SMP | seasonal monitoring program |
| TGM | treated granular mat |
| TFHRC | Turner-Fairbank Highway Research Center |
| TM | treated material |

**Symbols**

| | |
|---|---|
| $AREA_{12}$ | area of the deflection basin from 0 to 12 in normalized to $d_0$ |
| $AREA_{36}$ | area of the deflection basin from 0 to 36 in normalized to $d_0$ |
| $a_T$ | temperature shift factor |
| $\alpha_1$, $\alpha_2$, $\alpha_3$, $\alpha_4$ | temperature shift factor coefficients |
| $c_1$, $c_2$, $c_3$, $c_4$ | regression coefficients |
| D | total pavement thickness |
| $d_i$ | deflection measured i inches from the load center |
| $d_j$ | deflection measured j inches from the load center |
| $d_r$ | deflection measured r inches from the load center |
| $D_0$, $d_0$ | deflection measured under the load center |
| $D_4$, $d_4$ | deflection measured 4 inches from the load center |
| $D_8$, $d_8$ | deflection measured 8 inches from the load center |
| $D_{12}$, $d_{12}$ | deflection measured 12 inches from the load center |
| $D_{18}$, $d_{18}$ | deflection measured 18 inches from the load center |
| $D_{24}$, $d_{24}$ | deflection measured 24 inches from the load center |
| $D_{36}$, $d_{36}$ | deflection measured 36 inches from the load center |
| $D_{48}$, $d_{48}$ | deflection measured 48 inches from the load center |
| $D_{60}$, $d_{60}$ | deflection measured 60 inches from the load center |
| $DSI_{4\text{-}18}$ | Deflection Slope Index at deflections 4 and 18 in from the load center |
| $E_{ac}$ | elastic modulus of the asphalt concrete layer |
| $E_p$ | composite pavement modulus |
| E(t) | time dependent relaxation modulus |
| $\varepsilon_{ac}$ | tensile strain at the bottom of the asphalt concrete layer |
| *i, j, r* | radial distances from the load center |
| L | length |

| | |
|---|---|
| $M_R$ | subgrade resilient modulus |
| P | load |
| $R^2$ | coefficient of determination |
| $SN_{eff}$ | effective structural number |
| t | loading time |
| με | microstrain |

# CHAPTER 1. INTRODUCTION

## BACKGROUND

The U.S. Federal Highway Administration (FHWA) has funded the design, development, and demonstration of a prototype Rolling Wheel Deflectometer (RWD) for high-speed measurement of pavement structural response since the late 1990s. In 2002, a proof of concept study showed the device could successfully measure pavement deflections at highway speeds. From 2003 through 2013, the RWD was continuously developed and demonstrated to multiple Federal, State, and local transportation agencies through a cooperative research and development agreement (CRADA) with the FHWA Turner-Fairbank Highway Research Center (TFHRC).

Since that time, the original laser-based measurement system has been replaced with a camera and light combination known as RWD-Vision, shown in figure 1. The upgraded methodology allows for measurement of the full deflection basin, as opposed to limited deflection points. The RWD technology has potential for highway agencies to better assess their pavement structural conditions, enhance pavement management decision making, increase the effectiveness of maintenance and construction activities. However, the relationship between RWD deflections and falling weight deflectometers (FWDs)—which constitute the current state-of-the-practice, and for which current analysis tools and techniques are developed—should be better understood.


Source: FHWA

**Figure 1. Photo. The RWD measures pavement structural response at highway speeds.**

## PROJECT OBJECTIVE

The objective of this research is to compare RWD and FWD deflection basins and to provide a better understanding of their similarities and differences. The research team investigated the two devices through dynamic modeling of specific loading characteristics and field data collection on 23 State of Mississippi test sections to compare observed deflections to predicted trends. Furthermore, the team developed predictive equations to provide an efficient and reliable method for estimating critical asphalt concrete (AC) strains for use in network-level structural evaluation.

## SCOPE OF WORK

The research team developed the following scope of work for accomplishing the objectives:

- **Task 1: Review existing deflection technologies, applications, and needs.** The project began by reviewing the current state-of-the-practice in pavement deflection testing, analysis techniques, and applications to design and management. This included a review of existing FWD data analysis techniques, applications of RWD data to network-level evaluations, and previous research about implementing RWD data into routine pavement management activities.

- **Task 2: Determine the relationship between RWD and FWD deflections.** This task examined the differences between RWD and FWD devices, such as loading mode, loading rate, load configuration, speed influences, and dynamic loading effects. The ViscoWave[1] dynamic, finite layer algorithm was used to model the RWD and FWD with 324 pavement structures to determine their deflection relationships. In addition, the research team developed equations to predict AC critical strains based on selected curvature indices.

- **Task 3: Field testing and validation of theoretical predictions.** The research team collected field data on 23 established test sections in Mississippi to validate the theoretical RWD to FWD relationships and to provide input data for use in the strain predictive equations developed above. Field testing included the RWD, FWD, and accelerometer data collection and analysis.

## REPORT ORGANIZATION

The following list details the chapters in this report:

[1] Backcalculation analysis of layered pavements has been done using a number of static techniques for over 100 years. More recently, the Viscowave algorithm developed by Dr. Hyung Lee allowed analysis using dynamic properties more aligned to the rolling measurements taken by the RWD. Because of that unique capability, the algorithm was selected to be used in this project. A description and review of this algorithm may be found at: https://www.fhwa.dot.gov/publications/research/infrastructure/pavements/15063/005.cfm#01

- Chapter 2 provides a summary of the pertinent documents reviewed as part of this study. The purpose is to show the role of deflection testing in project- and network-level pavement evaluation, design, and management activities; demonstrate the use of RWD deflections in past studies; and identify analysis tools and techniques that have potential for adaptation to the RWD and its integration into network-level evaluation.

- Chapter 3 presents a description of the inherent differences between RWD and FWD devices and demonstrates the effects of various loading characteristics on thin and thick AC pavements.

- Chapter 4 presents the results of 324 dynamic, finite layer simulations of a wide range of pavement structures and subgrade conditions. The testing factorial covered pavements with variable AC and base layer thicknesses, and AC, base, and subgrade moduli. The outputs were used to compare RWD and FWD deflection basins, to calculate multiple basin shape parameters, and to correlate these basin shape parameters to critical AC strains.

- Chapter 5 documents the side-by-side RWD and FWD field testing performed on 23 Mississippi Department of Transportation (DOT) test sites. The testing also included accelerometer data collected to validate the RWD basins. The same basin shape parameters as used in the theoretical analysis were obtained from the field data for comparison in the next chapter.

- Chapter 6 compares the field results to the previously determined theoretical predictions regarding RWD and FWD relationships for deflections and basin shape parameters. In addition, the same parameters were used to estimate critical AC strain based on the predictive equations developed as part of this research.

- Chapter 7 summarizes the pertinent findings and conclusions of this study.

# CHAPTER 2. LITERATURE REVIEW

This chapter summarizes the key literature pertinent to the project objectives.

## CURRENT DEFLECTION TESTING AND ANALYSIS PRACTICES

### Deflection Analysis Techniques

The FWD has been the tool of choice for pavement structural testing and analysis in the United States since the 1980s. While it has been proven useful in many ways, the vast majority of its applications are limited to project-level studies, such as overlay design. Due to its stationary test nature, need for temporary lane closures, and limited productivity, the FWD has not been widely used for network-level evaluation. The data analysis techniques in use today have been developed around or adapted to the FWD and may not be directly applicable to moving wheel deflections, such as the RWD. Nevertheless, it is important to evaluate the existing techniques to assess their feasibility to be adapted to moving wheel deflections.

One of the most commonly used FWD analysis methodologies is the flexible pavement backcalculation method from the 1993 American Association of State Highway and Transportation Officials (AASHTO) pavement design guide.[(1)] This method models the pavement as a two-layer system—the sum of all pavement layers and the subgrade—and utilizes two sensors—an outer sensor to estimate the subgrade resilient modulus ($M_R$) and the maximum deflection ($D_0$) to determine the composite pavement modulus ($E_p$). The $E_p$ and total pavement thickness (D) are then used to determine the pavement's effective structural number ($SN_{eff}$). Although less sophisticated than other methods, the AASHTO method has been widely used due to its simplicity and integration into the pavement rehabilitation procedures based on the structural number concept.

The Asphalt Institute (AI) overlay design method presented in Manual Series No. 17 (MS-17) was originally developed for Benkelman Beam deflections and later adjusted for FWD loadings.[(2)] It calculates an estimate of load-carrying capacity based on maximum deflection. In the AI method, the design deflection is defined as the mean plus two standard deviations, taking into account not only deflection magnitude, but also section variability. The deflection is corrected for temperature, season, and multiplied by 1.61 to convert the FWD deflection to an equivalent Benkelman Beam rebound deflection.

Numerous deflection basin parameters (DBPs), also known as basin shape factors or deflection indices, have been defined and used for assessing the relative condition of the layers that make up the pavement structure. DBPs have the advantage of being calculated using only a few deflection measurements and eliminate the need for full characterization of the deflection basin. Extensive review and application of DBPs can be found in Xu, Ranjithan, and Kim; Kim and Park; and Horak.[(3,4,5)] Some of the more common DBPs include the Surface Curvature Index (SCI), the Radius of Curvature Index (RoC), and the Area Under the Pavement Profile (AUPP).

## Temperature Correction Methods

The stiffness of AC materials is temperature dependent, making AC pavement deflections dependent on the temperature conditions present at the time of testing. Therefore, common practice is to correct AC pavement deflections to a standard temperature to allow comparison between deflections collected at different temperatures. In general, deflection temperature adjustment is achieved by a two-step process. First, the effective temperature at a certain depth of the asphalt layer (e.g., mid-depth) is estimated from other variables that can be obtained more easily (e.g., air or surface temperature). Then, a correction factor for deflection is determined based on the estimated pavement temperature and applied to the measured deflection.

To estimate the AC mix temperatures during FWD testing, Baltzer et al. developed a model known as the BELLS equation (an acronym for the authors, Baltzer, Ertman-Larson, Lukanen, and Stubstad) based on the Long-Term Pavement Performance (LTPP) initial round of Seasonal Monitoring Program (SMP) data.[6] After completion of the second round of the LTPP SMP experiment, Lukanen et al. improved the original BELLS equation and supplied a new set of equations that are referred to as BELLS2 and BELLS3.[7] The authors recommended the BELLS3 equation for routine testing where the FWD measurement at a given location takes less than a minute. Its inputs include the pavement surface temperature, previous day's mean air temperatue, depth of interest, and time of day. Another method was developed by Park et al. using temperature data collected from six in-service pavements in Michigan.[8] The model was validated against LTPP's SMP data and uses all of the same inputs as the BELLS equation, except for the previous day's air temperature.

Once the AC temperature at the depth of interest is estimated, there are several deflection correction methods available, such as the AASHTO and AI procedures. The 1993 AASHTO guide provides two graphs for obtaining $D_0$ temperature correction factors to normalize deflections to 68 °F, based on the AC thickness and base type—granular or cement-stabilized. The AI method was developed based on the Benkelman Beam. It is presented in a graph and provides a factor to adjust $D_0$ to 70 °F based on the mean pavement temperature and untreated base thickness. Other deflection correction method developers include Chen et al., whose method allows for $D_0$ correction to a user-defined reference temperature, based on AC mid-depth temperature during testing and AC thickness.[9] Kim et al. developed a $D_0$ temperature correction model for North Carolina, which was further developed to account for correction of deflections at distances away from the load center, when appropriate.[10]

Other researchers have even proposed methods for correcting DBPs. Lukanen et al. developed semi-log models for some of the frequently used DBPs and outlined how these semi-log models could be used for adjusting the DBPs as well as the FWD center deflection.[7] The researchers provided the framework to correct curvature indices from 8 to 60 inches from the load center. They reported that the correction factors calculated using this method are very similar to those of the 1993 AASHTO guide. This $D_0$ temperature adjustment methodology was extended by Flintsch et al. to correct FWD deflections at all sensors during FWD and traffic speed deflectometer testing.[11]

## NETWORK-LEVEL DEFLECTION APPLICATIONS

As an alternative to the FWD, the RWD presents a feasible option for collecting data on large roadway networks or in areas where lane closures are not practical. It has been implemented in several ways over the past 12 years as part of pavement management systems (PMS) and large-scale structural evaluations.

One of the earliest implementations was an RWD-based PMS for local roads in Illinois. Vavrik et al. developed a pavement management strategy for Champaign County, Illinois, to assist the County Highway Department with allocating its roadway network maintenance budget.[12] They developed a treatment matrix to select the most appropriate maintenance or rehabilitation alternative for each road based on the RWD deflection, Pavement Condition Index (PCI) value, and traffic level. Through a multi-year simulation, the researchers were also able to recommend a budget necessary for the County to maintain the roadway network at its current condition and how additional funding may improve the roadway condition over time. The proposed pavement management strategy for Champaign County is unique in that the average RWD deflections are used directly in the decision-making process without any further analysis. This system has since been used for other Illinois local roads agencies.

In another study, Wilke used RWD and FWD data collected in Pennsylvania to compare the remaining service life (RSL) estimated from these devices to those predicted by the Pennsylvania DOT's existing roadway management system.[13] The RWD surveyed approximately 290 miles of the DOT's roadway network while the FWD testing was conducted on 16 selected projects. For the analysis of the RWD data, the AI overlay design methodology was used to calculate the RSL in terms of equivalent single axle loads (ESALs). FWD data were analyzed using the AASHTO backcalculation methodology, determining $SN_{eff}$ values used in the AASHTO flexible design equation to determine allowable ESALs. RWD- and FWD-based RSLs were compared to the DOT's roadway management system, and a consistent trend was observed between the remaining life estimates from all three methods.

Researchers at the Louisiana Transportation Research Center (LTRC) developed a model for estimating the $SN_{eff}$ of existing pavements from RWD deflections, based on the RWD and FWD data collected from 16 pavement sections, each 1.5 miles long, consisting of various cross sections and structural conditions.[14] After adjusting the RWD deflections for temperature using the BELLS3 and AASHTO methods, they calculated a new parameter called the RWD Index (RI), which is the mean RWD deflection per section, multiplied by that section's deflection standard deviation. The model was validated using 52 in-service pavement sections in Louisiana that were tested with both the RWD and the FWD. The structural number (SN) of the pavement was estimated from the RWD using the previously developed equation and compared to the FWD's $SN_{eff}$, based on the conventional AASHTO equations. With a coefficient of determination ($R^2$) value of 0.77, the researchers concluded that the model may be a good tool for identifying pavement structural condition at a network level.

To demonstrate the potential economic benefit of implementing RWD data in a statewide PMS, FHWA sponsored a study with the Oklahoma DOT.[15] According to Oklahoma's pavement management strategy, the overall condition of a pavement is assessed in terms of the Pavement Quality Index (PQI), which is a weighted sum of the individual indices for functional condition

(i.e., surface distress), ride quality, rutting, and structural condition. The indices, including the overall PQI, are on a scale of 0 to 100, with 100 representing a distress-free condition. In the DOT's system, the structural condition comes from FWD testing; however, this is limited to the National Highway System (NHS) and other high-volume roadways. The majority of the roadway network is primarily managed based on a subjective rating termed Base Condition. For the roadways where the FWD data are available, the ratio of the average deflection measured at the center of the load plate to the maximum deflection criteria is calculated for the structural assessment. Based on RWD data collected on approximately 1,000 centerline miles of the DOT's highway network and a 20-year simulation, the research team found that the annual budget could be reduced by 11.5 percent by incorporating a pavement preservation program in the PMS activities and using the RWD to identify candidate pavement sections for preservation (vs. overlay).

## POTENTIAL TOOLS FOR IMPLEMENTING RWD DATA IN PMS

The RWD has potential to benefit network-level evaluation and PMS; however, the vast majority of available data analysis techniques were developed around the FWD and are not directly applicable to the unique loading characteristics of moving wheel loads. Also, current moving wheel deflectometers do not provide comparable deflection accuracy to FWDs, making analyses such as layer moduli backcalculation through basin matching infeasible. Several researchers have investigated the application of DBPs to moving deflectometer data to estimate critical stresses and strains in the AC, base, and subgrade layers. These efforts have shown good results and have the potential to quickly and effectively determine critical responses in the pavement and subgrade layers, which in turn can be used to estimate structural capacity.

Thyagarajan et al. used the Jacob Uzan Layered Elastic Analysis (JULEA) program to generate synthetic deflections and strains of various flexible pavements (thickness and modulus) subjected to an RWD dual tire load.[16,17] Using the deflections and strains, the researchers indicated that the peak deflection alone is not a good indicator of the structural condition of the pavement. Instead, the researchers indicated that the Curvature Index (CI) is a better measure of the asphalt condition. The study considered three CIs--$delta_8$, $delta_{12}$, and $delta_{18}$. The researchers developed linear correlations between the CIs and the critical AC strains for AC thicknesses ranging from 3 to 14 inches in 1-inch increments.

Rada et al. performed a similar analysis using a combination of forward run programs for 75 DBP definitions.[18] Their study began with dynamic modeling of three MnROAD test sites using the 3D-Move finite element program, calibrating the program outputs to measured data from two moving wheel deflectometers. They used the resultant deflections as inputs in the numerous DBP definitions and correlated to critical strains in the AC, base, and subgrade layers. Next, they evaluated the sensitivity of the correlations to 36 variations in the pavement structure and vehicle speeds, also using the 3D-Move program. Finally, they performed approximately 15,000 JULEA runs to evaluate the robustness of the correlations, noting the limitations of this method, which models static, instead of dynamic, loads and linear elastic AC behavior, instead of viscoelastic. Different indices performed better at different stages of the evaluation, and the researchers determined that better results were obtained by developing correlations for different AC thicknesses. Based on all AC thicknesses evaluated, they recommended the Deflection Slope

Index (DSI) using the $d_4$ and $d_{18}$ deflections ($DSI_{4-18}$) developed as part of their study as the most effective index, followed closely by $SCI_{12}$.

Carvalho et al. also looked into using DBPs as part of simplified procedures for incorporating FWD deflection testing and structural analysis into network-level analysis.[19] They concluded that consideration of structural condition improved performance, minimized maintenance, and reduced maintenance and rehabilitation (M&R) costs per mile and that the decreased M&R costs easily surpassed the FWD testing cost.

The experience of these researchers indicates that implementation of RWD testing at the network level has the potential to optimize the use of agency resources and decrease costs. The previous research with DBPs shows that they are a suitable approach to incorporating RWD data at the network level, but that it is important to develop procedures adapted to moving wheel basins, not FWD deflections, and not using analysis techniques based on static loading.

One viable method of modeling dynamic pavement loading—both FWD and RWD—is ViscoWave, developed by Lee.[20] ViscoWave is a finite layer solution capable of modeling the pavement dynamics and material viscoelasticity under a transient, non-periodic loading. It was used extensively in this study to simulate the pavement response under dynamic FWD loadings, as it is capable of modeling the full time-history of an impact load and deflections, not just the peak deflections at each sensor. ViscoWave is capable of simulating not only the pavement response at a fixed point in the pavement but also the pavement response at fixed distances from the moving load along the length of the pavement (i.e, similar to the deflections measured by the RWD).[21]

# CHAPTER 3. RWD VS. FWD DEVICE COMPARISON

## DEVICE DESCRIPTIONS

The RWD and FWD both deliver dynamic loads to the pavement and measure resultant deflections; however, there are differences in their loading characteristics that produce different deflection basins. This section describes each device, the inherent differences between them, and the effect of each loading characteristic on the relationship between FWD and RWD basins.

### RWD

The current RWD is an imaged-based system for measuring pavement deflections beneath the dual tires of an 18,000-lb, single-axle semi-trailer, as shown in figure 2. The system collects pairs of spatially coincident images of the pavement surface; first, in the undeflected pavement area forward of the rubber tires, and second, when the truck has advanced to where the wheels occupy the previously undeflected area. A customized image processing algorithm overlaps the two images and determines differences between them, corresponding to vertical pavement deflection. It uses light emitting diode (LED) flashes to light the deflected and undeflected pavement areas, thereby overcoming changes in ambient lighting throughout the day and minimizing the effects of hard shadows, such as those cast by the rubber tires.

The key RWD components include:

- Two high-speed, high-resolution digital cameras.
- Two banks of high-intensity, short-flash duration LED lights.
- A distance measuring instrument (DMI).
- Triggering mechanism to synchronize cameras and flashes.
- Operating computer and software.
- Infrared pavement surface temperature sensor.
- Global positioning system (GPS).

The measurement system is mounted on a 53-ft trailer and operated by a laptop computer placed in the cab. The RWD is two-person operation—one driver and one operator. The RWD typically collects images every 25 ft and averages deflection basins every 500 ft for use in network-level management. It operates at prevailing highway speeds and does not involve lane closures or traffic control.

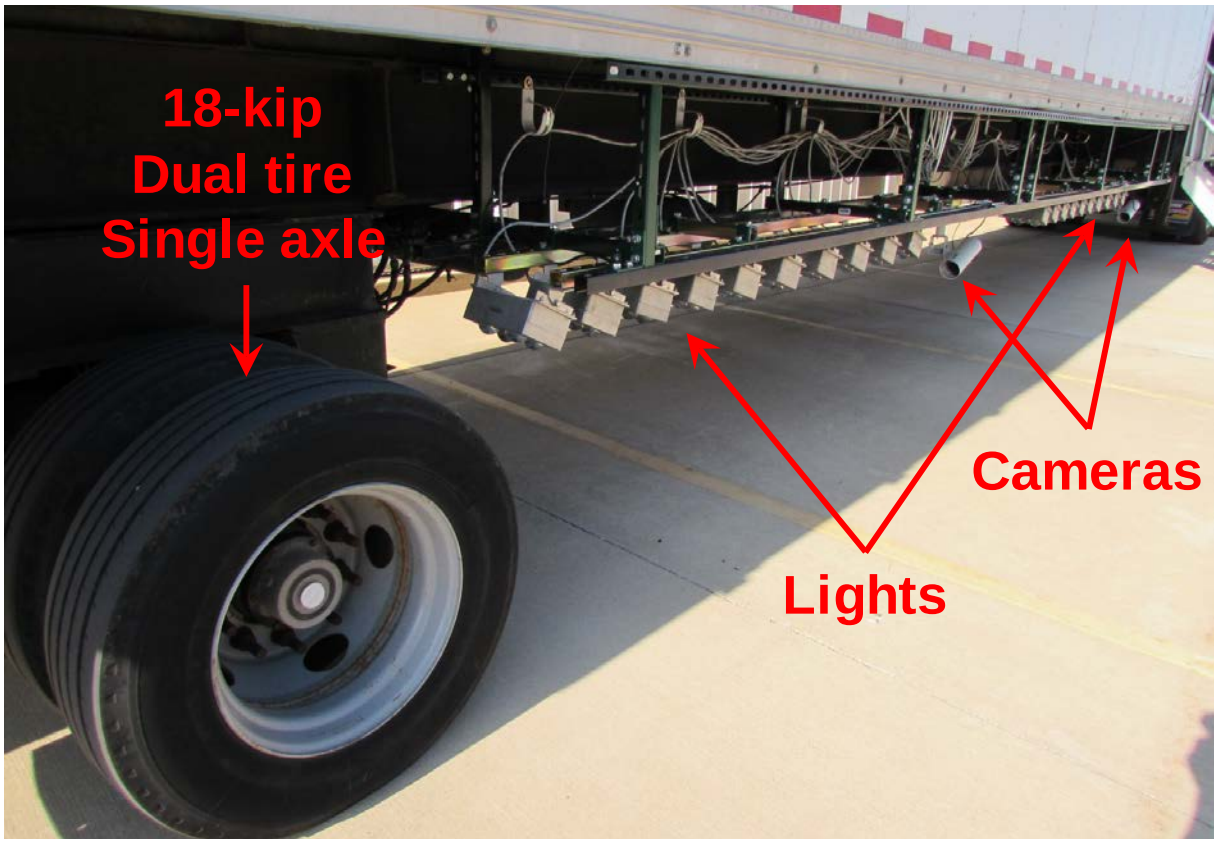


Source: FHWA

**Figure 2. Photo. Essential RWD components.**

**FWD**

The FWD is a widely understood nondestructive deflection testing device that delivers an impact load to the pavement surface by means of dropping a falling mass/spring combination on a load plate placed on the pavement surface. The resultant pavement deflections are measured by sensors placed radially in one direction from the center of the load plate. For this study, data were collected with a truck-mounted FWD, meaning the falling mass assembly and sensors are mounted in the bed of a heavy-duty pickup truck and lowered to the pavement at each test point. The FWD generates multiple target loads by varying the drop height, and all operations are performed from a laptop computer that records the resulting load and deflection data. Figure 3 shows the FWD used for this project.

The FWD performed a single, unrecorded seating drop at each test point, followed by a single drop each at 9,000-, 12,000, and 16,000-lbf target loads. It measured deflections with sensors placed at 0, 8, 12, 18, 24, 36, 48, and 60, and -12 inches from the load plate. In addition to the load and deflection data, the FWD also records air and pavement surface temperatures, GPS coordinates, and a linear reference at each test point. The FWD is a single operator system.

Source: FHWA

**Figure 3. Photo. The FWD and sensor bar.**

## INHERENT DIFFERENCES BETWEEN DEVICES

Although the FWD and RWD are both dynamic deflection testing devices, their loading characteristics have inherent differences, and therefore they produce different pavement responses, including deflection magnitudes, basin shapes, and critical stresses and strains. These differences include:

- Loading mode—impact vs. moving loads.
- Loading rate—speed effects.
- Load configuration—single plate vs. dual tires.
- Half- vs. full-axle configurations.
- Deflections between the tires vs. under a dual tire.
- Constant target loads vs. dynamic variations.

## Loading Mode Effect

Both the FWD and RWD apply dynamic loads to the pavement; however, their loading modes are different. The FWD is an impact device, delivering a vertical impact force to the pavement surface by dropping a falling mass/spring combination on a load plate placed on the pavement surface. The RWD is a moving wheel load, normally operating at highway speeds. Typical loading durations for an FWD are 12 to 20 ms rise times (i.e., time from rest to peak load), while the RWD may range from 150 to 200 ms, depending on truck speed. The difference in loading rate affects the response of bituminous materials due to their viscoelastic properties, with longer loading durations resulting in a greater response (i.e., higher deflections).

The research team evaluated the sensitivity of pavement deflections due to different loading modes by modeling pavement responses due to FWD (i.e., impact) and RWD (i.e., moving wheel) loads. For this comparison, a single, circular loading area with a constant 9,000-lb load was modeled for both FWD and RWD simulations. Two AC thicknesses—4 and 12 inches—were modeled over a granular base over subgrade. The only difference between the two simulations was loading mode. The simulated RWD truck speed was 60 mph, and the FWD load pulse was a haversine wave with a 12.5 ms rise time (i.e., 25 ms duration). Figure 4 shows the results.

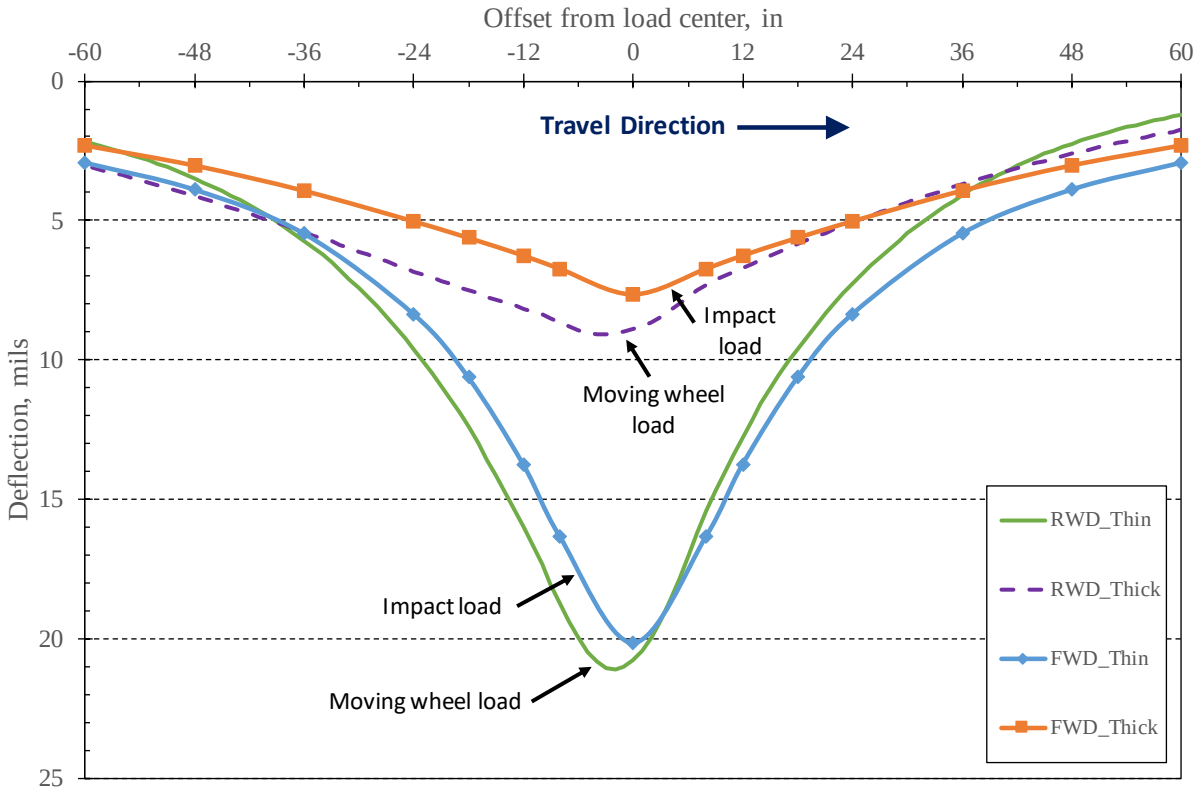


Source: FHWA

**Figure 4. Loading mode effect—thin and thick AC.**

The results show that, with all other parameters being equal, the moving wheel load produces higher deflections than the impact load, especially for the thicker AC pavement. The results also highlight the asymmetry of the RWD basin, due to the delay in recovery behind the moving wheel. The figure also illustrates the slight lag in the the RWD maximum deflection with respect to the center of the wheel load, which in this case is about 2 inches.

**Loading Rate Effect**

To study the effect of RWD truck speed, and therefore loading rate, on the viscoelastic AC response and resulting deflections, the RWD was simulated at speeds ranging from 10 to 60 mph in 10 mph increments. Figures 5 and 6 show the results for sample thin and thick pavements, respectively. For comparison purposes, these figures also show the FWD deflection basins previously presented in figure 4.

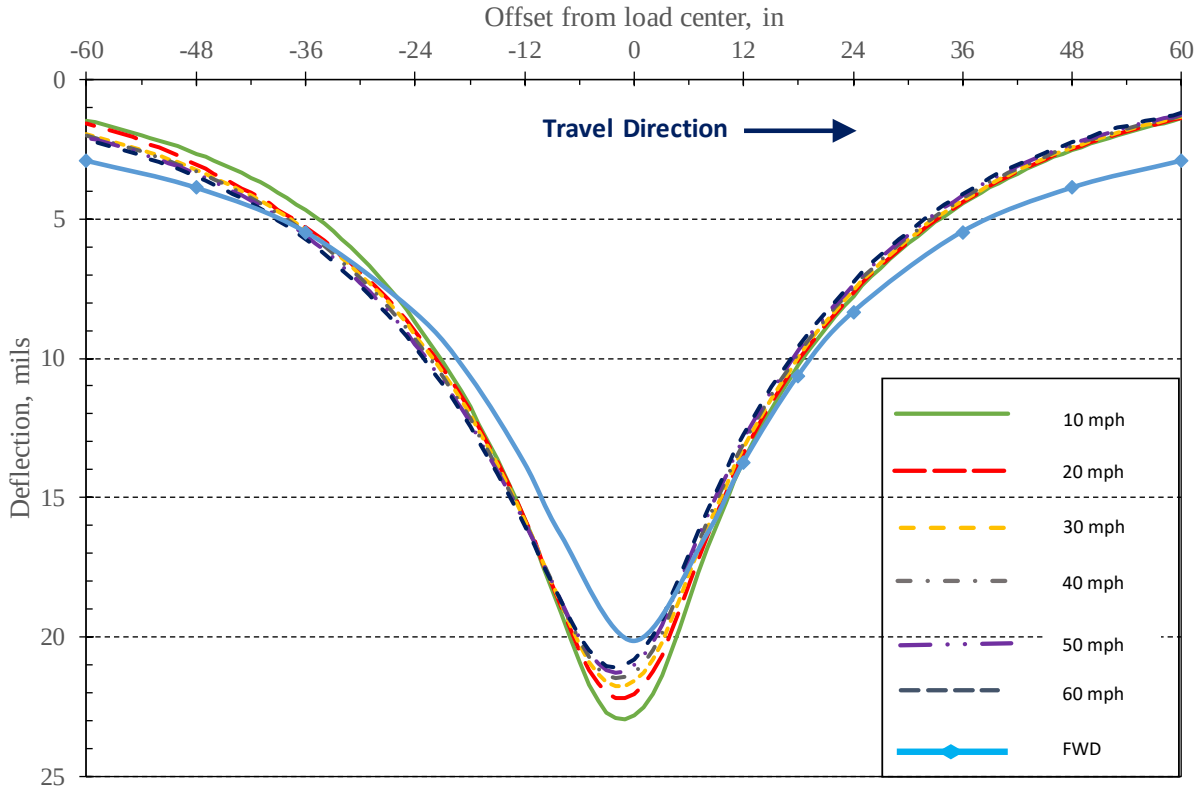


Source: FHWA

**Figure 5. Graph. RWD speed effect—thin AC.**

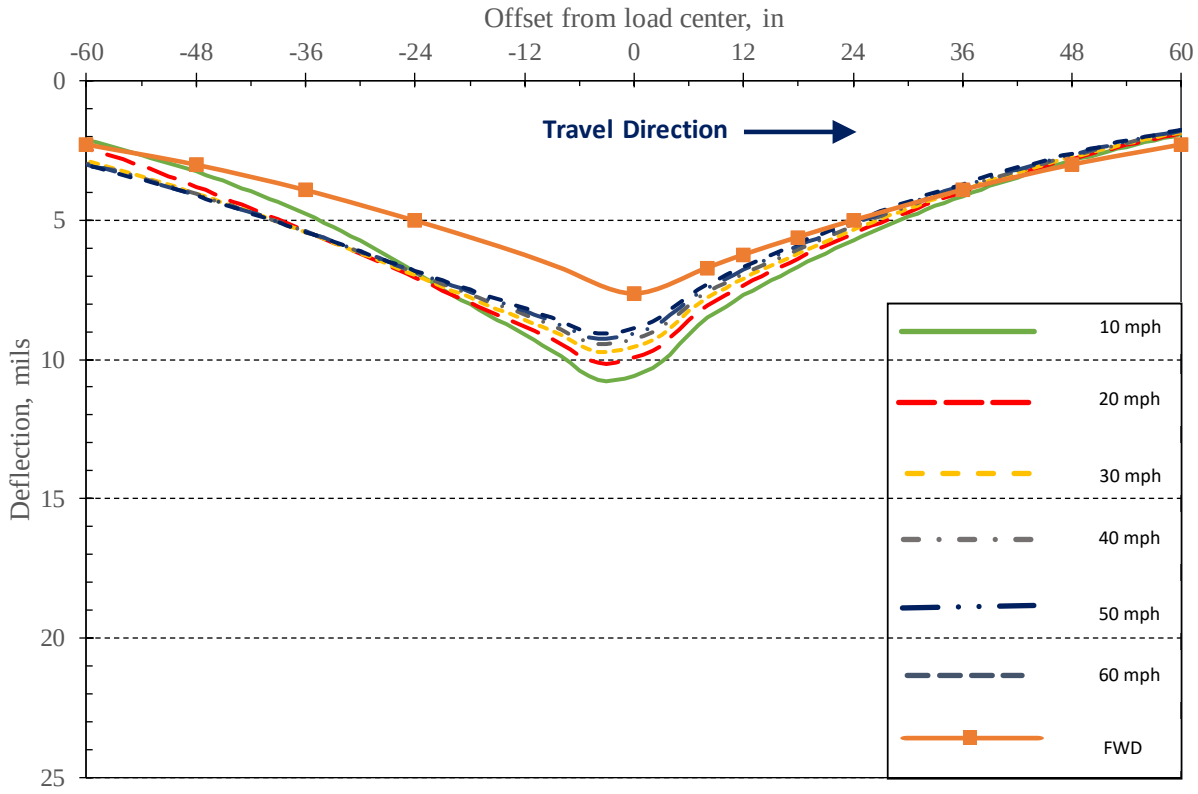


Source: FHWA

**Figure 6. Graph. RWD speed effect—thick AC.**

The data show that truck speed has an effect on deflections, primarily at and near the center of the deflection basin, and at lower speeds. The 10 mph simulations produced the largest maximum deflections, with diminishing effect above 40 mph, and become more asymptotic at 60 mph. Although deflections decrease at higher speeds, they do not reach the FWD maximum deflections, indicating that there are other differences between the moving and impact load types besides truck speed. Other possibilities for the larger RWD deflections include the shape and extent of the stress bulb generated beneath the moving wheel load, as well as the effect of pavement inertia (i.e., dynamic effect) in the FWD simulation, as some of the FWD's energy goes into accelerating the at-rest pavement. Overall, the results indicate that when operating at speeds greater than 40 mph, speed effect does not have a significant effect on deflections.

### Load Configuration Effect

A primary difference between the FWD and RWD is the load configuration. The FWD applies its entire target load over a circular plate, while the RWD splits the load between two tires (i.e., dual tires) spaced 13 inches apart. The effect of the RWD's distributed load decreases the deflections near the dual tires, producing a shallower basin. Figure 7 presents the results of distributing the load over two tires, as compared to a single plate load. The dual tire deflections are measured between the two tires.

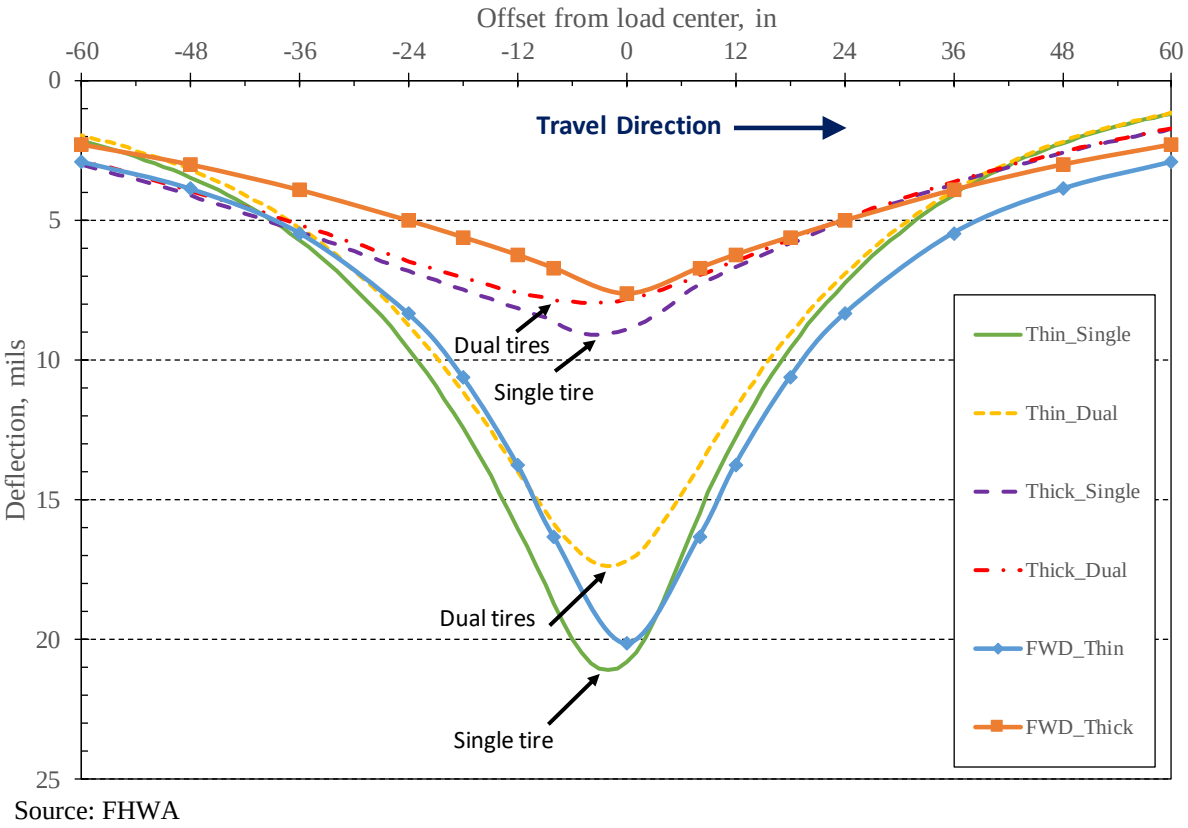


Source: FHWA

**Figure 7. Graph. Load configuration effect—thin and thick AC.**

The results show a dramatic deflection decrease for the distributed load, especially in the case of the thin AC pavement. In fact, the maximum deflection between the dual tires becomes significantly less than that of the single plate load for the thin AC pavement. Deflections for the thick AC pavement also decrease but remain slightly higher than the corresponding FWD deflections.

### Half- vs. Full-Axle

A special consideration for the RWD is the deflection contribution from the other half of the axle load to the deflection basin on the side of the axle where deflection is measured. Basically, the outer portions of the deflections basins from each set of wheel loads superimpose on the opposite side basin, slightly increasing deflecitons. To gain an understanding of the amount of increase, ViscoWave was used to simulate half- and full-axle loadings. Figure 8 shows the results.

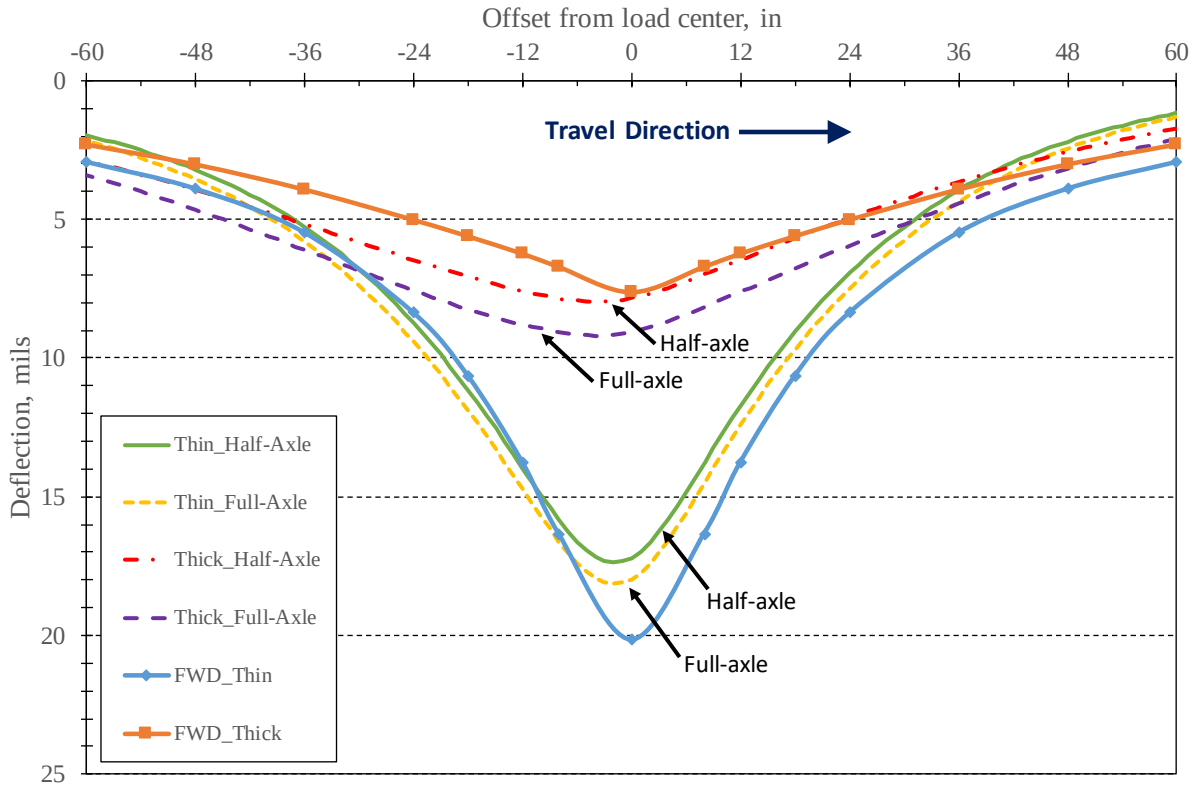


Source: FHWA

**Figure 8. Graph. Half- and full-axle deflecitons—thin and thick AC.**

The simulations show that half-axle deflections increase considerably when the second half of the axle is considered, especially in the case of thicker, stiffer pavements.

### Deflections Between the Tires vs. Under a Dual Tire

The RWD measurement system calculates deflections between the RWD's dual tires, as it is not possible to measure directly underneath the moving wheel loads. To study the difference in deflections between the tires vs. under the tires, the deflections were calculated along both locations in ViscoWave for the full-axle case. Figure 9 presents the results for deflections under the inner dual tire. Deflections under the inner tire are slightly higher than the outer tire, due to a greater contribution from the other half of the axle.

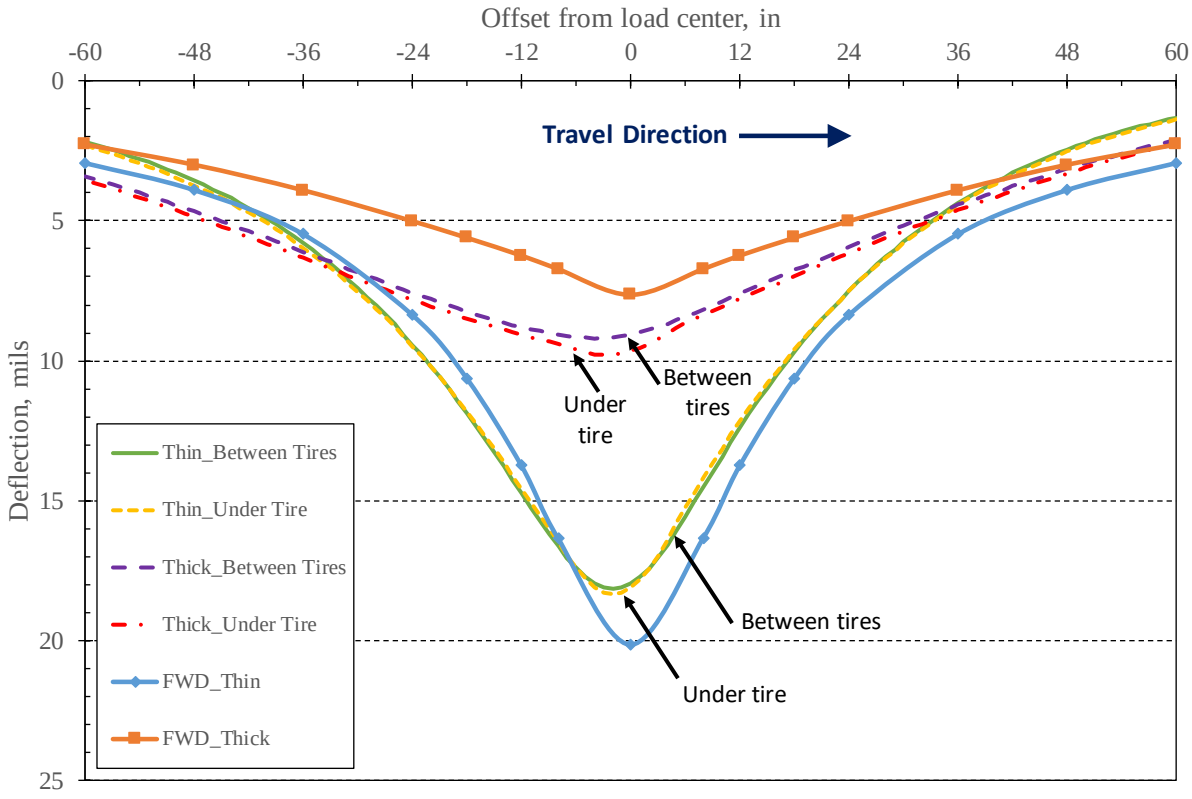


Source: FHWA

**Figure 9. Graph. Deflections between the tires vs. under the tire—thin and thick AC.**

The results show that deflections under the inner tire are slightly higher than those of the RWD's measurement system, which calculates deflections between the tires. The effect is minimal on the thin AC pavement and slightly higher on the thick AC pavement.

### Combined Effect of All Loading Characteristics on FWD and RWD Basins

Figure 10 shows the combined effect of all loading characteristics on FWD and RWD basins for the thin and thick AC pavements used in the above simulations. For these two specific pavement structures, ViscoWave predicts lower deflections for the RWD than for the FWD on the thin AC pavement, but higher deflections for the RWD than for the FWD on the thick AC pavement.

### Load Variations—Constant vs. Variable Dynamic Loading

The final loading characteristic distinguishing the RWD from FWDs is the aspect of truck bounce creating a variable dynamic load on the pavement, in addition to its static 18-kip axle load. During steady state operation, the RWD experiences a sinusoidal load variation due to road roughness. The variation in dynamic load on the pavement surface is a function of several road and truck factors, including pavement roughness, truck speed, truck weight, and suspension stiffness and damping.

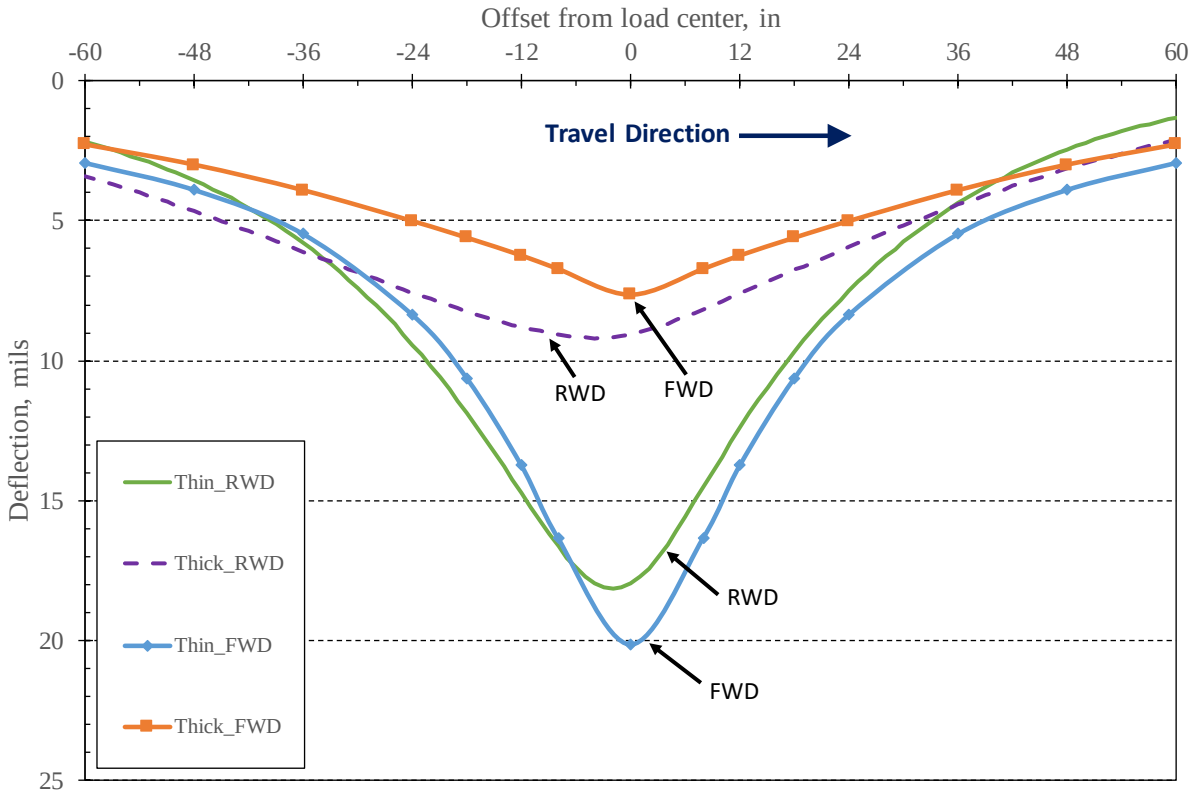


Source: FHWA

**Figure 10. Graph. Resulting FWD and RWD deflections—thin and thick AC.**

Figure 11 shows a sample of load variation data recorded by monitoring the RWD's air suspension pressure during field testing on two pavements—smooth and rough. The data show that on smooth pavements, the RWD experiences very little bounce, and therefore, very little variation from its 9,000-lb static load on each half axle. In the case of the rough pavement, the load on the pavement surface varies significantly, ranging from 7,300 to 12,300 lb. The load standard deviations over the 500-ft sections are 64 and 757 lb for the smooth and rough pavements, respectively, corresponding to coefficients of variation of 1 and 8 percent, respectively.

Figure 12 illustrates the effect of load variations on pavement deflections for a medium-thick (8-inch AC) pavement, as simulated in ViscoWave. As expected, the deflection variations follow the same trend as load variations. The deflection standard deviations for the smooth and rough pavements are 0.10 and 1.11 mils, respectively, resulting in coefficients of variation of 1 and 8 percent each. As truck bounce tends to follow a sinusoidal pattern, deflection variations due to dynamic loads are typically removed through averaging of multiple RWD readings over a fixed distance, say every 100 to 500 ft.

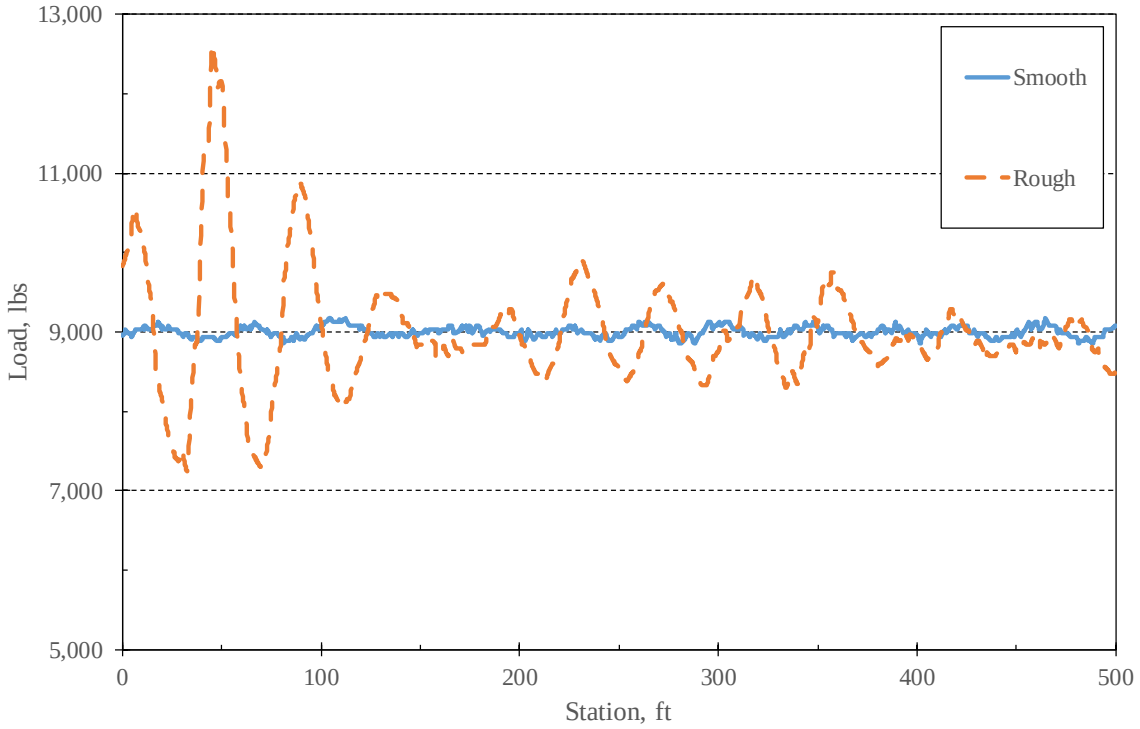


Source: FHWA

**Figure 11. Graph. Load variations from truck bounce—smooth and rough pavements.**

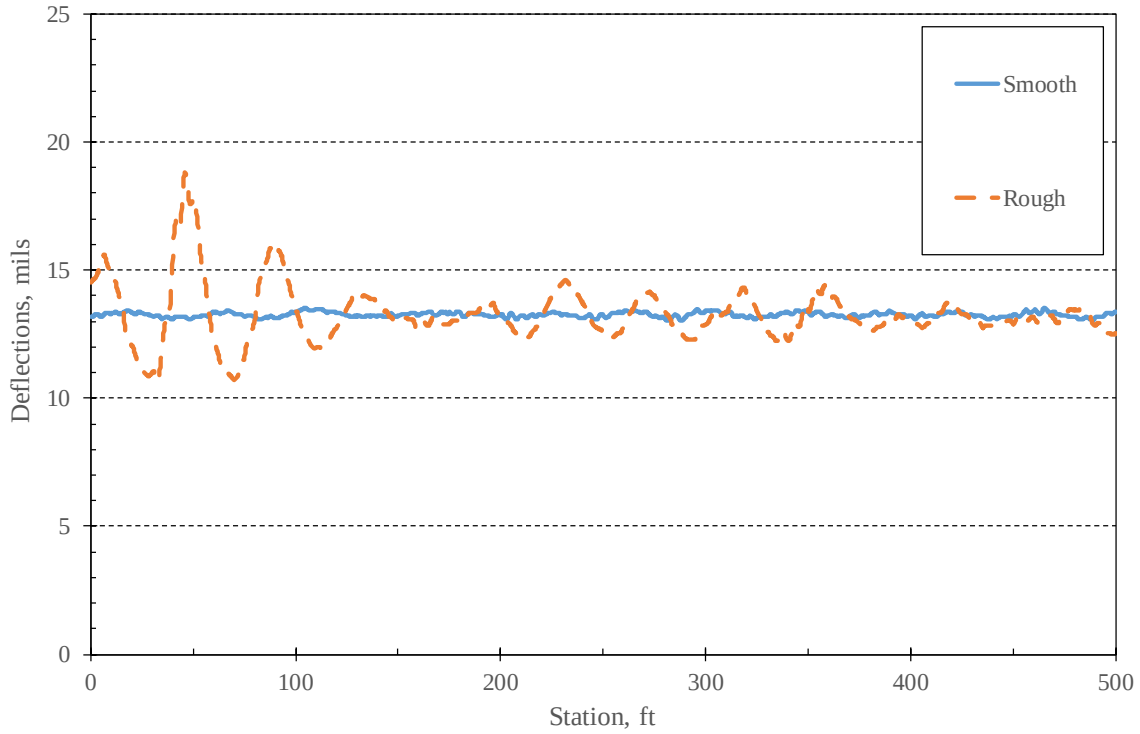


Source: FHWA

**Figure 12. Graph. Deflection variations from truck bounce—smooth and rough pavements.**

# CHAPTER 4. DYNAMIC MODELING OF RWD AND FWD RESPONSES

## SIMULATION DESCRIPTION

The research team performed dynamic modeling of a diverse range of pavement and subgrade layer thicknesses and moduli to generate a synthetic data set of pavement responses for both FWD and RWD loadings. ViscoWave[20] was used for this task. The goal was to develop a large data set to determine the relationship between FWD and RWD deflections over a broad range of pavement thicknesses and moduli. In addition, the resultant deflections and critical AC strains were used to develop several relationships between basin shape factors and critical AC strains.

## FACTORIAL DESIGN

The research team selected the following input variables and values for evaluation in the dynamic analysis:

- AC thicknesses: 4, 8, 12, and 16 inches.
- Base thicknesses: 8, 10, and 12, inches.
- Subgrade thickness: 120 inches with a semi-infinite stiff layer.
- AC modulus: Time dependent relaxation modulus, E(t), of form shown in figure 13 was used with coefficients $c_1 = 3.5$, $c_2 = 3$, $c_3 = -0.2$, and $c_4 = 0.45$ to produce E(t) in units of psi. In figure 13, $t$ is the loading time and $a_T$ is the temperature shift factor obtained using the equation shown in figure 14, with $\alpha_1 = 0.0006$, $\alpha_2 = -0.1518$, and $\alpha_3 = 2.5456$. Using these variables, the AC modulus was simulated at 50, 70, and 90 °F.
- Base moduli: 40,000, 60,000, and 80,000 psi.
- Subgrade moduli: 10,000, 20,000, and 30,000 psi.

$$\log\left(E\left(t\right)\right) = c_1 + \frac{c_2}{1 + e^{c_3 + c_4\left\{\log\left(t\right) - \log\left(a_T\right)\right\}}}$$

**Figure 13. Equation. Sigmoidal function for AC relaxation modulus.**

$$\log\left(a_T\right) = \alpha_1 \cdot T^2 + \alpha_2 \cdot T + \alpha_3$$

**Figure 14. Equation. Temperature shift factor.**

This resulted in 324 individual ViscoWave runs for both the FWD and RWD simulations.

The FWD simulation modeled a haversine impact load of 25 ms duration and a peak force of 9,000 lbf over a 12-inch diameter circular load plate. The simulation outputs included surface deflections and horizontal strain at the bottom of the AC layer at offsets of 0, 8, 12, 18, 24, 36, 48, and 60 inches from the center of the load plate.

The RWD simulation modeled an 18,000-lbf, dual tire, single axle (i.e., four tires at 4,500 lb each) traveling at 60 mph. The outputs included deflections and strains at every 1-inch interval, beginning at the axle centerline (i.e., 0 inches) and extending forward and backward from -60 to 60 inches. Pavement response was simulated at two transverse offsets for these deflection locations—between the dual tires and directly beneath the inner tire. However, the resulting differences were not significant enough to affect the subsequent correlation developments. Therefore, only the responses from the basins between the dual tires were used in the remainder of this analysis, as this is where the RWD device measures deflections.

## FWD AND RWD DEFLECTION RESULTS

Figures 15 and 16 show sample outputs for thin and thick pavements (4 and 12 inches of AC), respectively. The FWD output is forward of the load plate, while the RWD simulation produces deflections both forward and rear of the RWD tires. The figures show that the rebound portion of the RWD basins (i.e., the area behind the moving wheel loads) has a slight lag, relative to the forward RWD deflections. The figures also illustrate that there is no consistent relationship between FWD and RWD basins, meaning that one device may produce deflections higher or lower than the other device, depending on the pavement characteristics.

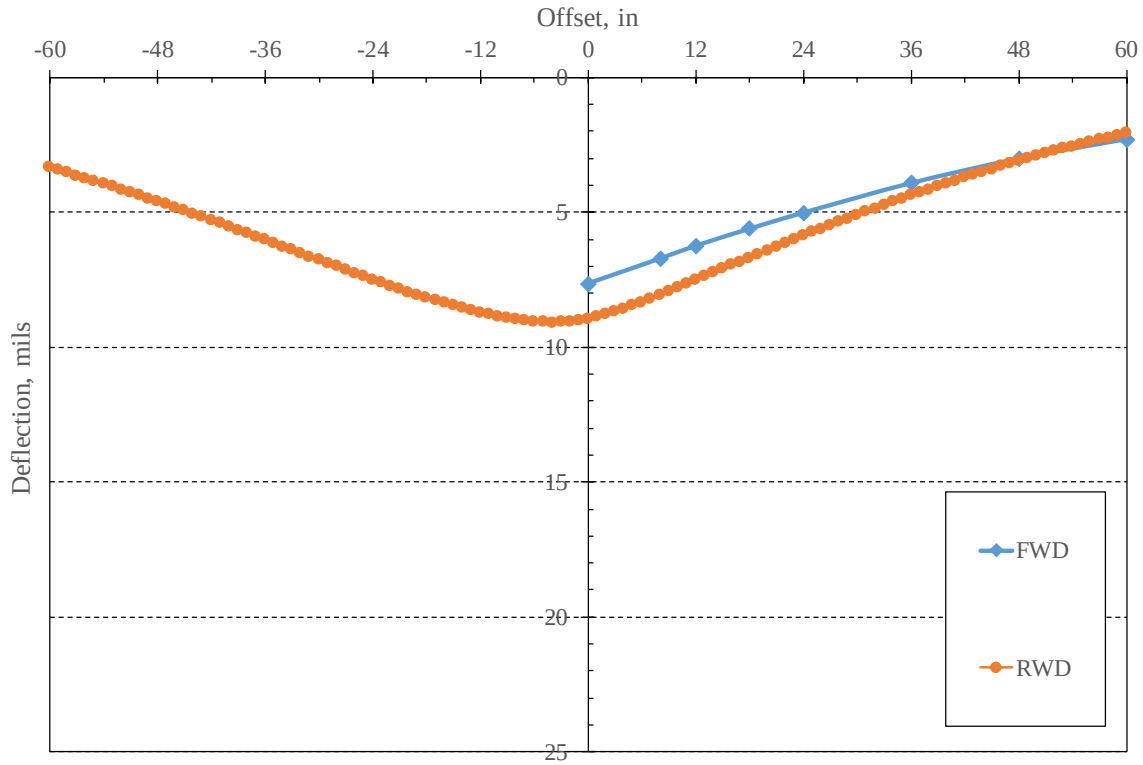


Source: FHWA

**Figure 15. Graph. Sample ViscoWave FWD and RWD basins—12-inch AC.**

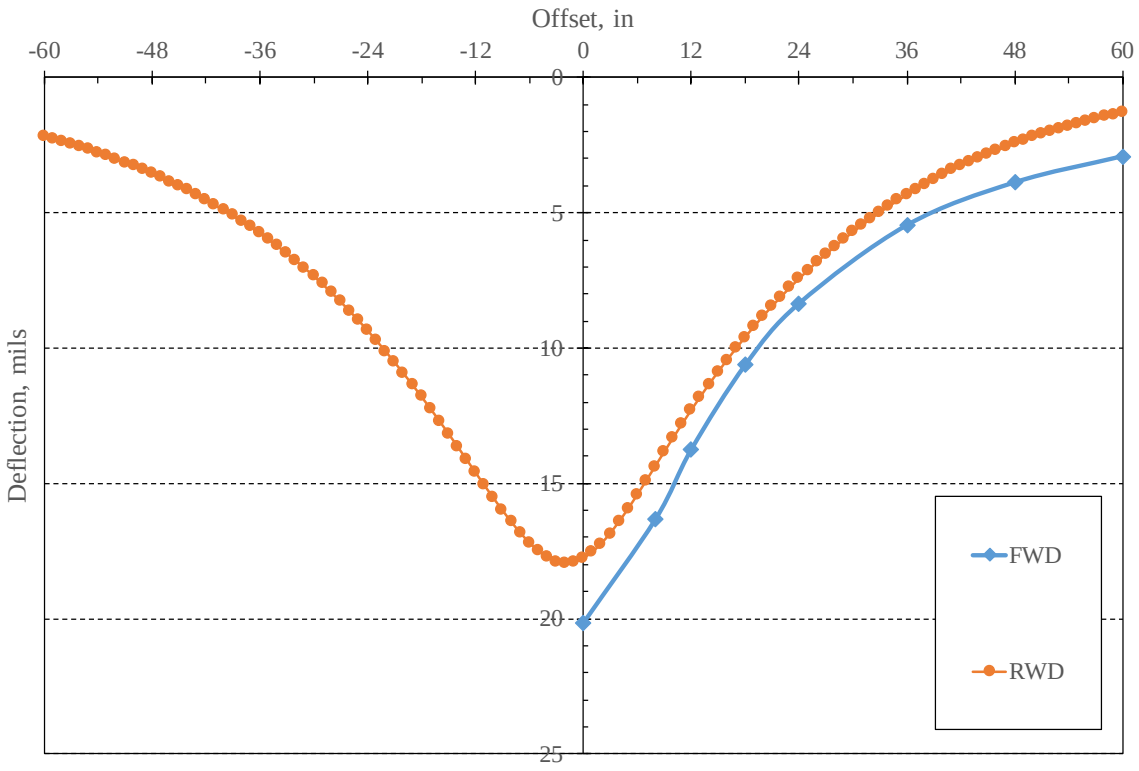


Source: FHWA

**Figure 16. Graph. Sample ViscoWave FWD and RWD basins—4-inch AC.**

To further characterize the relationship between FWD and RWD basins for a broad range of pavement factors, the research team compared deflections at 0, 36, and 60 inches forward from the load center for both devices for all 324 pavement combinations. Figures 17 to 19 show these results.

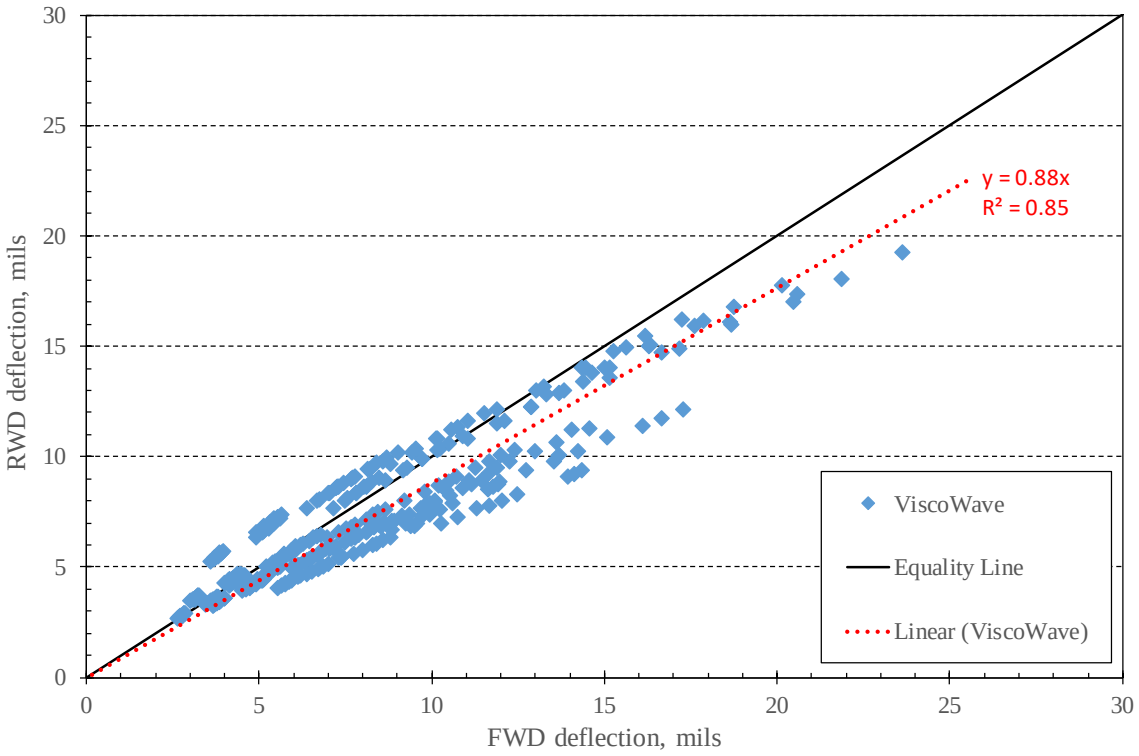


Source: FHWA

**Figure 17. Graph. FWD vs. RWD comparison—$D_0$.**

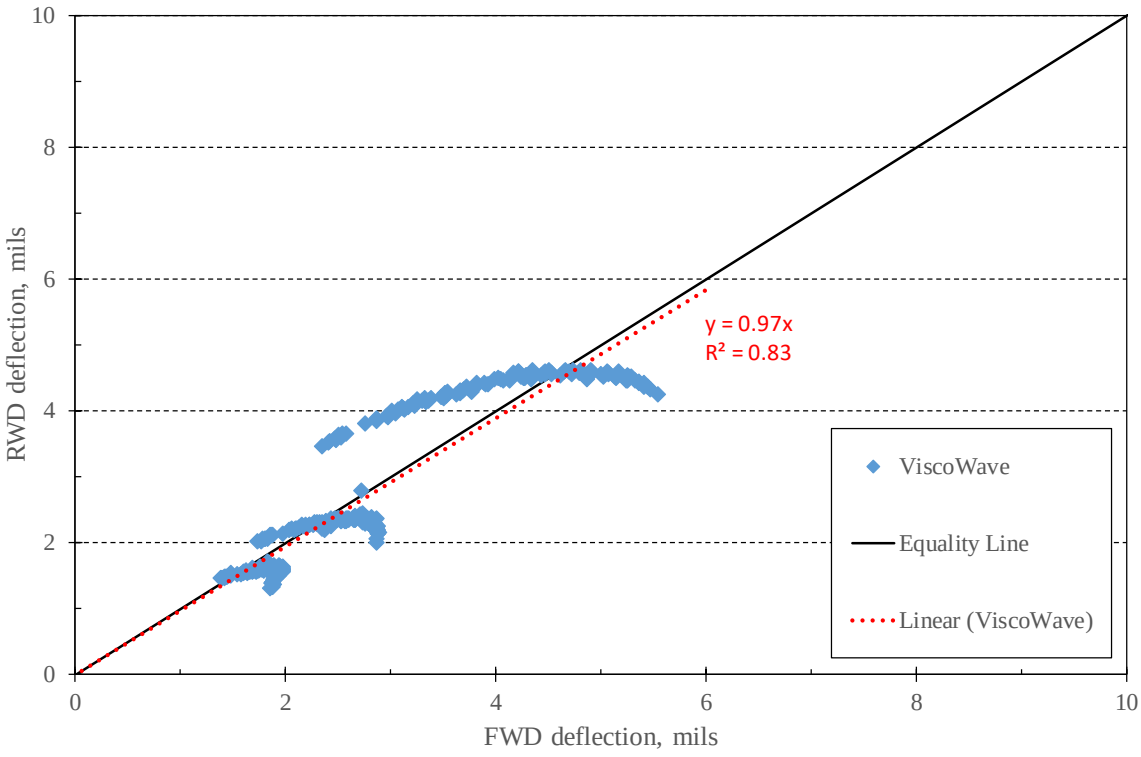


Source: FHWA

**Figure 18. Graph. FWD vs. RWD comparison—$D_{36}$.**

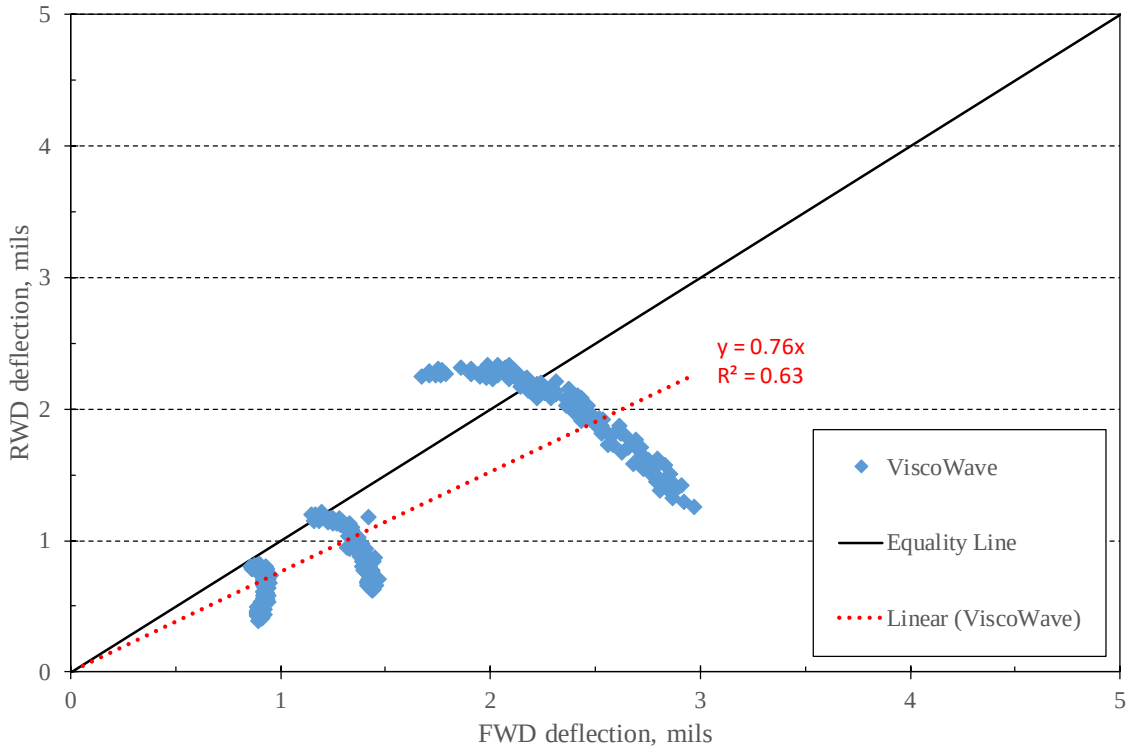


Source: FHWA

**Figure 19. Graph. FWD vs. RWD comparison—$D_{60}$.**

Figure 17 shows the general trend for FWD and RWD basins is to produce similar maximum deflections for low deflection pavements (i.e, thick or stiff pavements), with slightly lower RWD deflections compared to the FWD for medium- and high-deflection pavements (i.e., thin or weak pavements). The primary pavement factors influencing the relationship between devices are AC thickness, AC modulus, and subgrade modulus.

In both figure 18 and 19 the data fall into three distinct groups depending on the $M_R$ used to generate the deflections—10,000, 20,000, or 30,000 psi. The lowest deflections are produced by the highest $M_R$ and vice versa.

Overall, these results agree with the limited examples shown in the previous chapter regarding the inherent loading differences between the two devices. The RWD moving wheel load produces higher deflections relative to the FWD for thick AC pavements due to the greater response (higher deflection) of the viscoelastic AC layer subjected to the RWD's slower loading rate. However, this is offset by a significant decrease in RWD maximum deflection due to its dual-tire, distributed load. On thinner, weaker pavements, the FWD's single plate loading produces larger maximum deflections than the RWD.

Pavement deflections at 36 inches from the load center are similar for both devices, with the primary pavement factor being the subgrade modulus. This reinforces the common practice of using an outer deflection sensor, many times the 36-inch FWD sensor, for estimating the subgrade modulus. Deflections at 60 inches are also primarily influenced by subgrade modulus, and the trend shows RWD deflections slightly lower than those of the FWD.

## CALCULATED PARAMETERS

### Basin Shape Factors

Previous research has shown that basin shape parameters are more reliable predictors of pavement strains than maximum deflection alone; therefore, the research team evaluated several parameters that have shown good potential for network-level application.[5,17] Based on an initial screening of multiple methods, and variations within a method, the following three parameters were identified for further evaluation:

- SCI based on deflections at 0- and 12-inch offsets from the load center.
- RoC based on deflections at 0- and 8-inch offsets from the load center.
- AUPP based on deflections at 0-, 12-, 24-, and 36-inch offsets from the load center.

Curvature index is a generic term to describe the deflection difference between two points on a basin. SCI is a specific case of a curvature index when the deflection difference is between the maximum deflection ($D_0$) and the deflection at 12 inches from the load center ($D_{12}$), as shown in figure 20:

$$SCI = d_0 - d_{12}$$

**Figure 20. Equation. SCI.**

RoC is another means of characterizing the curvature of the pavement surface and has an inverse relationship with SCI. In other words, as SCI increases, RoC decreases. According to Horak, the L value was originally 5 inches for the curvature meter, but it is 7.9 inches for an FWD.[5] Therefore; in this study the deflection at 8 inches from the load center has been used, along with $D_0$. RoC is calculated using the equation in figure 21:

$$RoC = \frac{L^2}{2d_0\left(1 - \frac{d_8}{d_0}\right)}$$

**Figure 21. Equation. RoC.**

AUPP has also been used for characterizing the curvature of the pavement surface and the stiffness of the AC layer, as it isolates the stiffness of the AC layer from the subgrade.[22] It is calculated based on $D_0$, $D_{12}$, $D_{24}$, and $D_{36}$, as shown in figure 22:

$$AUPP = \frac{5d_0 - 2d_{12} - 2d_{24} - d_{36}}{2}$$

**Figure 22. Equation. AUPP.**

Figure 23 to 25 show the calculated SCI, RoC, and AUPP indices for the FWD and RWD, based on the ViscoWave-generated deflections.

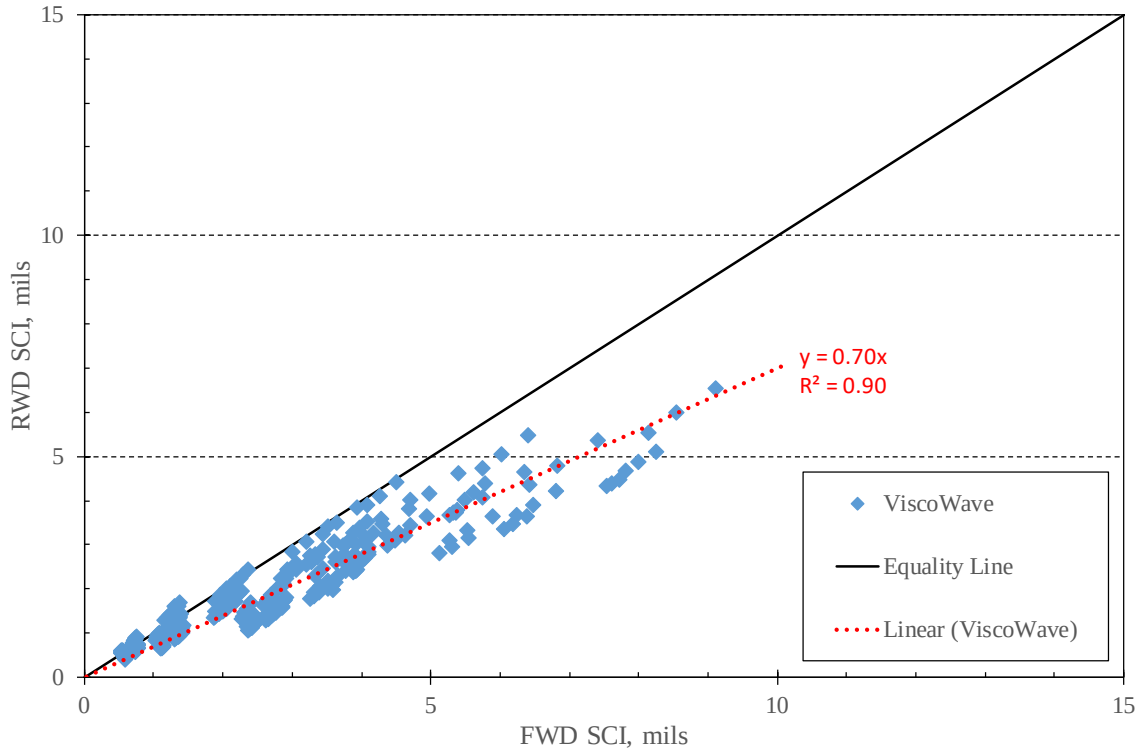


Source: FHWA

**Figure 23. Graph. FWD vs. RWD comparison—SCI.**

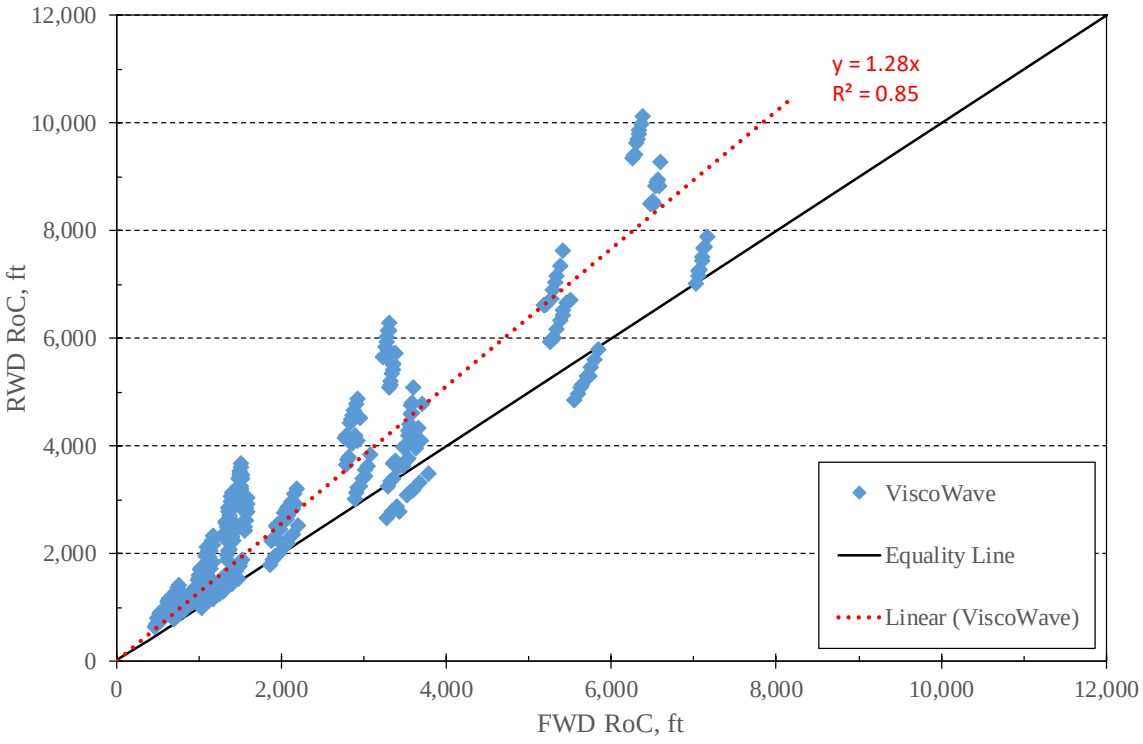


Source: FHWA

**Figure 24. Graph. FWD vs. RWD comparison—RoC.**

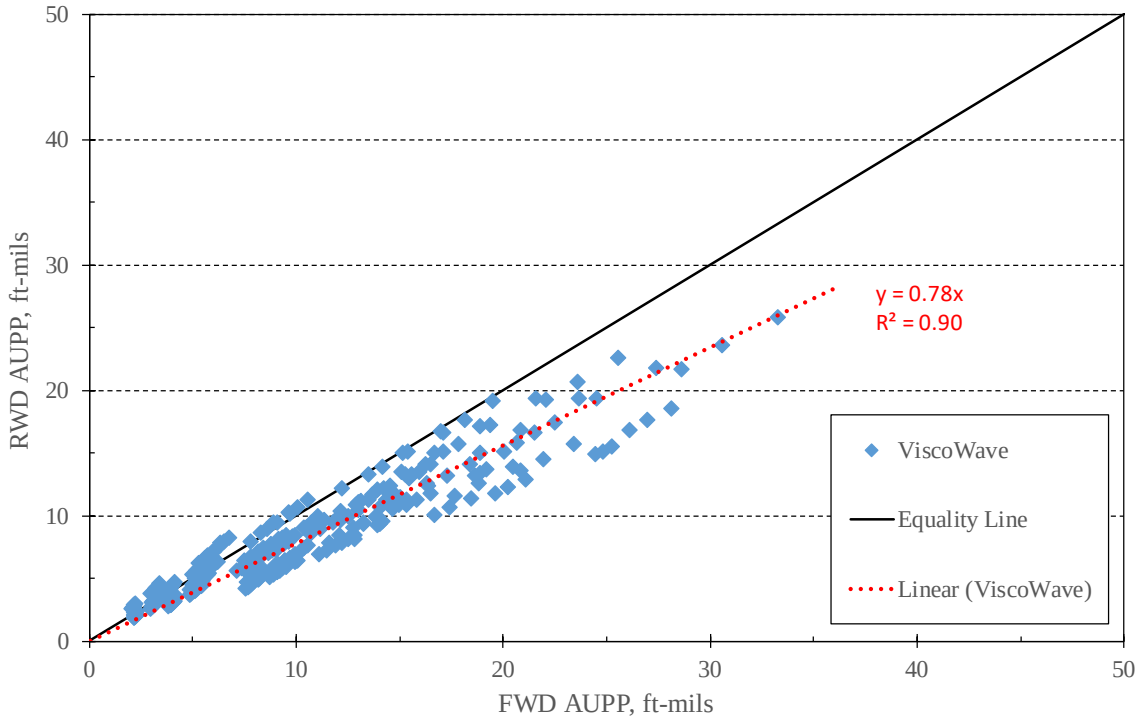


Source: FHWA

**Figure 25. Graph. FWD vs. RWD comparison—AUPP.**

The results show that basin shape factors between the RWD and FWD have good correlations, but not a 1:1 ratio. This is expected, as the two devices produce different deflection basins. The SCI and AUPP comparisons show that the FWD values increase at a faster rate than those of the RWD, while the RoC results show the opposite trend. The SCI and AUPP parameters produced better correlation coefficients between the RWD and FWD data than did RoC.

### AASHTO Flexible Pavement Backcalculation Equations

The 1993 AASHTO pavement design guide introduced a two-layer solution for backcalculation of flexible pavements. Although two layers is a simplification of most in-service pavements today, agencies continue to use this method because of its simplicity and integration in the accompanying overlay design procedure. The outputs of this method are the subgrade resilient ($M_R$), the effective pavement modulus ($E_p$), and the effective structural number ($SN_{eff}$).

The first step in the backcalculation procedure is the determination of the subgrade modulus, based on an outer sensor deflection sufficiently far from the load that it reflects deflection in the subgrade only, and not the influence of the overlying pavement layers. The equation for determing the subgrade modulus is shown in figure 26.

$$M_R = \frac{0.24P}{d_r \cdot r}$$

**Figure 26. Equation. $M_R$.**

where,

$M_R$ = Subgrade resilient modulus, psi
$P$ = Applied load, lbf
$r$ = Distance from load center, inches
$d_r$ = Deflection (in mils) at a distance $r$ (in inches) from the load center

The next step is determination of the effective pavement modulus, which represents the composite modulus of all layers above the subgrade. The equation is solved in an iterative manner by assuming different $E_p/M_R$ ratios until a match is achieved between the calculated $D_0$ and the FWD-measured $D_0$. The resultant ratio is multiplied by the previously determined $M_R$ to calculate $E_p$. The equation to calculate $d_0$, and therefore $E_p$, is shown in figure 27.

$$d_0 = 1.5pa\left\{\frac{1}{M_R\sqrt{1+\left(\frac{D}{a}\sqrt[3]{\frac{E_p}{M_R}}\right)^2}}+\frac{\left[1-\frac{1}{\sqrt{1+\left(\frac{D}{a}\right)^2}}\right]}{E_p}\right\}$$

**Figure 27. Equation. $d_0$.**

where,

$E_p$ = Effective modulus, psi
$d_0$ = Deflection (in inches) measured at the load center adjusted to 68 °F
$p$ = Applied pressure, psi.
$a$ = Radius of the load plate, inches
$D$ = Total thickness (in inches) of all pavement layers above the subgrade

The final step is calculation of the pavement's effective structural number based on the total pavement thickness and effective pavement modulus. Structural number is the method used in the design guide to characterize the load carrying capacity of the pavement layers. Figure 28 shows the equation.

$$SN_{eff} = 0.0045 \cdot D \cdot \sqrt[3]{E_p}$$

**Figure 28. Equation. $SN_{eff}$.**

Figures 29 to 31 display the $M_R$, $E_p$, and $SN_{eff}$ backcalculation results for the RWD and FWD data from the ViscoWave runs. The $M_R$ results show that the RWD deflections produce slightly higher $M_R$ values than the corresponding FWD deflections, and that the backcalculated $M_R$ values from the FWD were more variable than those from the RWD data. The data fall into three distinct groups depending on the $M_R$ used to generate the deflections—10,000, 20,000, or 30,000 psi. The lowest deflections are produced by the highest $M_R$ and vice versa.

The RWD to FWD relationship for backcalculated $E_p$ shows a linear, almost 1:1 trend, but with systematic shifts higher and lower than the equality line, depending on the input subgrade modulus. The highest $M_R$—30,000 psi—produced backcalculated $E_p$ values below the equality line, while the lowest $M_R$—10,000 psi—produced backcalculated $E_p$ values above the equality line.

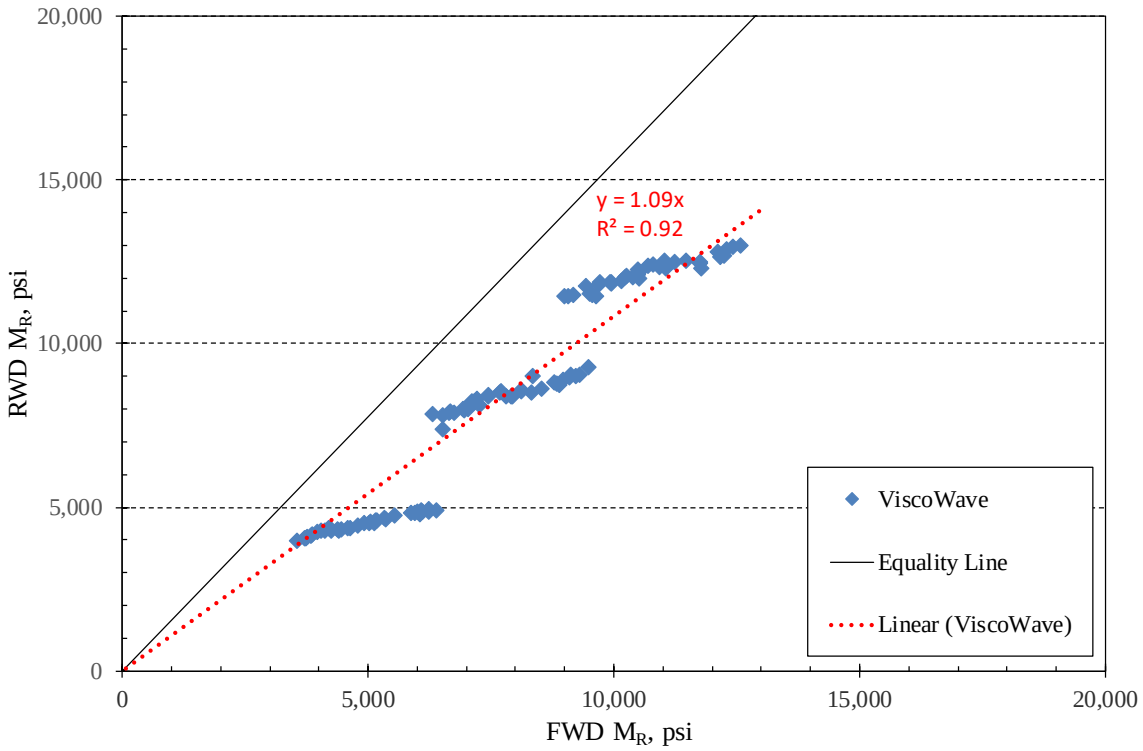


Source: FHWA

**Figure 29. Graph. FWD vs. RWD comparison—$M_R$.**

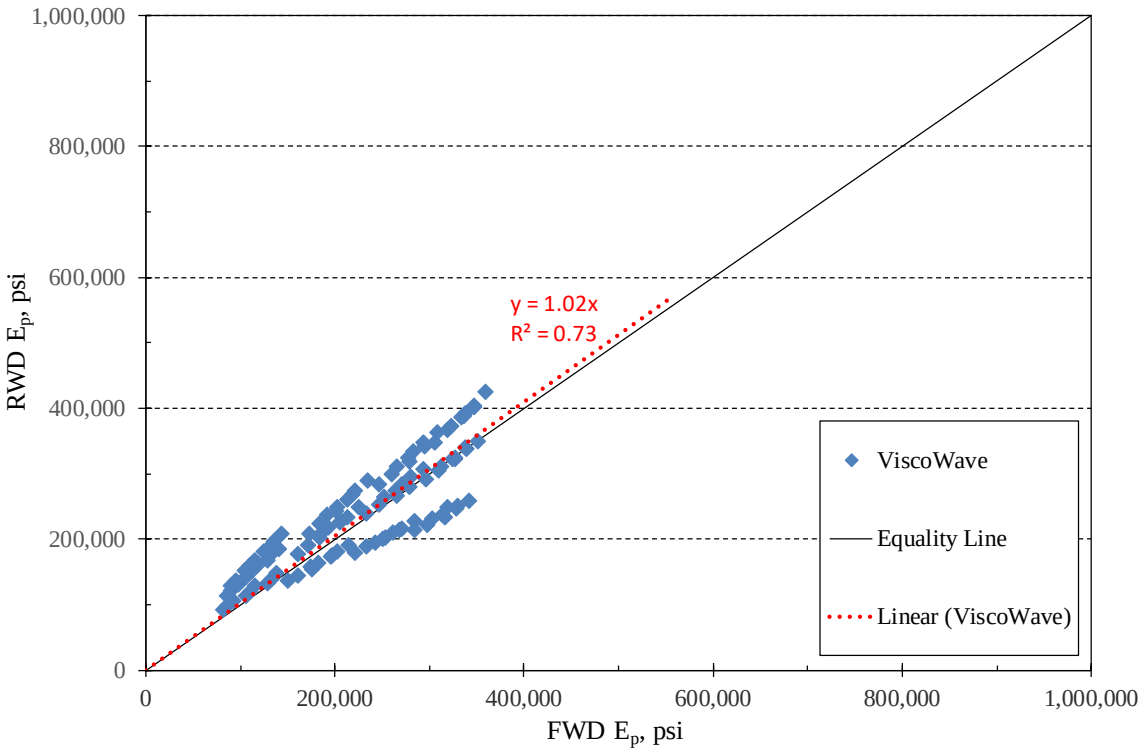


Source: FHWA

**Figure 30. Graph. FWD vs. RWD comparison—$E_p$.**

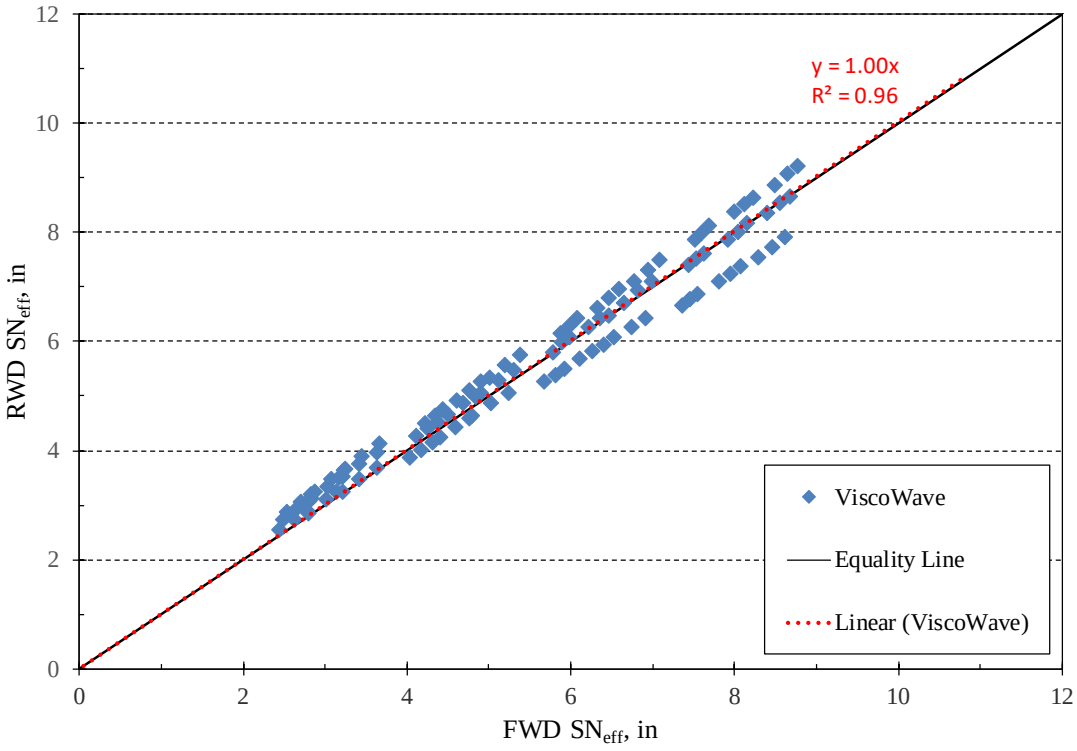


Source: FHWA

**Figure 31. Graph. FWD vs. RWD comparison $SN_{eff}$.**

The RWD to FWD correlation for $SN_{eff}$ is very good and the relationship is 1:1. This is consistent with the $E_p$ trend and also shows the effect of thickness on $SN_{eff}$, which is more influential than $E_p$.

## STRAIN CORRELATIONS

Horizontal strain at the bottom of the AC layer directly affects pavement structural life. Therefore, being able to efficiently and accurately predict critical AC strains from pavement deflections is a significant benefit for network-level analysis. Prior research has shown that basin shape parameters can be effective predictors of AC strain; however, these correlations were developed using pavement response programs that model static loads, not dynamic. A goal of this research was to develop strain prediction equations based on modeling dynamic loads, as well as the AC layer's viscoelastic properties. We have done this for both FWD and RWD loads, based on the ViscoWave determined surface deflections and horizontal strain at the bottom of the AC.

Figure 32 illustrates the relationship of critical AC strains with respect to the deflection basin for an RWD load, based on the ViscoWave runs. The data show that the critical AC strain occurs approximately at the point of greatest deflection and drops off quickly with distance from the load center. In fact, at distances greater than approximately 12 inches forward of the RWD tires, the bottom of the AC layer is not in tension.

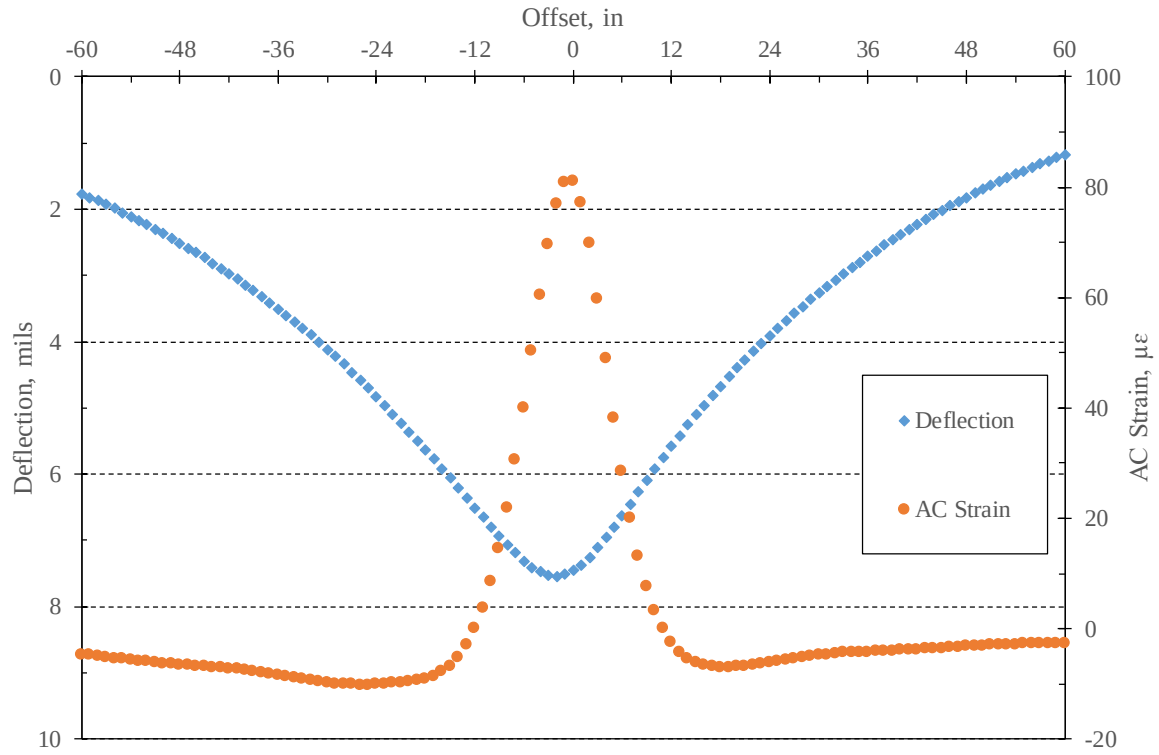


Source: FHWA

**Figure 32. Graph. Example AC strain distribution due to RWD loading.**

Furthermore, the AC strains due to FWD and RWD loadings are different, following a similar trend as those of maximum deflection, shown earlier, as shown in figure 33. AC strains due to the RWD are approximately 23 percent lower than those due to FWD loads, due mainly to the decrease in deflection from the dual tires distributing the load, especially on thinner or weaker pavements with higher deflections.

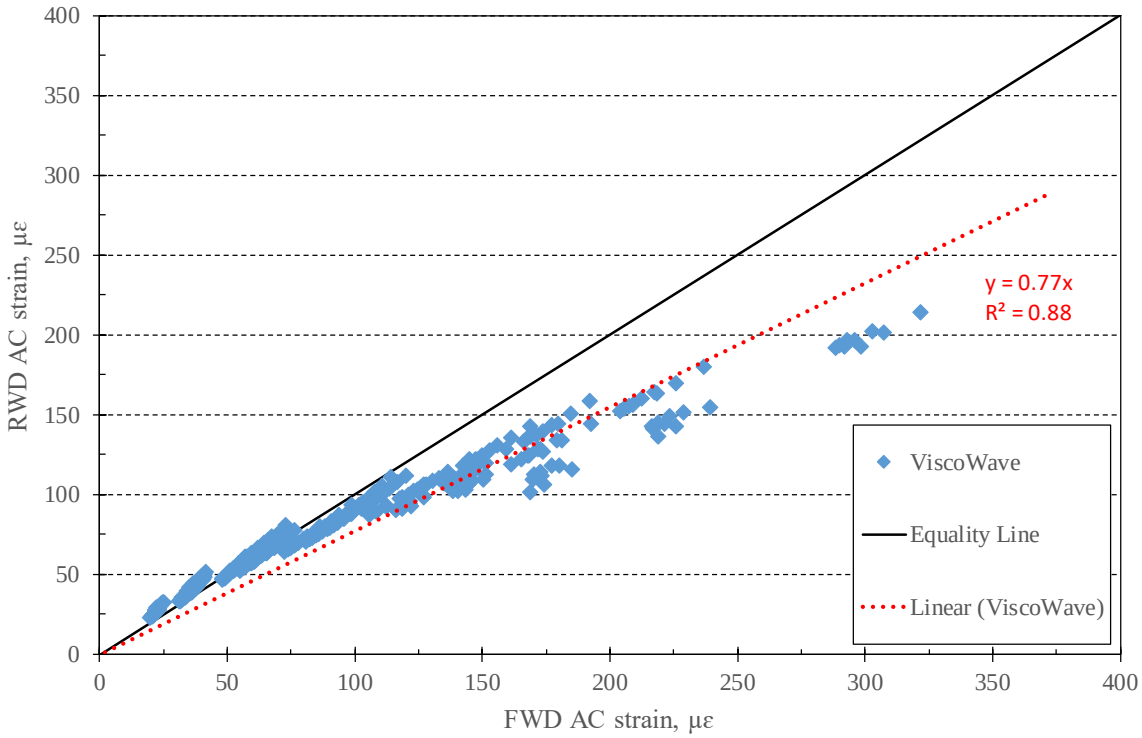


Source: FHWA

**Figure 33. Graph. FWD vs. RWD AC strain comparison.**

Figures 34 to 36 display the strain correlations to SCI, RoC, and AUPP for the FWD loading scenario, while figure 37 to 39 present the corresponding correlations for the RWD. In all cases, the basin shape factors correlated well to AC strain, making them all potential candidates for use in network-level analysis.

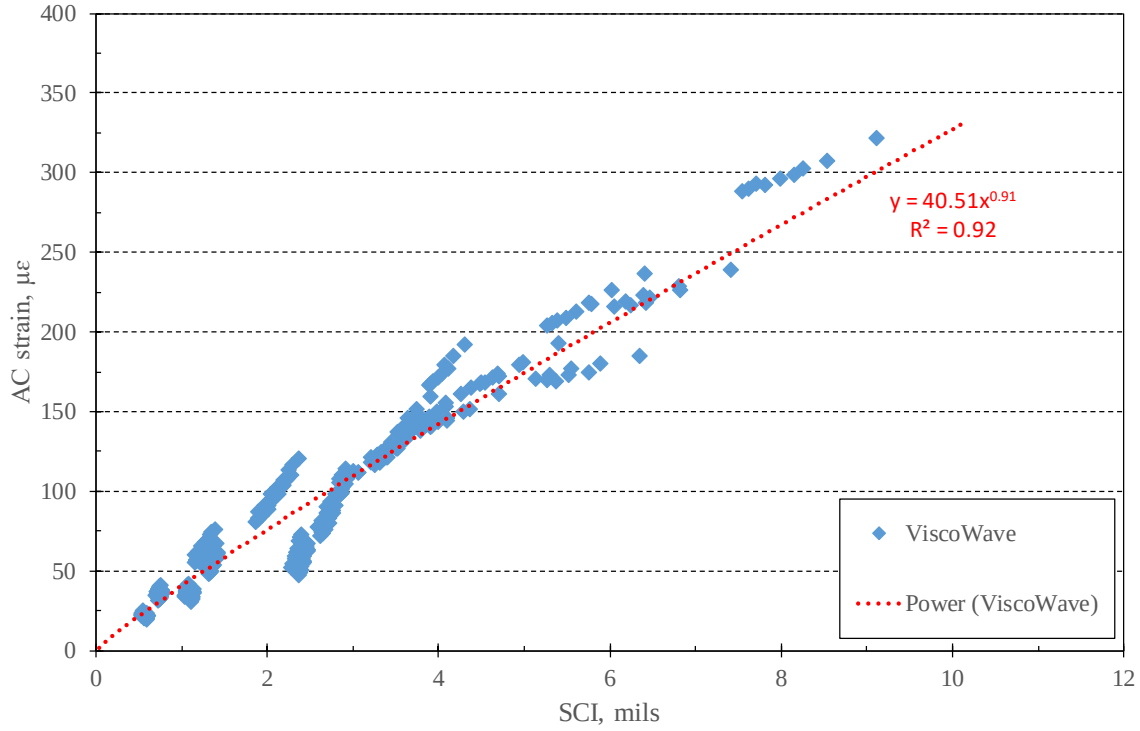


Source: FHWA

**Figure 34. Graph. SCI vs. AC strain—FWD.**

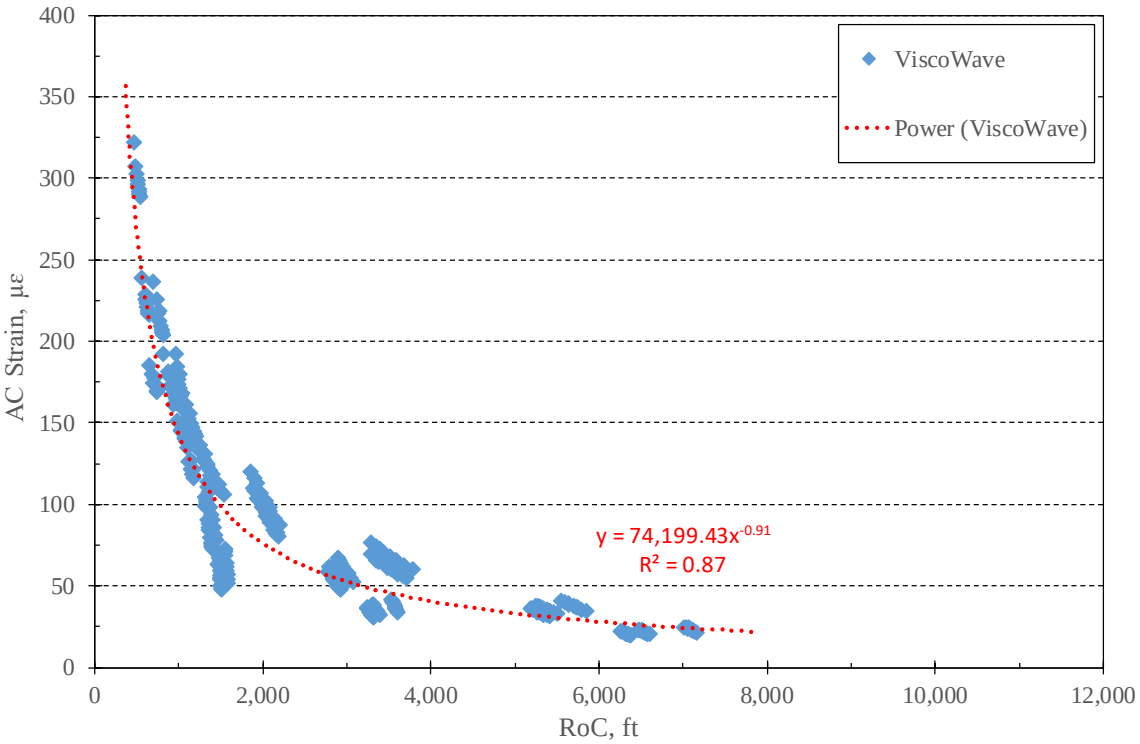


Source: FHWA

**Figure 35. Graph. RoC vs. AC strain—FWD.**

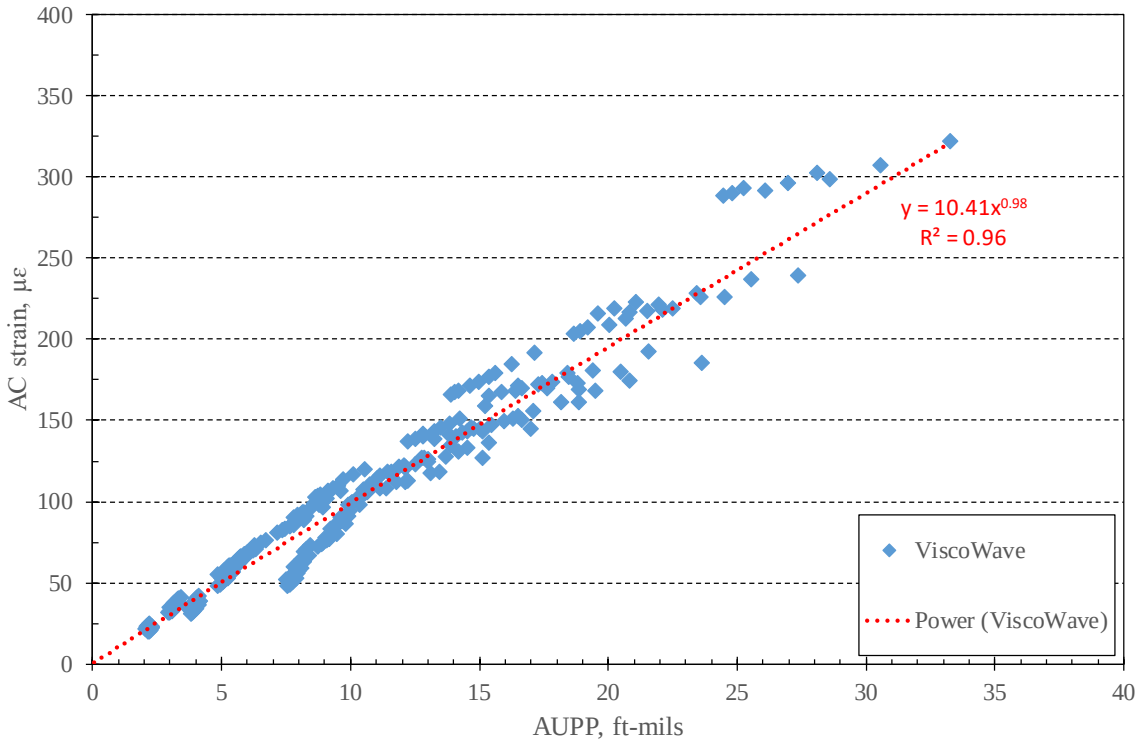


Source: FHWA

**Figure 36. Graph. AUPP vs. AC strain—FWD.**

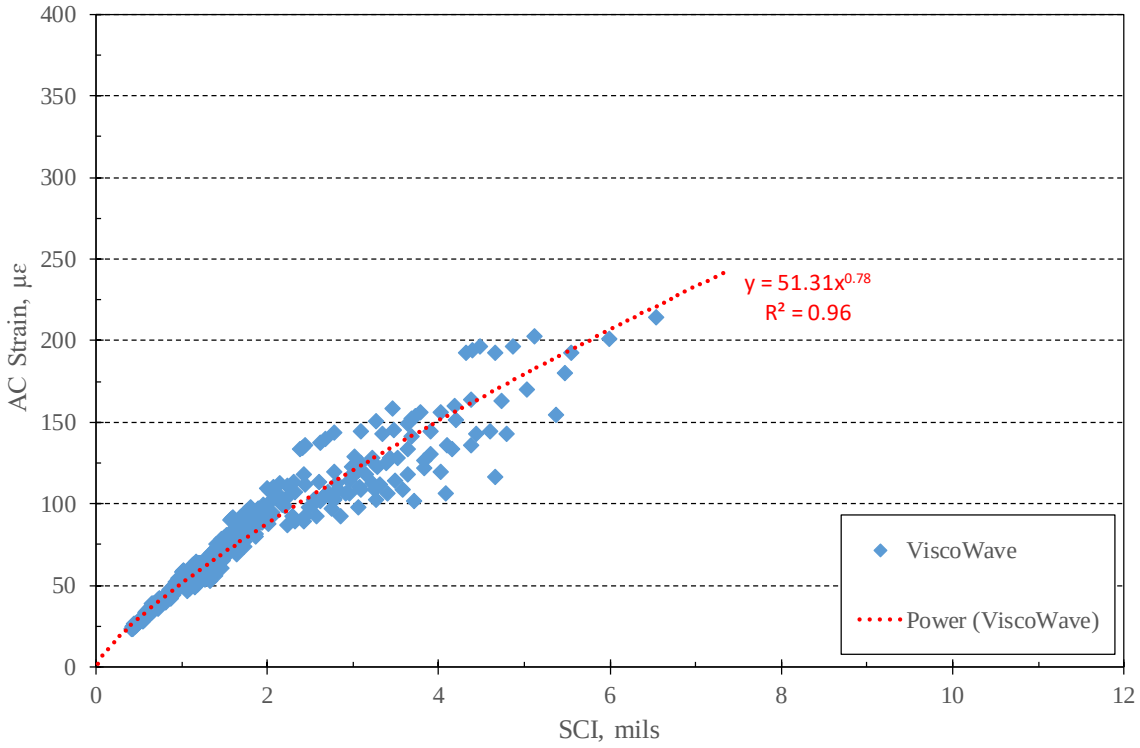


Source: FHWA

**Figure 37. Graph. SCI vs. AC strain—RWD.**

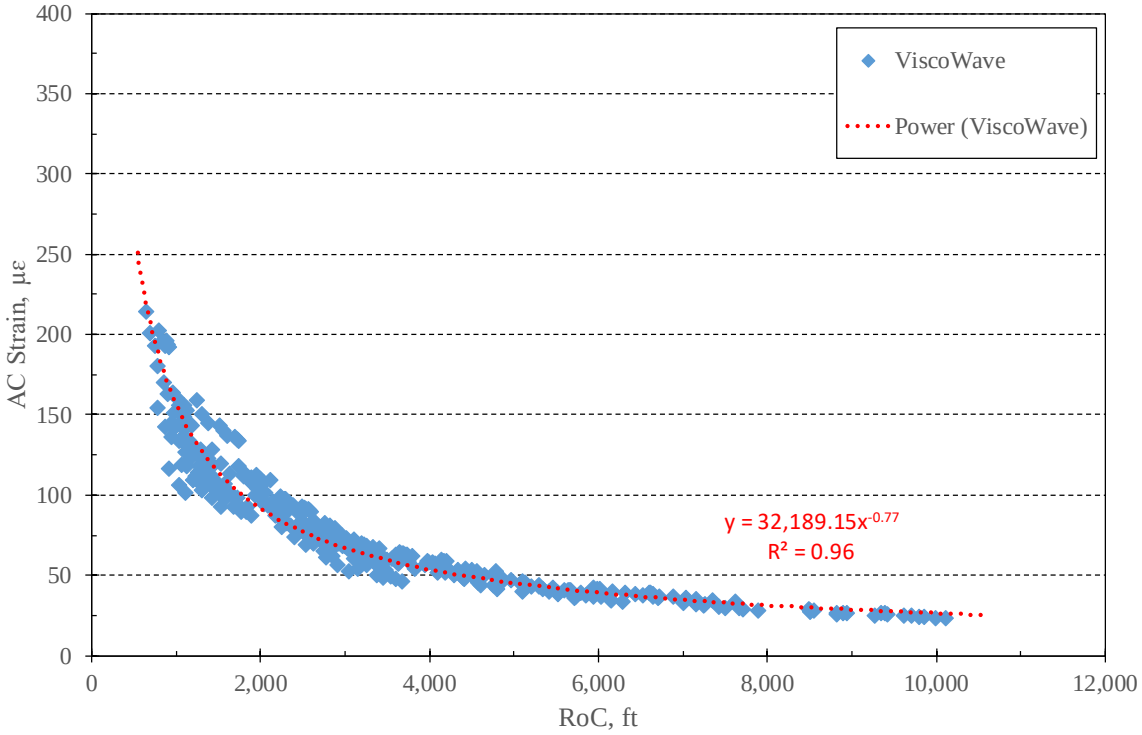


Source: FHWA

**Figure 38. Graph. RoC vs. AC strain—RWD.**

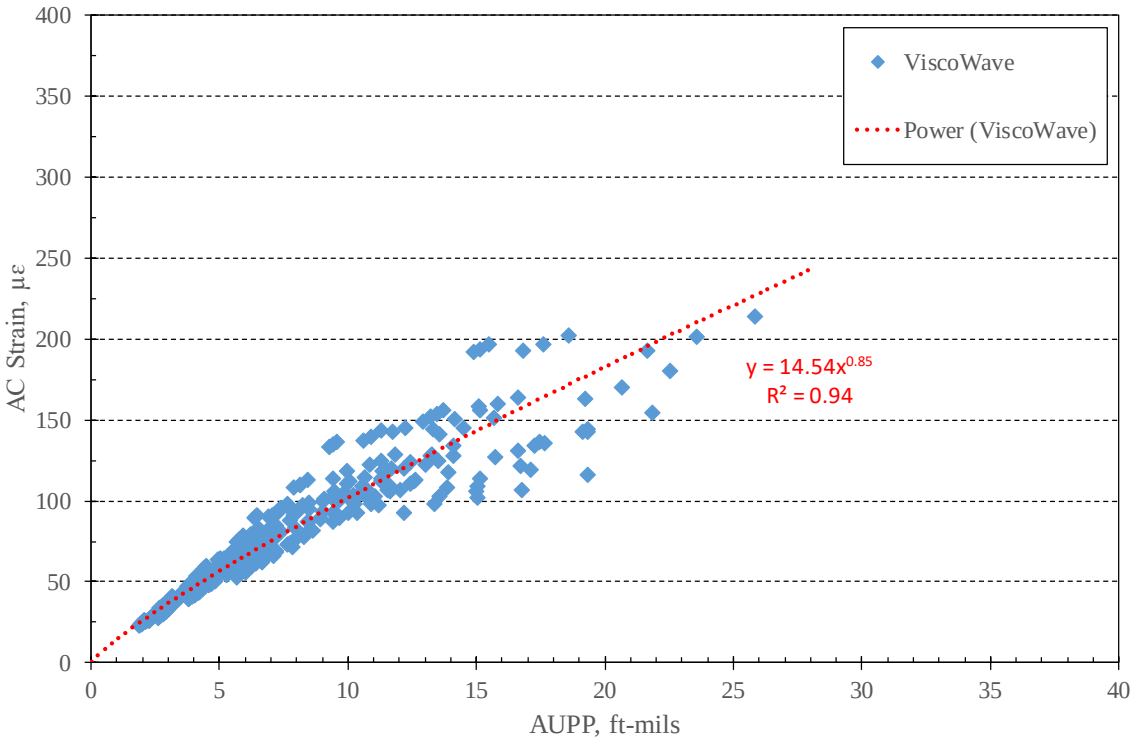


Source: FHWA

**Figure 39. Graph. AUPP vs. AC strain—RWD.**

The strain correlations are best represented by power curves with the general form of the equation shown in figure 40.

$$y = a \cdot x^b$$

**Figure 40. Equation. General form of the power regression.**

where,

*a*, *b* = regression coefficients
*y* = Dependent variable (i.e., AC strain)
*x* = Independent variable (i.e., SCI, RoC, or AUPP)

The research team developed power regression curves in Microsoft® Excel, and Table 1 summarizes the regression coefficients and $R^2$ values for SCI, RoC, and AUPP vs. AC critical strain for both the RWD and FWD. The $R^2$ values showed good correlations for both the RWD and FWD in the cases of SCI and AUPP. The correlation was slightly lower for RoC.

**Table 1. Summary of AC strain power equation coefficients.**

| Device | Input Parameter | a | b | $R^2$ |
|---|---|---|---|---|
| RWD | SCI | 40.51 | 0.91 | 0.92 |
| | RoC | 74,199.43 | -0.91 | 0.87 |
| | AUPP | 10.41 | 0.98 | 0.96 |
| FWD | SCI | 51.31 | 0.78 | 0.96 |
| | RoC | 32,189.15 | -0.77 | 0.96 |
| | AUPP | 14.54 | 0.85 | 0.94 |

# CHAPTER 5. FIELD DATA COLLECTION AND ANALYSIS

## PURPOSE

The research team performed a large-scale field study on 23 test sites in Mississippi to compare FWD and RWD deflection basins and to validate the theoretically predicted RWD to FWD relationships developed using ViscoWave. The testing program took place in May 2019 over 500-ft test sections and included RWD, FWD, accelerometer, and pavement condition data collection. The test sections are all Mississippi DOT established calibration sites for the Mechanistic-Empirical Pavement Design Guide (MEPDG).

## TEST SITES AND CHARACTERISTICS

The research team reviewed a list of 65 potential test sites provided by the Mississippi DOT, consisting of new, rehabilitated, and recently overlaid AC pavements representing a wide range of functional classifications, layer types and thicknesses, traffic, and pavement conditions. The list was narrowed to include sites with a representative range of AC thicknesses, base types and thicknesses, and subgrade types. Table 2 summarizes general information about the test sites.

**Table 2. Test site locations and general characteristics.**

| Section Identifier | Route Name | County | Pavement Category | Condition Rating |
|---|---|---|---|---|
| 1703 | US 45 | Lee | Overlay | Very Good |
| 1797 | US 45A | Clay | Overlay | Good |
| 1799 | US 45A | Clay | Overlay | Good |
| 2202 | US 51 | Montgomery | New | Poor |
| 2824 | US 78 | Desoto | Overlay | Fair |
| 2830 | I-22 | Itawamba | Overlay | Good |
| 2833 | I-22 | Itawamba | Overlay | Good |
| 2851 | I-22 | Lee | Overlay | Fair |
| 4580 | SR 16 | Neshoba | New | Good |
| 4588 | SR 302 | Desoto | New | Very Good |
| 4742 | SR 302 | Desoto | Rehabilitated | Poor |
| 4784 | US 45 | Clarke | New | Very Good |
| 4834 | US 72 | Benton | New | Very Good |
| 4889 | SR 302 | Marshall | Rehabilitated | Good |
| 4894 | SR 302 | Marshall | Rehabilitated | Good |
| 4933 | SR 16 | Neshoba | New | Good |
| 5105 | SR 12 | Oktibbeha | New | Very Good |
| 5210 | SR 19 | Winston | New | Poor |
| 5230 | SR 15 | Winston | New | Poor |
| 5506 | US 45 | Monroe | New | Poor |
| 5511 | US 45 | Monroe | Rehabilitated | Very Poor |
| 5616 | SR 302 | Marshall | New | Fair |
| 6015 | SR 8 | Grenada | New | Good |

The condition rating in Table 2 was determined by the field crew at the time of data collection.

Figure 41 shows the locations of the 23 test sites with the Mississippi DOT section names. All sites were located on either State routes, U.S. routes, or interstates, and all were four-lane roads.

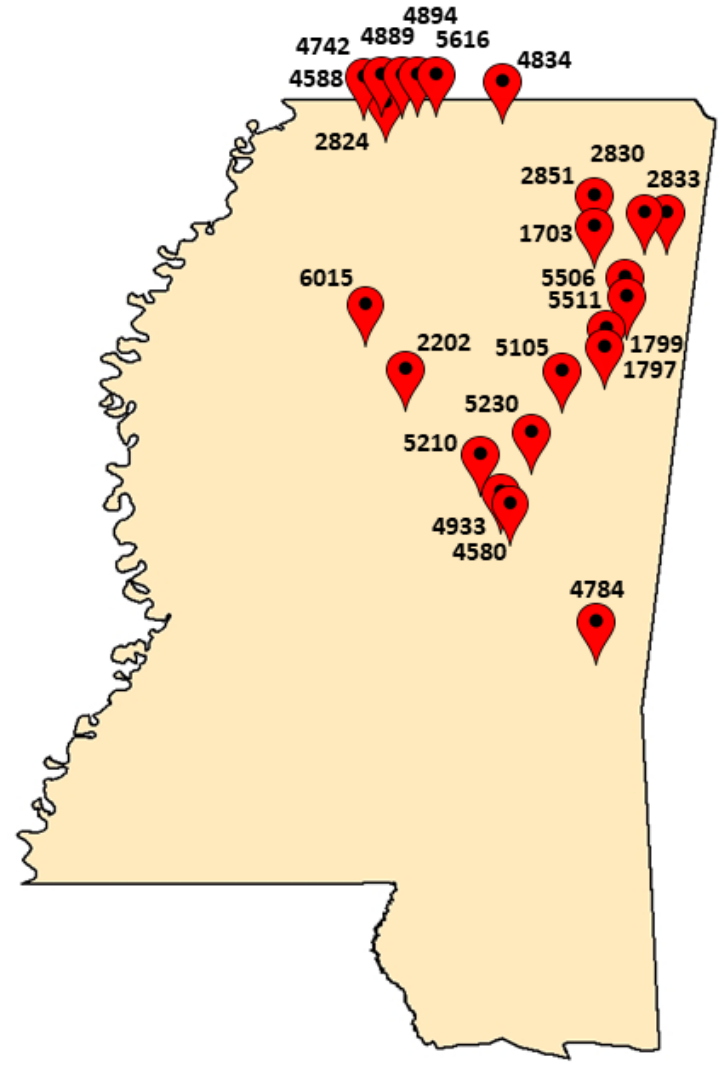




**Figure 41. Map. Mississippi test sites.**

Table 3 summarizes the layer type and thickness characteristics for the test sites. The total AC thicknesses (i.e., the sum of all surface, binder, and aphalt-treated base layers) ranged from 5.8 to 16.8 inches with a mean of 10.7 inches. Eighteen of the sites contained an asphalt-treated base (ATB). Base layer thicknesses ranged from 2.7 to 13 inches with a mean of 6.6 inches and were typically treated with lime, lime-fly ash, or cement. Five sites were built with unbound granular layers, and 12 sites contained either a treated or untreated subbase. In general, all test roads are medium to thick AC pavements capable of carrying heavy wheel loads.

Table 4 provides definitions of the pavement codes and other abbreviations used in Table 3.

**Table 3. Pavement layer types and thicknesses.**

| Section Identifier | AC | | | Base | | Subbase | |
|---|---|---|---|---|---|---|---|
| | SC+BC, inches | ATB, inches | Total, inches | Thickness, inches | Type | Thickness, inches | Type |
| 1703 | 8.7 | 4.5 | 13.2 | 10.0 | LTM | None | None |
| 1797 | 1.9 | 11.0 | 12.9 | None | None | None | None |
| 1799 | 4.8 | 11.0 | 15.8 | None | None | None | None |
| 2202 | 7.0 | 9.5 | 16.5 | 13.0 | GB | None | None |
| 2824 | 7.9 | 8.5 | 16.4 | 5.3 | LTM | None | None |
| 2830 | 7.4 | 6.5 | 13.9 | 9.0 | LTM | None | None |
| 2833 | 8.1 | 4.5 | 12.6 | 5.3 | CTM | None | None |
| 2851 | 12.3 | 4.5 | 16.8 | 6.8 | CTM | None | None |
| 4580 | 10.3 | None | 10.3 | 4.0 | CSDC | 6.5 | LFA |
| 4588 | 8.9 | None | 8.9 | 7.4 | LFA | 5.7 | CSM |
| 4742 | 7.3 | None | 7.3 | 6.5 | TGM | 9.1 | CSM |
| 4784 | 3.6 | 2.3 | 5.8 | 7.7 | LFA | None | None |
| 4834 | 3.5 | 4.6 | 8.1 | 6.2 | LFA | 9.3 | CSM |
| 4889 | 3.0 | 3.8 | 6.8 | 6.3 | LFA | None | None |
| 4894 | 7.3 | None | 7.3 | 8.2 | CSM | 5.3 | CSM |
| 4933 | 9.8 | None | 9.8 | 4.0 | CSDC | 10.8 | LFA |
| 5105 | 6.4 | 3.0 | 9.4 | 6.0 | CLS | 6.0 | CSA |
| 5210 | 4.0 | 5.0 | 9.0 | 5.6 | TM | 7.1 | TM |
| 5230 | 2.0 | 8.4 | 10.4 | 6.6 | LFA | 4.5 | CSM |
| 5506 | 6.8 | 3.0 | 9.8 | 5.5 | LA | 1.8 | SBC |
| 5511 | 4.3 | 3.0 | 7.3 | 7.2 | LFA | 2.0 | GB |
| 5616 | 9.2 | None | 9.2 | 2.7 | CLS | 6.8 | LFA |
| 6015 | 8.3 | None | 8.3 | 6.2 | GB | None | None |

**Table 4. Material Codes.**

| Category | Code | Mateial |
|---|---|---|
| Asphalt Material | AC | Asphalt Concrete |
| | SC | Surface Course |
| | BC | Binder Course |
| | ATB | Asphalt-Treated Base |
| Unbound base or subbase | CLS | Crushed Limestone |
| | CSA | Concrete Sand |
| | CSDC | Crushed Stone Drainage Course |
| | CSM | Crushed Stone Material |
| | GB | Granular Base |
| Treated base or subbase | CTM | Cement Treated Material |
| | LA | Lime Ash |
| | LFA | Lime-Fly Ash |
| | LTM | Lime-Treated Material |
| | SBC | Stabilized Base Course |
| | TGM | Treated Granular Mat |
| | TM | Treated Material |

## TESTING PROGRAM

Field testing took place from May 13 to May 22, 2019, as summarized in Table 5. Mississippi DOT provided lane closures, and all testing was performed in the outer lane in either the northbound or eastbound traffic direction. The research team referenced each 500-ft section beginning with station 0+00 and ending at station 5+00. Weather conditions were sunny and clear for all days, and the average air temperature and estimated AC mid-depth temperature using the BELLS3 method are shown in the table.

At each site, the research team performed the following sequence of activities in the closed lane:

- FWD testing at 25-ft intervals in the right wheel path using a seating drop followed by a single drop each at 9-, 12-, and 16-kip loads. The FWD was configured with a 12-inch-diameter load plate and sensors placed at 0, 8, 12, 18, 24, 36, 48, 60, and -12 inches from the load center. At each test point, the FWD recorded the air and pavement surface temperatures, linear reference, and GPS coordinates, in addition to the load and deflection data. This resulted in 21 test points per site.

- Foot-on-ground pavement condition survey between stations 1+50 and 3+50, using the PCI rating method (simultaneous to FWD testing).

- Accelerometer installation at an FWD test station determined to be representative of the section mean deflection. This included partial-depth coring and cleaning of a 2-inch-diameter hole to allow temporary installation of a wireless accelerometer, verified with an FWD test at the start of each day, and used to validate RWD readings.

- RWD testing at 45 mph over the 500-ft section, plus sufficient lead-in and run-out distances to allow for accelerating and braking at each end within the lane closure. The RWD recorded an image set every 25 ft to correspond to the FWD test spacing, resulting in 21 test points per site.

- Removal of the wireless accelerometer and patching of the partial-depth, 2-inch-diameter corehole using AC cold patch.

- Video recording of the 500-ft section using a camera phone mounted on the front of the FWD vehicle to record the pavement and surrounding right-of-way conditions for future reference.

Figure 42 shows a sample overview of a test site closed for data collection.

**Table 5. Summary of field data collection.**

| Date | Section Identifier | Start Time | Air Temperature at Start, °F | Estimated AC Mid-Depth Temperature, °F |
|---|---|---|---|---|
| 5/13/2019 | 4588 | 8:41 AM | 72.5 | 66.3 |
| | 4742 | 11:23 AM | 87.2 | 81.2 |
| | 4889 | 1:16 PM | 83.0 | 86.6 |
| | 4894 | 3:01 PM | 84.7 | 88.0 |
| 5/14/2019 | 2824 | 8:22 AM | 68.7 | 65.3 |
| | 5616 | 11:50 AM | 81.2 | 82.6 |
| | 4834 | 2:06 PM | 81.1 | 91.5 |
| 5/15/2019 | 2833 | 9:06 AM | 72.1 | 69.6 |
| | 2830 | 11:51 AM | 89.8 | 81.5 |
| | 2851 | 1:48 PM | 93.7 | 84.4 |
| | 1703 | 3:46 PM | 96.2 | 90.9 |
| 5/16/2019 | 5506 | 9:56 AM | 103.1 | 82.7 |
| | 5511 | 12:24 PM | 97.5 | 95.8 |
| | 1799 | 1:58 PM | 99.0 | 93.3 |
| | 1797 | 3:46 PM | 105.3 | 99.7 |
| 5/20/2019 | 5105 | 8:36 AM | 89.3 | 82.8 |
| | 5230 | 12:19 PM | 92.9 | 92.7 |
| | 5210 | 3:03 PM | 96.2 | 101.0 |
| 5/21/2019 | 4933 | 8:55 AM | 79.3 | 82.5 |
| | 4580 | 11:17 AM | 94.1 | 91.6 |
| | 4784 | 2:38 PM | 92.0 | 102.4 |
| | 2202 | 11:45 AM | 89.3 | 91.8 |
| | 6015 | 2:05 PM | 102.1 | 106.4 |

Source: FHWA

**Figure 42. Photo. Example overview of a test site closed for data collection.**

## FWD RESULTS

The research team analyzed the raw FWD data in two ways:

- $D_0$ profiles based on maximum deflections normalized to 9,000 lbf using a linear extrapolation of the raw load and deflection data.
- Average deflection basins based on the 21 test points collected at each site for data normalized to 9,000 lbf.
- Deflection data were not temperature corrected, as the FWD and RWD were tested within several minutes of each other, under similar climatic conditions.

Figure 43 shows sample $D_0$ profiles for three sections representing a range of deflection magnitudes and variability. Figure 44 displays the average deflection basins for the same three sections. Table 6 summarizes the FWD data by section, including the mean $D_0$, coefficient of variation (COV), station selected for accelerometer installation, $D_0$ at the accelerometer station, and the deflection difference between the mean $D_0$ and the accelerometer station $D_0$. The table shows that accelerometer stations were selected that generally produced deflections within +/- 1 mil of the mean, with the exception of two sites (5230 and 6015). Locations at these two sites were intentionally chosen due to their high deflections.

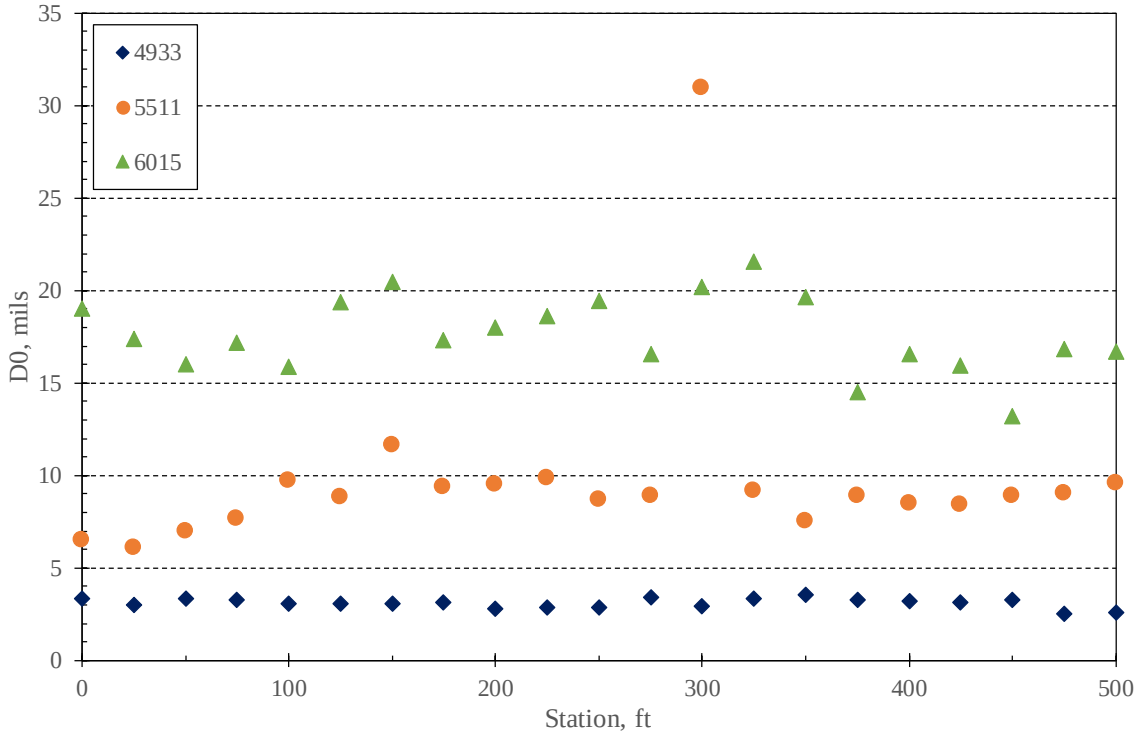


Source: FHWA

**Figure 43. Graph. Example FWD profiles showing deflection magnitude and variability.**

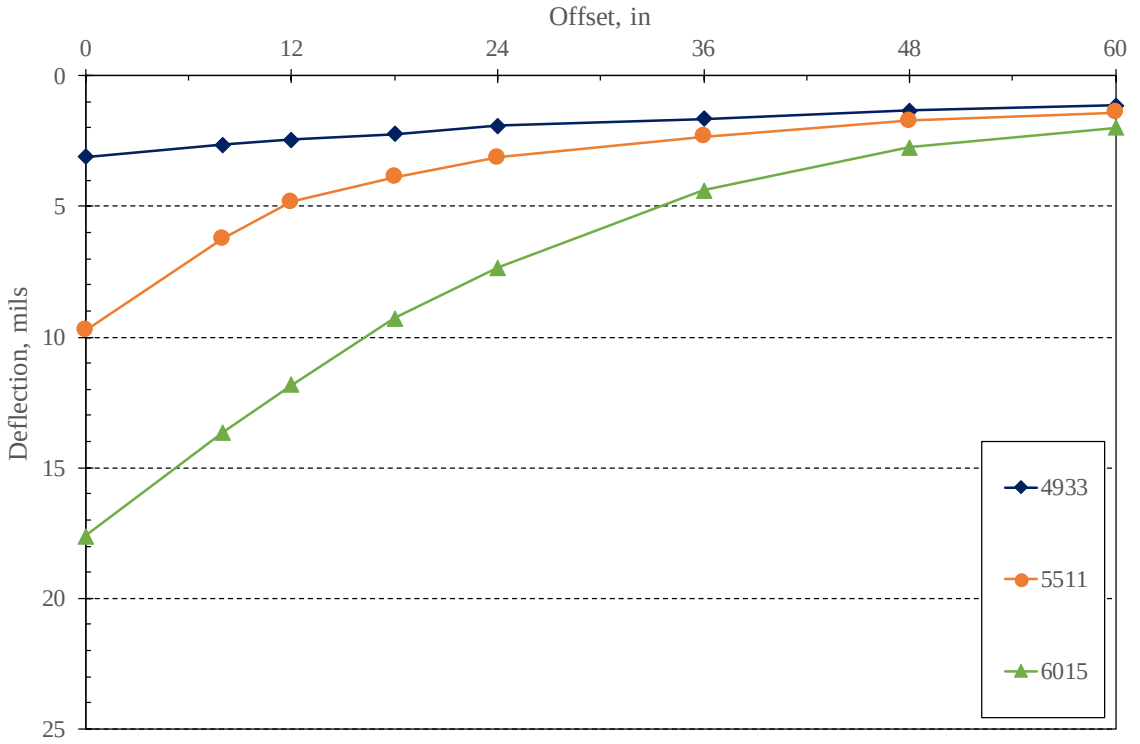


Source: FHWA

**Figure 44. Graph. Example mean FWD basins for three sections.**

**Table 6. Summary of FWD results by section.**

| Section Identifier | $D_0$ | | Accelerometer Location and $D_0$ | | $D_0$ @ Accel - Mean, mils |
|---|---|---|---|---|---|
| | Mean, mils | COV, percent | Station | $D_0$, mils | |
| 1703 | 13.36 | 11.0 | 3+00 | 13.69 | 0.33 |
| 1797 | 13.08 | 8.7 | 2+50 | 13.31 | 0.23 |
| 1799 | 13.10 | 10.6 | 2+75 | 14.04 | 0.93 |
| 2202 | 8.81 | 18.1 | 2+50 | 9.66 | 0.85 |
| 2824 | 3.61 | 26.1 | 3+25 | 3.89 | 0.28 |
| 2830 | 6.03 | 9.7 | 2+50 | 5.90 | -0.13 |
| 2833 | 7.99 | 34.7 | 2+50 | 7.25 | -0.74 |
| 2851 | 5.88 | 18.1 | 2+25 | 5.84 | -0.04 |
| 4580 | 4.11 | 20.7 | 2+25 | 3.77 | -0.34 |
| 4588 | 7.61 | 19.3 | 3+00 | 7.57 | -0.05 |
| 4742 | 10.63 | 36.7 | 2+00 | 9.44 | -1.20 |
| 4784 | 12.34 | 13.4 | 2+75 | 13.06 | 0.72 |
| 4834 | 6.96 | 12.9 | 2+00 | 7.13 | 0.17 |
| 4889 | 7.73 | 28.9 | 2+25 | 8.45 | 0.72 |
| 4894 | 12.55 | 18.7 | 3+00 | 12.26 | -0.29 |
| 4933 | 3.10 | 8.6 | 2+50 | 2.88 | -0.22 |
| 5105 | 10.37 | 6.8 | 2+75 | 10.36 | -0.01 |
| 5210 | 11.85 | 29.5 | 2+25 | 11.35 | -0.50 |
| 5230 | 12.35 | 61.0 | 2+00 | 16.78 | 4.44 |
| 5506 | 6.99 | 17.9 | 3+25 | 7.68 | 0.69 |
| 5511 | 9.73 | 51.5 | 2+50 | 8.68 | -1.05 |
| 5616 | 8.37 | 17.6 | 2+00 | 8.69 | 0.32 |
| 6015 | 17.63 | 11.8 | 3+00 | 20.20 | 2.57 |

## ACCELEROMETER TESTING

The research team temporarily installed a wireless accelerometer at each test section to provide a recording of the entire RWD event (i.e., all three axle sets) and to validate the RWD readings. At each test site FWD data were reviewed to select a test point location where the maximum deflection generally represented the mean for the entire 500-ft section. At this location, a partial-depth 2-inch-diameter corehole was drilled in the right wheel path in which the accelerometer was placed and secured by a rubber stopper recessed approximately 0.25 inches below the pavement surface. The research team recorded and reviewed the accelerometer readings from a laptop computer located on the roadway shoulder during testing. Figure 45 shows the accelerometer used for testing and an example corehole.

Source: FHWA

**Figure 45. Photo. The accelerometer used for pavement instrumentation.**

At the beginning of each day, the research team tested the accelerometer with the FWD with the $D_0$ sensor located directly above the sensor. The FWD performed a single drop each at 9,000-, 12,000-, and 16,000-lbf target loads and an accelerometer trace was obtained for each drop. The raw acceleration signal was double-integrated in Microsoft® Excel to obtain the deflection trace, which was then compared to the FWD deflection time history to verify that the accelerometer system was functioning correctly.

Figure 46 shows an example FWD vs. accelerometer-based deflection time history, showing excellent agreement between the two devices. Figure 47 displays the maximum deflection comparison between FWD and accelerometer-based maximum deflections for all test days. The two devices agreed extremely well, verifying the accelerometer was working and accurate each day.

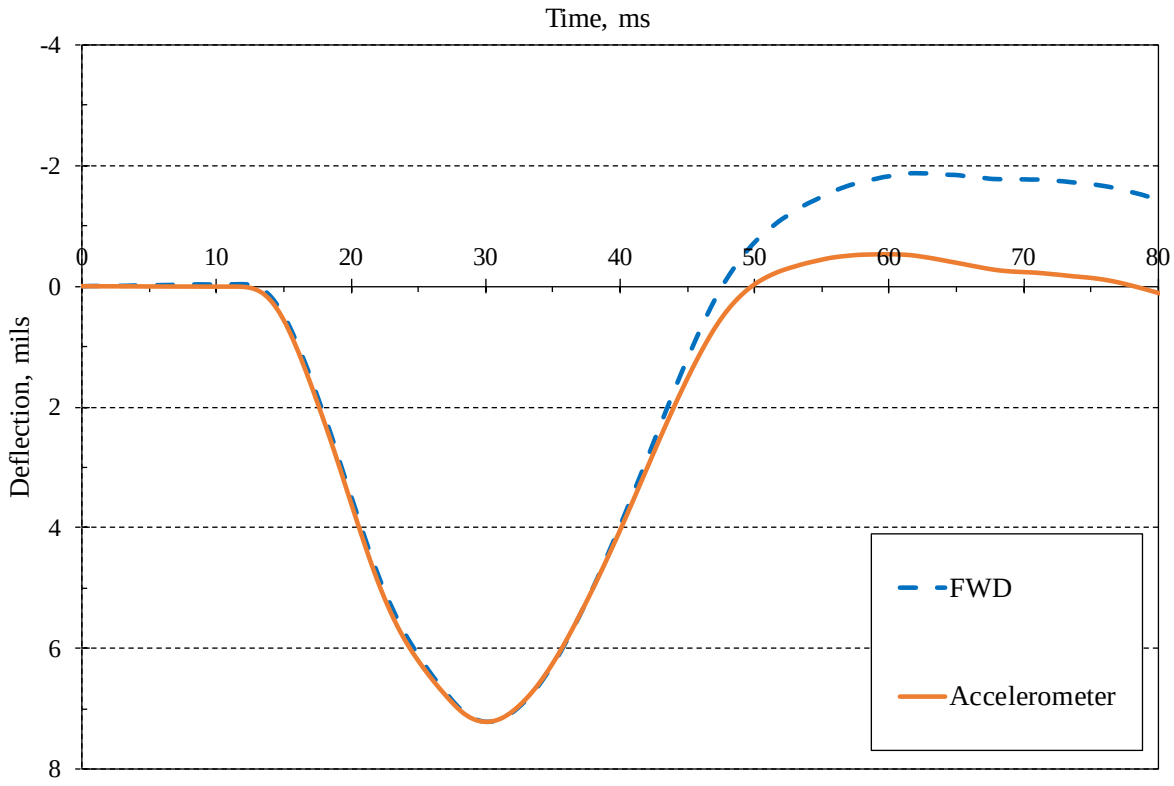


Source: FHWA

**Figure 46. Graph. Accelerometer validation using the FWD $D_0$ sensor—Section 4588.**

Following accelerometer validation, the RWD made a test pass, which was recorded by the accelerometer to capture the entire RWD event. This was done to document the RWD event and to provide reference data for validation. Figure 48 shows an example accelerometer-based deflection profile. The readings were converted to the distance domain and the output clearly shows all three truck-trailer axles—steering, tandem drive, and RWD. For each RWD pass, the area beginning at the maximum deflection between the RWD axle's rubber tires and extending 5 ft forward was extracted. The RWD's deflection basin was then validated against the independent reference. Figure 49 shows an example comparison, confirming that the RWD was functioning and compared well to an independent device.

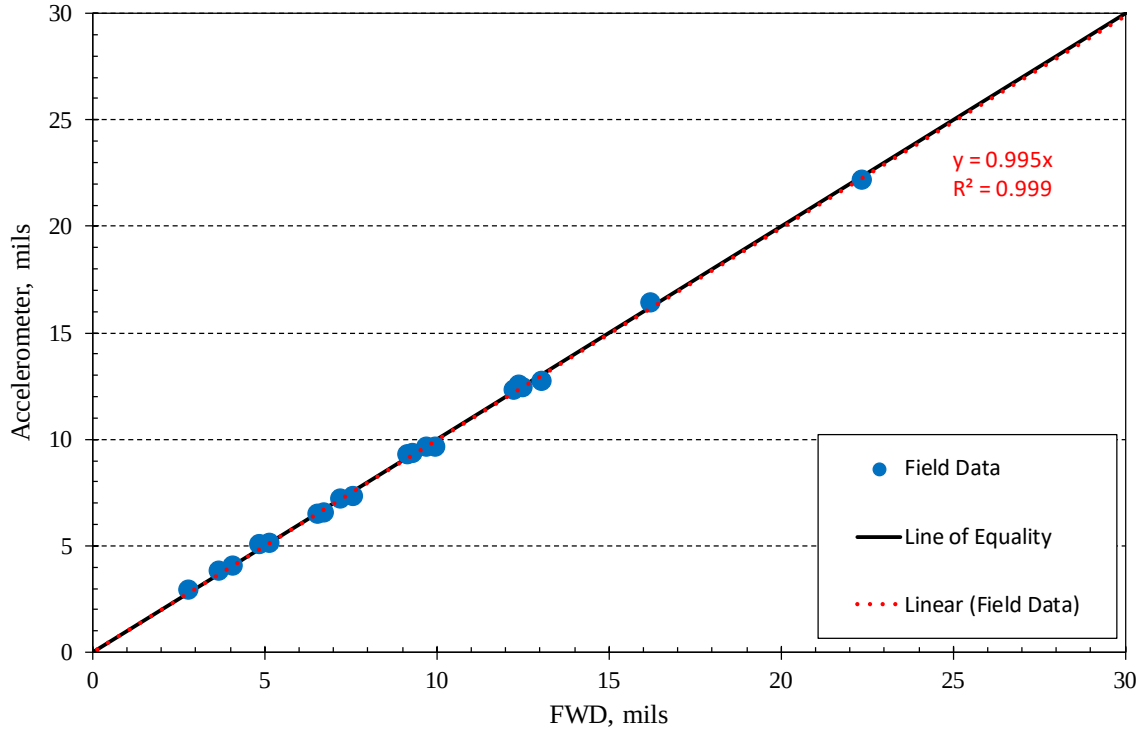


Source: FHWA

**Figure 47. Graph. Accelerometer vs. FWD comparison—7 sections (19 drops).**

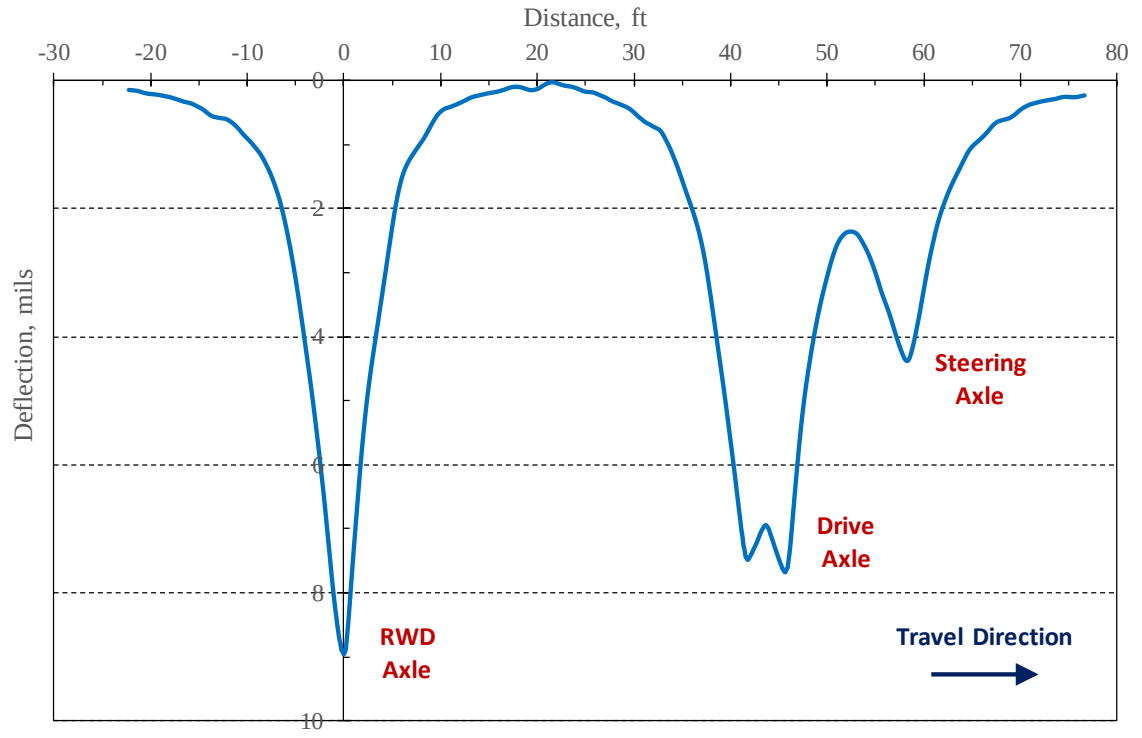


Source: FHWA

**Figure 48. Graph. Accelerometer-based recording of the entire RWD event—Section 4588.**

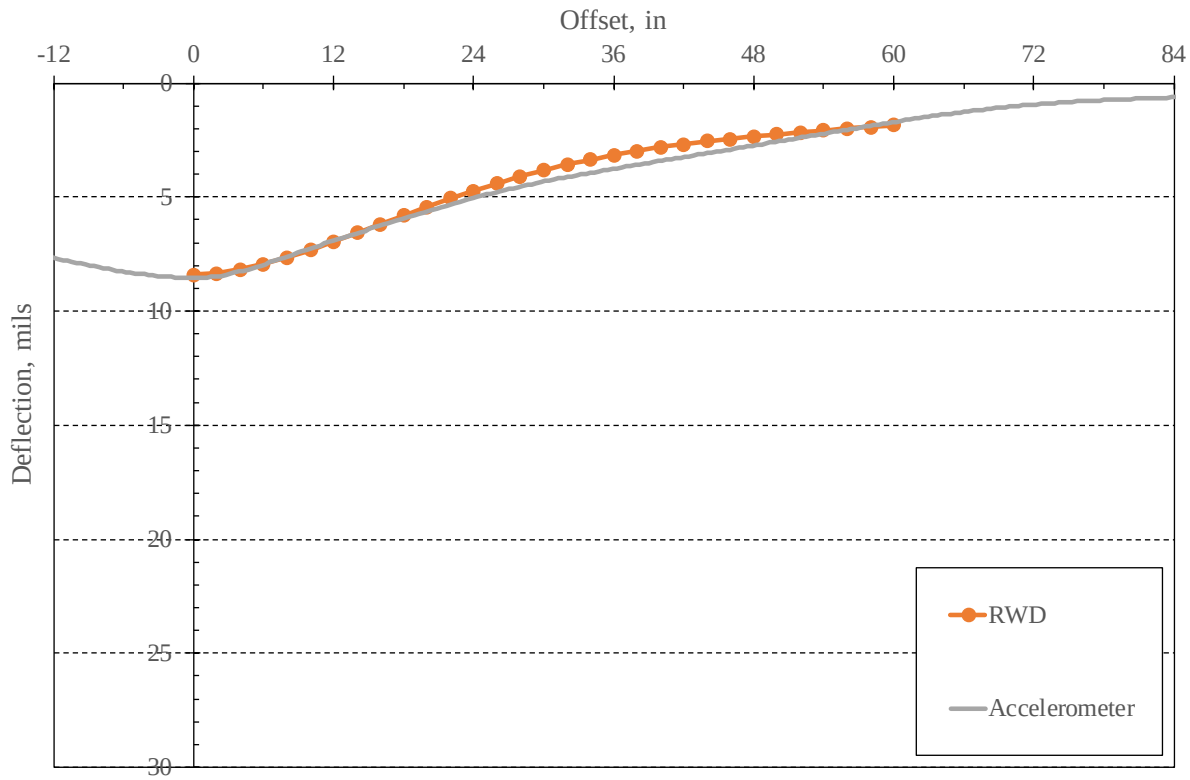


Source: FHWA

**Figure 49. Graph. RWD vs. accelerometer comparison—Section 4588.**

## RWD RESULTS

The research team processed the RWD data collected at 25-ft intervals to determine the maximum deflection in the right wheel path, providing data for direct comparison to the FWD. In addition, the basins for the 21 test points at each site were averaged to determine the mean basin. Figure 50 to 52 show the maximum deflection results for low, medium, and high deflections, along with the corresponding FWD data. Figure 53 summarizes the mean RWD and FWD basins for the same three sites. The results demonstrate that the relationship between RWD and FWD basins changes as deflection magnitudes increase. Overall, as FWD deflection increases, the RWD deflection also increases, but at a lower rate, due to the RWD's distributed load. The deflections have not been temperature corrected, as RWD and FWD testing were performed at the same time under the same climatic conditions.

Table 7 summarizes the RWD results by section, showing the mean RWD $D_0$, coefficient of variation, the accelerometer-based reference deflection, and the difference between the mean RWD $D_0$ and the acclerometer. In general, the RWD agrees within +/- 1 mil of the reference, as expected, as the accelerometer location was selected to be representative of the section mean, with the exception of two sites (5230 and 6015).

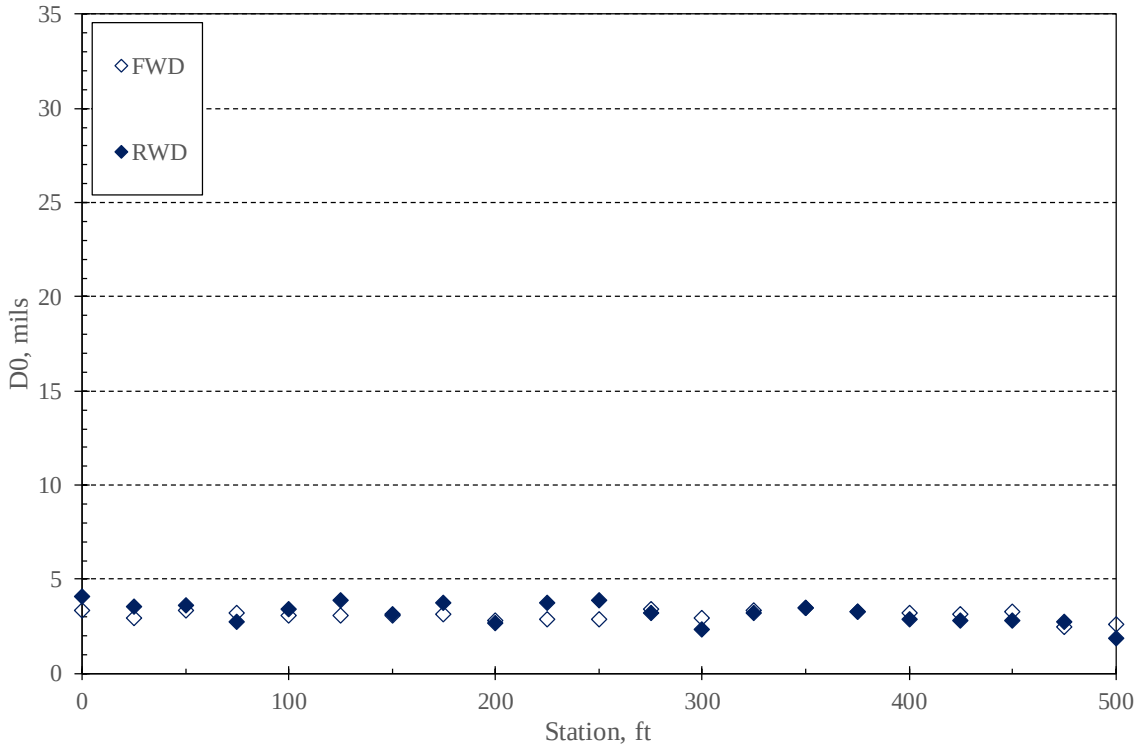


Source: FHWA

**Figure 50. Graph. RWD maximum deflection profile vs. FWD—Section 4933.**

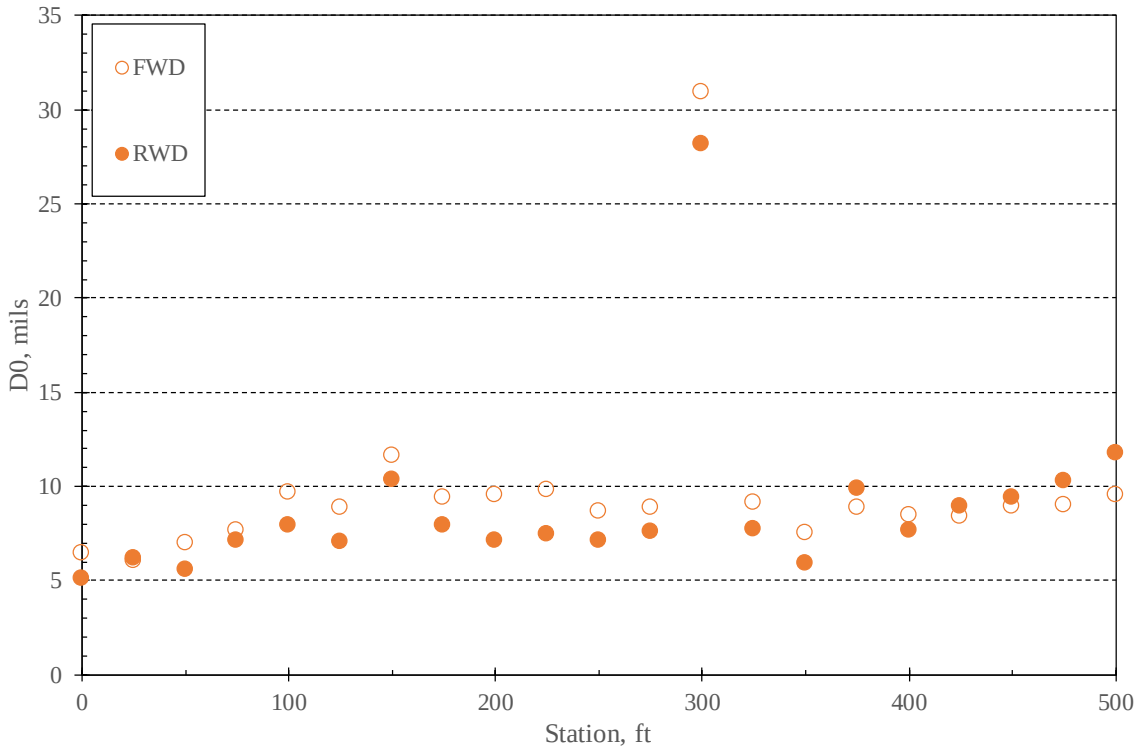


Source: FHWA

**Figure 51. Graph. RWD maximum deflection profile vs. FWD—Section 5511.**

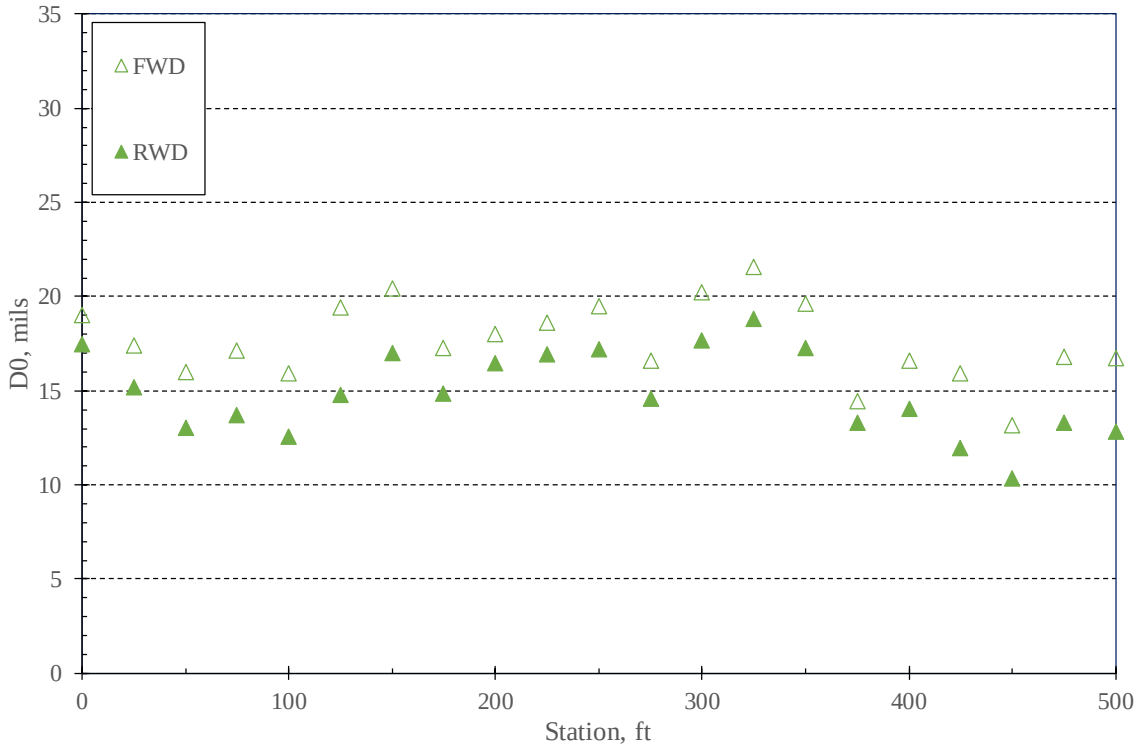


Source: FHWA

**Figure 52. Graph. RWD maximum deflection profile vs. FWD—Section 6015.**

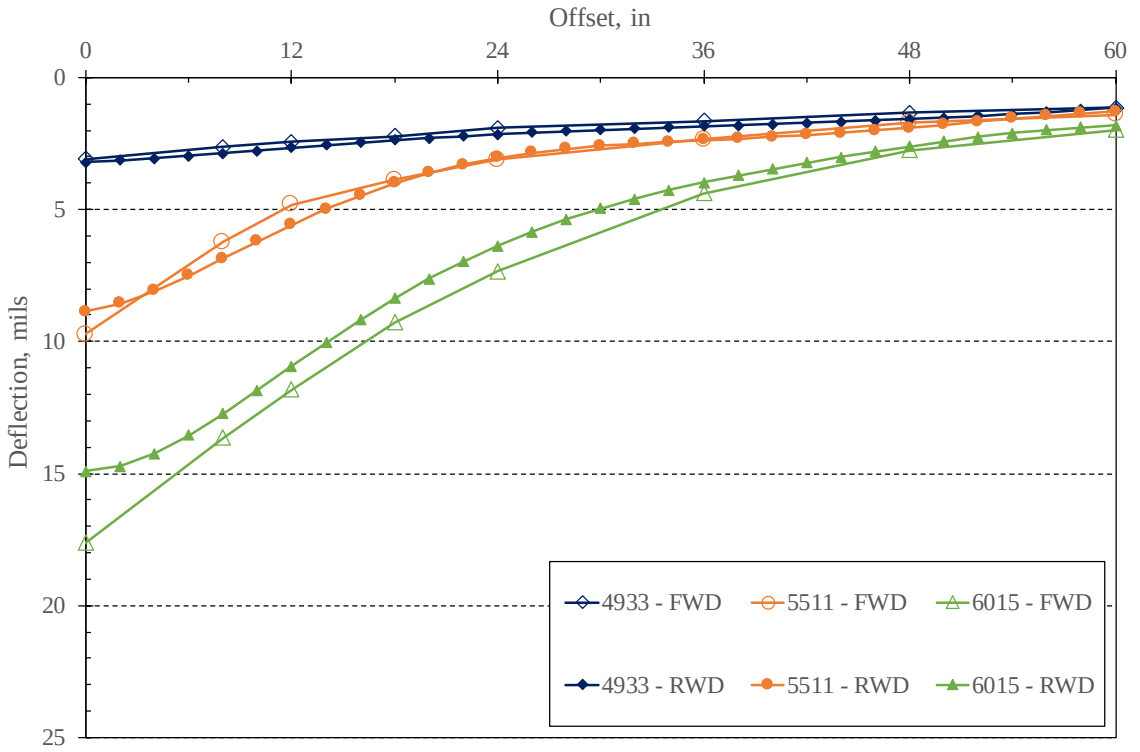


Source: FHWA

**Figure 53. Graph. RWD vs. FWD basin comparison—three sections.**

**Table 7. Summary of RWD results by section.**

| Section Identifier | $D_0$ | | Accelerometer | | D0 @ Accel - Mean, mils |
|---|---|---|---|---|---|
| | Mean, mils | COV, percent | Station | $D_0$, mils | |
| 1703 | 10.89 | 11.2 | 3+00 | 11.39 | 0.50 |
| 1797 | 12.06 | 7.2 | 2+50 | 12.06 | 0.00 |
| 1799 | 11.97 | 13.2 | 2+75 | 12.70 | 0.74 |
| 2202 | 8.28 | 24.9 | 2+50 | 7.70 | -0.58 |
| 2824 | 4.11 | 21.0 | 3+25 | 4.06 | -0.05 |
| 2830 | 5.08 | 22.0 | 2+50 | 5.12 | 0.04 |
| 2833 | 7.75 | 22.9 | 2+50 | 7.51 | -0.24 |
| 2851 | 6.24 | 24.9 | 2+25 | 6.25 | 0.01 |
| 4580 | 4.18 | 19.8 | 2+25 | 4.11 | -0.07 |
| 4588 | 8.40 | 20.3 | 3+00 | 8.55 | 0.15 |
| 4742 | 10.52 | 37.2 | 2+00 | 9.25 | -1.27 |
| 4784 | 10.42 | 13.1 | 2+75 | 10.49 | 0.07 |
| 4834 | 6.05 | 21.6 | 2+00 | 5.78 | -0.27 |
| 4889 | 7.46 | 23.6 | 2+25 | 8.06 | 0.61 |
| 4894 | 12.30 | 19.1 | 3+00 | 12.53 | 0.23 |
| 4933 | 3.20 | 17.5 | 2+50 | 2.96 | -0.24 |
| 5105 | 10.91 | 6.2 | 2+75 | 11.11 | 0.19 |
| 5210 | 11.15 | 34.8 | 2+25 | 10.78 | -0.37 |
| 5230 | 11.80 | 66.7 | 2+00 | 15.81 | 4.01 |
| 5506 | 6.74 | 29.1 | 3+25 | 7.23 | 0.49 |
| 5511 | 8.86 | 53.4 | 2+50 | 7.78 | -1.08 |
| 5616 | 6.98 | 19.5 | 2+00 | 7.03 | 0.05 |
| 6015 | 14.91 | 15.1 | 3+00 | 17.57 | 2.66 |

## CALCULATED PARAMETERS

Table 8 to Table 10 summarize the key parameters used to compare RWD and FWD deflection basins and backcalculated parameters, including:

- Deflections $D_0$, $D_{36}$, and $D_{60}$.
- Basin shape parameters SCI, RoC, and AUPP.
- Backcalculated parameters $M_R$, $E_p$, and $SN_{eff}$.

In the next chapter, these parameters are analyzed with respect to each other and to compare the field data results to the previously determined theoretical predictions based on ViscoWave.

**Table 8. FWD vs. RWD $D_0$, $D_{36}$, and $D_{60}$ deflections.**

| Section Identifier | FWD | | | RWD | | |
|---|---|---|---|---|---|---|
| | $D_0$, mils | $D_{36}$, mils | $D_{60}$, mils | $D_0$, mils | $D_{36}$, mils | $D_{60}$, mils |
| 1703 | 13.36 | 2.79 | 1.13 | 10.89 | 2.98 | 1.23 |
| 1797 | 13.08 | 3.61 | 2.08 | 12.06 | 4.04 | 1.47 |
| 1799 | 13.10 | 3.80 | 2.05 | 11.97 | 3.62 | 1.70 |
| 2202 | 8.81 | 2.77 | 1.62 | 8.28 | 2.67 | 1.27 |
| 2824 | 3.61 | 1.84 | 1.20 | 4.11 | 1.83 | 0.97 |
| 2830 | 6.03 | 1.96 | 1.10 | 5.08 | 2.14 | 1.17 |
| 2833 | 7.99 | 3.53 | 2.22 | 7.75 | 3.51 | 2.06 |
| 2851 | 5.88 | 2.50 | 1.55 | 6.24 | 2.87 | 1.47 |
| 4580 | 4.11 | 1.86 | 1.24 | 4.18 | 1.94 | 1.29 |
| 4588 | 7.61 | 3.31 | 1.84 | 8.40 | 3.16 | 1.84 |
| 4742 | 10.63 | 3.53 | 1.67 | 10.52 | 3.04 | 1.39 |
| 4784 | 12.34 | 2.12 | 0.97 | 10.42 | 2.96 | 0.76 |
| 4834 | 6.96 | 2.15 | 1.28 | 6.05 | 2.30 | 1.44 |
| 4889 | 7.73 | 2.16 | 1.42 | 7.46 | 2.43 | 0.93 |
| 4894 | 12.55 | 4.13 | 2.16 | 12.30 | 4.11 | 1.45 |
| 4933 | 3.10 | 1.64 | 1.13 | 3.20 | 1.85 | 1.14 |
| 5105 | 10.37 | 4.23 | 2.45 | 10.91 | 3.66 | 1.99 |
| 5210 | 11.85 | 4.41 | 2.59 | 11.15 | 4.39 | 2.06 |
| 5230 | 12.35 | 3.26 | 1.72 | 11.80 | 3.56 | 1.78 |
| 5506 | 6.99 | 2.60 | 1.48 | 6.74 | 1.96 | 1.19 |
| 5511 | 9.73 | 2.34 | 1.41 | 8.86 | 2.38 | 1.29 |
| 5616 | 8.37 | 2.56 | 1.33 | 6.98 | 2.52 | 1.57 |
| 6015 | 17.63 | 4.39 | 1.98 | 14.91 | 3.98 | 1.82 |

**Table 9. FWD vs. RWD basin shape parameters.**

| Section Identifier | FWD | | | RWD | | |
|---|---|---|---|---|---|---|
| | SCI, mils | RoC, ft | AUPP, ft-mils | SCI, mils | RoC, ft | AUPP, ft-mils |
| 1703 | 6.41 | 633 | 20.8 | 3.74 | 1,186 | 14.5 |
| 1797 | 6.20 | 548 | 19.1 | 3.35 | 1,324 | 13.8 |
| 1799 | 5.75 | 624 | 18.2 | 3.42 | 1,444 | 14.6 |
| 2202 | 4.13 | 832 | 12.3 | 2.75 | 1,543 | 10.4 |
| 2824 | 0.81 | 4,476 | 3.1 | 0.72 | 6,191 | 3.4 |
| 2830 | 2.55 | 1,293 | 8.1 | 1.11 | 3,871 | 4.8 |
| 2833 | 1.96 | 1,941 | 7.6 | 1.51 | 3,285 | 6.9 |
| 2851 | 1.97 | 1,648 | 6.5 | 1.13 | 3,953 | 5.3 |
| 4580 | 1.12 | 3,205 | 4.1 | 0.82 | 5,434 | 3.6 |
| 4588 | 1.68 | 2,178 | 7.1 | 1.44 | 3,585 | 7.7 |
| 4742 | 3.18 | 1,190 | 12.2 | 2.84 | 1,717 | 12.5 |
| 4784 | 6.14 | 624 | 20.0 | 3.26 | 1,347 | 13.1 |
| 4834 | 3.14 | 1,012 | 9.7 | 1.54 | 2,879 | 6.5 |
| 4889 | 3.14 | 1,087 | 10.5 | 1.90 | 2,445 | 8.3 |
| 4894 | 4.28 | 836 | 15.2 | 3.09 | 1,494 | 13.5 |
| 4933 | 0.65 | 5,822 | 2.6 | 0.54 | 8,024 | 2.3 |
| 5105 | 2.57 | 1,526 | 10.3 | 2.18 | 2,285 | 11.1 |
| 5210 | 4.15 | 996 | 13.9 | 2.95 | 1,529 | 11.9 |
| 5230 | 4.56 | 893 | 16.5 | 2.89 | 1,738 | 13.4 |
| 5506 | 2.48 | 1,357 | 8.3 | 1.45 | 3,558 | 7.4 |
| 5511 | 4.91 | 763 | 15.2 | 3.29 | 1,329 | 12.3 |
| 5616 | 2.76 | 1,345 | 10.3 | 1.32 | 3,820 | 6.8 |
| 6015 | 5.81 | 669 | 22.7 | 3.98 | 1,225 | 18.0 |

**Table 10. FWD vs. RWD backcalculated parameters.**

| Section Identifier | FWD | | | RWD | | |
|---|---|---|---|---|---|---|
| | $M_R$, psi | $E_p$, psi | $SN_{eff}$, in | $M_R$, psi | $E_p$, psi | $SN_{eff}$, in |
| 1703 | 7,165 | 115,615 | 5.1 | 6,645 | 161,495 | 5.7 |
| 1797 | 5,515 | 369,370 | 4.2 | 4,901 | 518,902 | 4.7 |
| 1799 | 5,311 | 250,983 | 4.5 | 5,469 | 281,059 | 4.6 |
| 2202 | 7,400 | 219,575 | 8.0 | 7,399 | 224,056 | 8.1 |
| 2824 | 10,975 | 482,794 | 7.6 | 10,814 | 343,413 | 6.8 |
| 2830 | 10,133 | 268,210 | 6.6 | 8,876 | 388,796 | 7.5 |
| 2833 | 5,964 | 377,409 | 5.4 | 5,449 | 266,022 | 5.2 |
| 2851 | 8,253 | 386,050 | 7.7 | 6,785 | 372,527 | 7.6 |
| 4580 | 9,655 | 833,826 | 8.7 | 9,083 | 778,153 | 8.6 |
| 4588 | 6,188 | 196,964 | 5.7 | 6,270 | 155,252 | 5.3 |
| 4742 | 6,367 | 157,938 | 5.5 | 6,513 | 129,221 | 5.2 |
| 4784 | 8,472 | 182,975 | 3.4 | 6,682 | 322,351 | 4.2 |
| 4834 | 9,474 | 251,712 | 6.7 | 7,435 | 364,430 | 7.6 |
| 4889 | 9,838 | 490,979 | 4.4 | 8,145 | 397,418 | 4.4 |
| 4894 | 4,897 | 151,580 | 5.0 | 4,813 | 147,995 | 5.0 |
| 4933 | 10,594 | 769,137 | 10.2 | 9,410 | 791,799 | 10.3 |
| 5105 | 4,680 | 188,840 | 5.5 | 5,276 | 155,532 | 5.2 |
| 5210 | 4,493 | 269,874 | 6.2 | 4,510 | 261,197 | 6.2 |
| 5230 | 6,376 | 205,571 | 5.6 | 5,466 | 168,241 | 5.4 |
| 5506 | 7,856 | 345,718 | 5.4 | 9,361 | 289,922 | 5.1 |
| 5511 | 8,402 | 262,628 | 4.7 | 7,809 | 270,645 | 4.8 |
| 5616 | 8,372 | 209,813 | 5.0 | 7,551 | 297,440 | 5.6 |
| 6015 | 4,093 | 231,746 | 4.0 | 4,665 | 275,468 | 4.2 |

# CHAPTER 6. THEORETICAL VS. FIELD DATA COMPARISONS

The researchers compared field data and theoretical results for the RWD and FWD for two main purposes:

- To compare deflection, basin shape, and backcalculated parameters to identify trends between RWD and FWD results.

- To validate the trends determined with theoretical data (ViscoWave).

In addition, the calculated parameters from the field data were used as inputs to the strain prediction correlations to estimate critical AC strain for each test site and to compare the predictions from the different basin shape factors. The following sections present the results.

## RWD VS. FWD DEFLECTIONS

RWD and FWD basins were compared for three key deflections—$D_0$, $D_{36}$, and $D_{60}$. In general, the maximum deflection is a good indicator of overall pavement stiffness, while the outer sensors reflect subgrade support. Figure 54 to 56 present the RWD to FWD comparisons of both theoretical and field results for $D_0$, $D_{36}$, and $D_{60}$, respectively.

In almost all cases the field data fall within the bounds of the theoretical data sets, validating the ViscoWave analysis. This allows for drawing broader conclusions for the RWD to FWD relationships, based on the theoretical results, which represented a much broader range of pavement structures than the field data. The results show:

- The general relationship between RWD and FWD $D_0$ is linear, but the ratio of RWD to FWD deflections is not the same for all deflection levels. Overall, thick pavements with lower deflections (e.g., 5 mils) produce similar $D_0$ values under similar FWD and RWD loadings, while FWD maximum deflections are generally higher than those of the RWD on thinner pavements with higher deflections (e.g., 15 mils). These differences are due mainly to the FWD's single plate load vs. the RWD's dual-tire distributed load. Also, the effect of the RWD's slower loading rate resulting in larger deflections is less influential for higher deflection pavements, which typically have thinner AC layers that are less influenced by their viscoelastic properties.

- The $D_{36}$ deflections are very similar for both devices, although there is a wide range of possibilities, depending on the specific combination of pavement layer thicknesses and moduli. The theoretical data show the significant influence of subgrade moduli on $D_{36}$. The three distinct horizontal data bands in the theoretical data correspond to the input subgrade moduli usd to generate the data set, with the lowest deflections corresponding to the stiffest subgrade, and vice versa.

- The $D_{60}$ trend shows slightly higher FWD deflections than RWD deflections, especially for weaker subgrades. This may be due to the practice of recording peak deflections at each FWD sensor, rather than the instantaneous basin present at the time that $D_0$ reaches

peak. Peak deflections at the outer sensors are typically slightly higher than instantaneous ones.

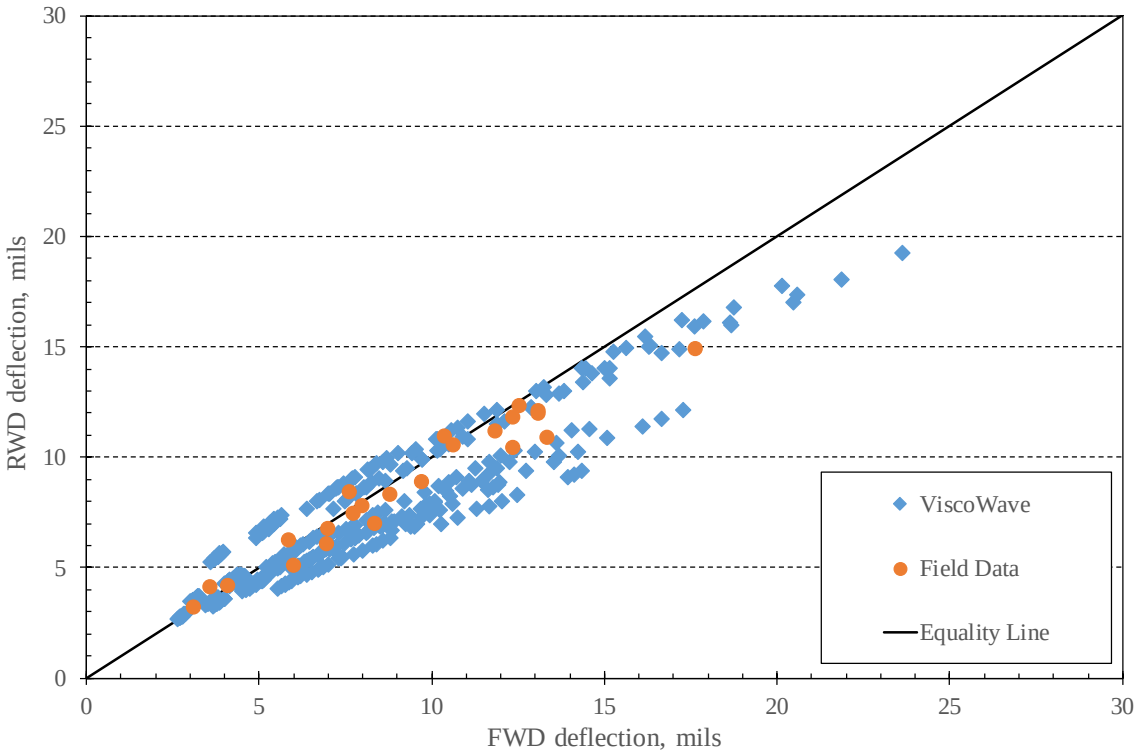


Source: FHWA

**Figure 54. Graph. Field vs. ViscoWave data—RWD vs. FWD $D_0$.**

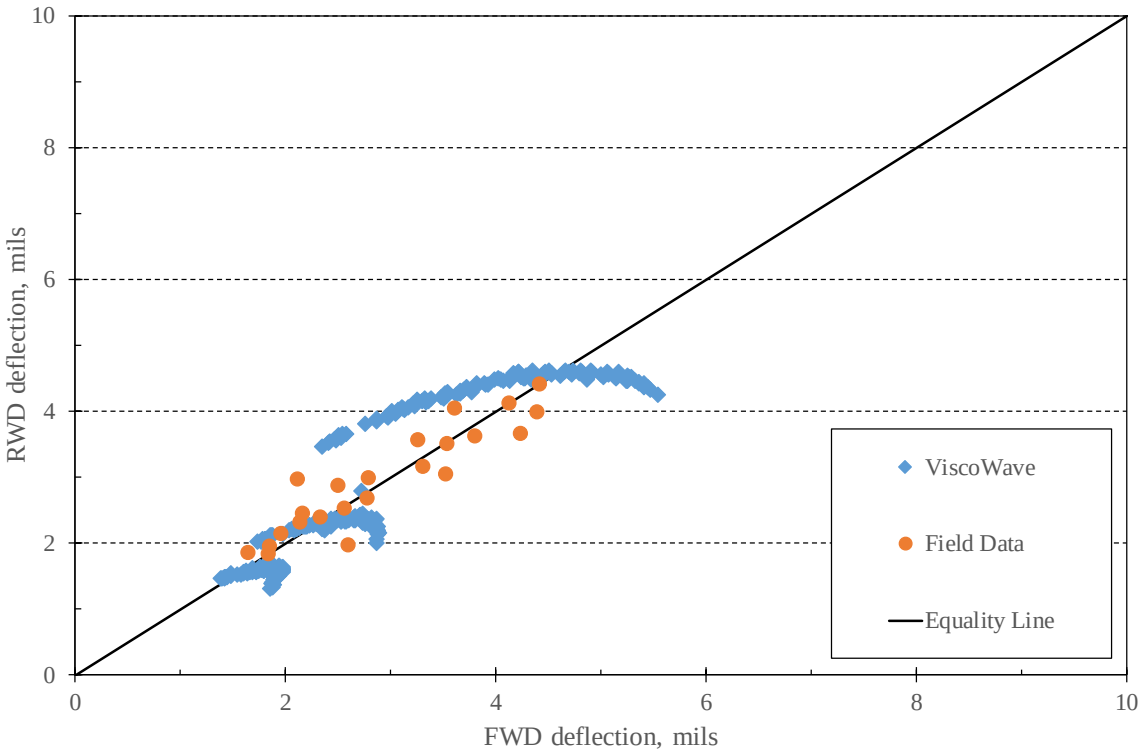


Source: FHWA

**Figure 55. Graph. Field vs. ViscoWave data—RWD vs. FWD $D_{36}$.**

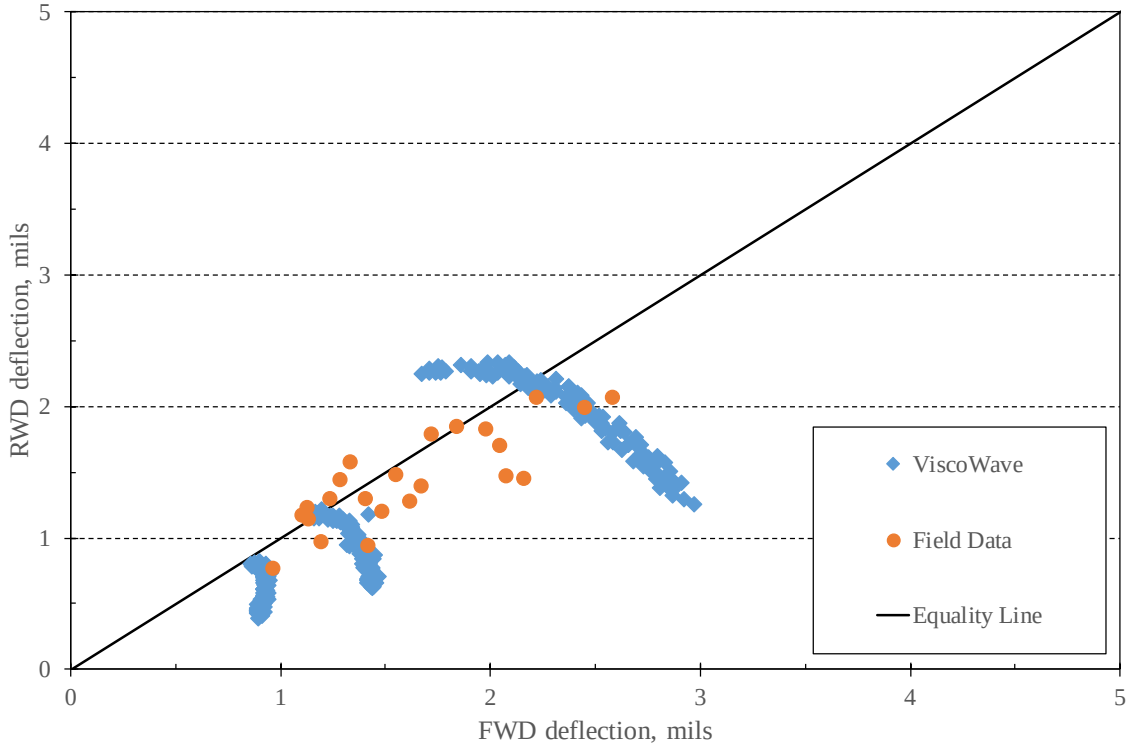


Source: FHWA

**Figure 56. Graph. Field vs. ViscoWave data—RWD vs. FWD $D_{60}$.**

## RWD VS. FWD BASIN SHAPES

Figure 57 to 59 present the RWD vs. FWD relationships for both the theoretical and field data for the three basin shape parameters chosen for evaluation in this study—SCI, RoC, and AUPP. The field data for SCI and RoC agree less well when compared to the theoretical data than the deflection results (i.e., $D_0$, $D_{36}$, and $D_{60}$); however, the field data-based AUPP values agree with the ViscoWave-predicted data. The data show:

- The field data exhibited systematically higher FWD SCI values than RWD SCI values, compared to the theoretical predictions. Although the field data still plot in the predicted range, most values are at the lower limit of the prediction.

- The opposite trend exists for the RoC field data, which plot near the upper limit predicted by ViscoWave. This demonstrates the inverse relationship between SCI and RoC, meaning an increased SCI corresponds to a decreased RoC. This indicates that the RWD basin around the load (i.e., within 12 inches) is flatter for the RWD relative to the FWD, than that predicted.

- AUPP, on the other hand, is based on four deflections spaced 12 inches each from 0 to 36 inches. It is less sensitive to curvature within 12 inches of the load center, but it still relates well to critical AC strain. The field data-based AUPP values plotted within the ViscoWave predicted range.

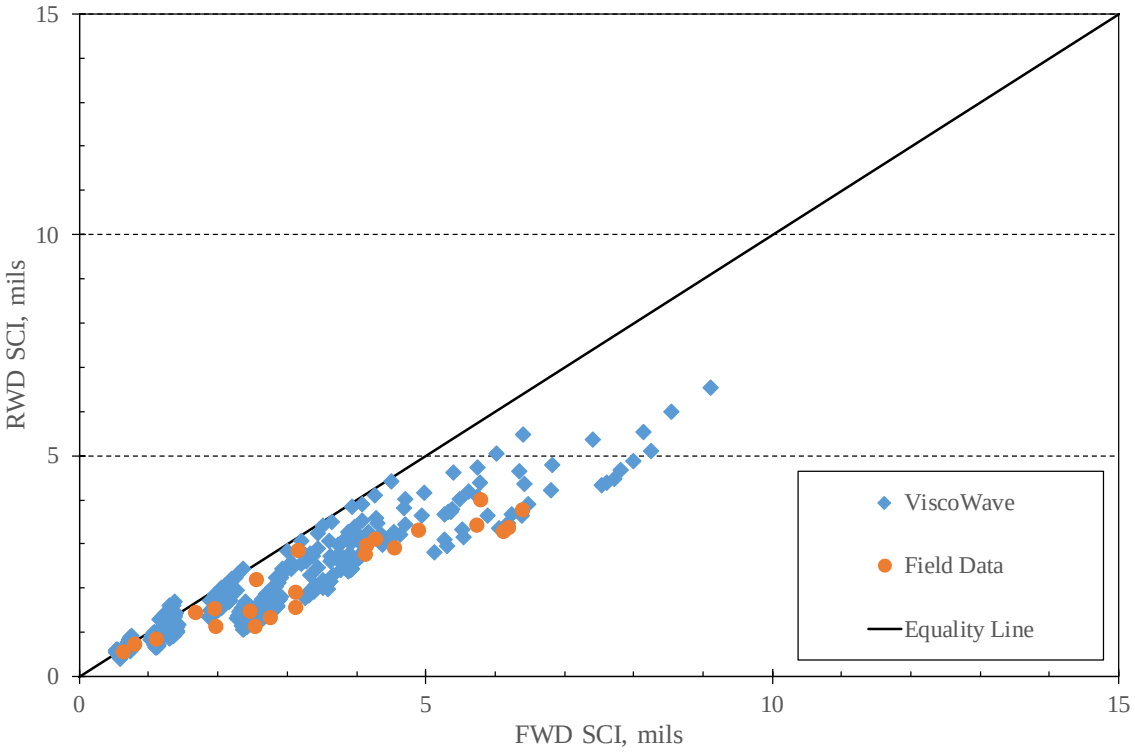


Source: FHWA

**Figure 57. Graph. Field vs. ViscoWave data—FWD vs. RWD SCI.**

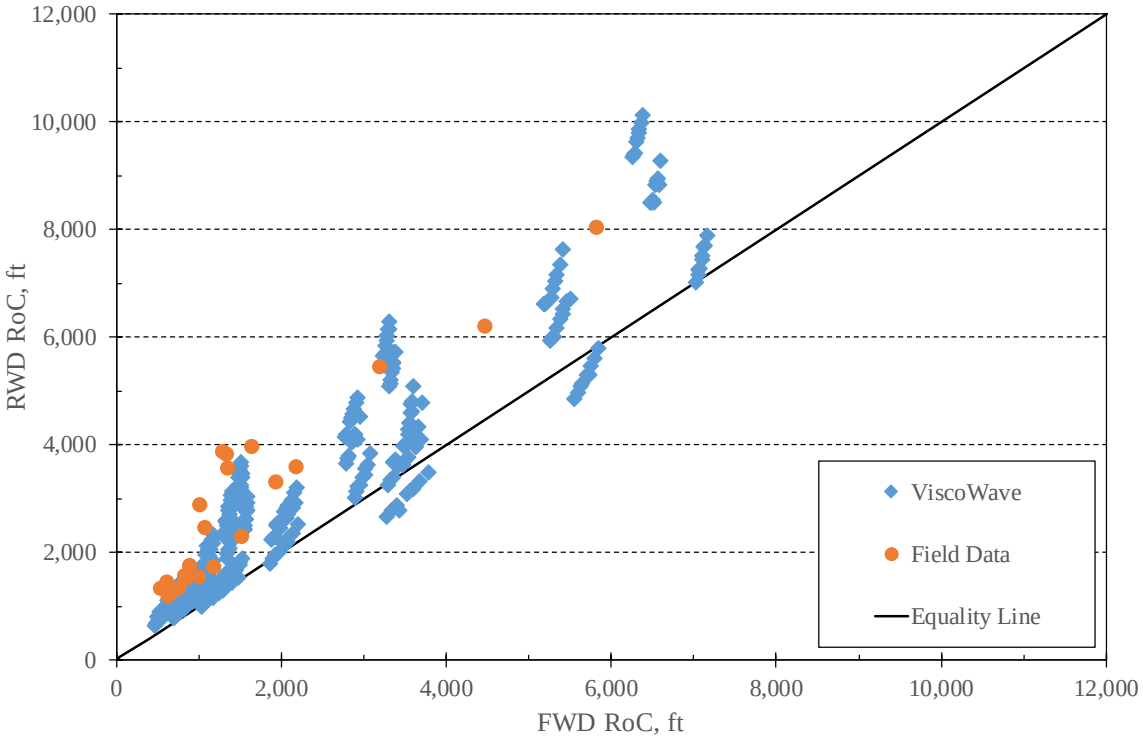


Source: FHWA

**Figure 58. Graph. Field vs. ViscoWave data—FWD vs. RWD RoC.**

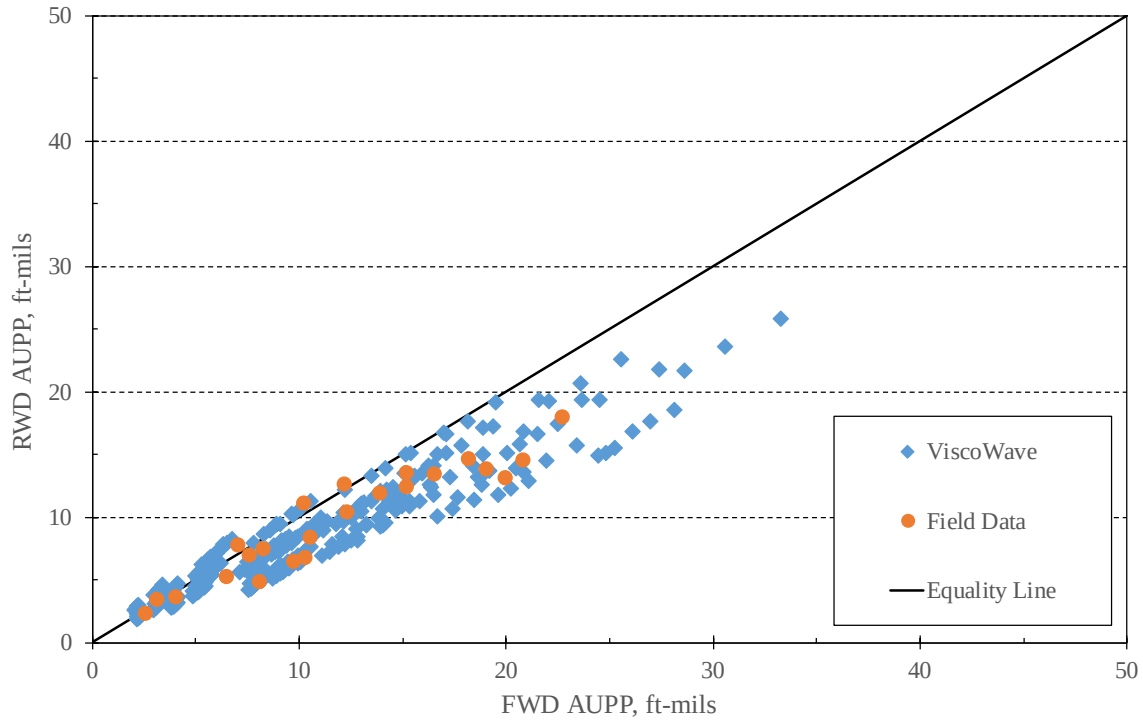


Source: FHWA

**Figure 59. Graph. Field vs. ViscoWave data—FWD vs. RWD AUPP.**

## RWD VS. FWD BACKCALCULATED PARAMETERS

Figure 60 to 62 present the RWD vs. FWD relationships for both the theoretical and field data for the three backcalculated parameters considered—$M_R$, $E_p$, and $SN_{eff}$. The field data for $M_R$ and $E_p$ have only a fair relationship with the theoretical data; however, the $SN_{eff}$ values agree very well with the ViscoWave-predicted data. The figures show:

- The backcalculated $M_R$ values for the RWD and FWD field data follow a similar trend; however, ViscoWave predicted higher $M_R$ values for the RWD than for the FWD, consistent with the higher outer sensor deflections predicted by ViscoWave, as discussed above. Higher outer sensor deflections result in lower backcalculated $M_R$ values and vice versa in the AASHTO flexible backcalculation method.

- Backcalculated $E_p$ values for the field data showed a similar overall trend to the theoretical values, but with more scatter. This demonstrates the sensitivity of backcalculated moduli to field measurements, which are affected by factors not considered in idealized pavement models, such as stress-sensitivity of materials. Backcalculated moduli based on field data are expected to have more scatter than those determined from theoretical deflections. Several field data-based $E_p$ values are much higher than the ViscoWave data set, due to extremely thick or stiff stabilized bases not considered in the theoretical runs.

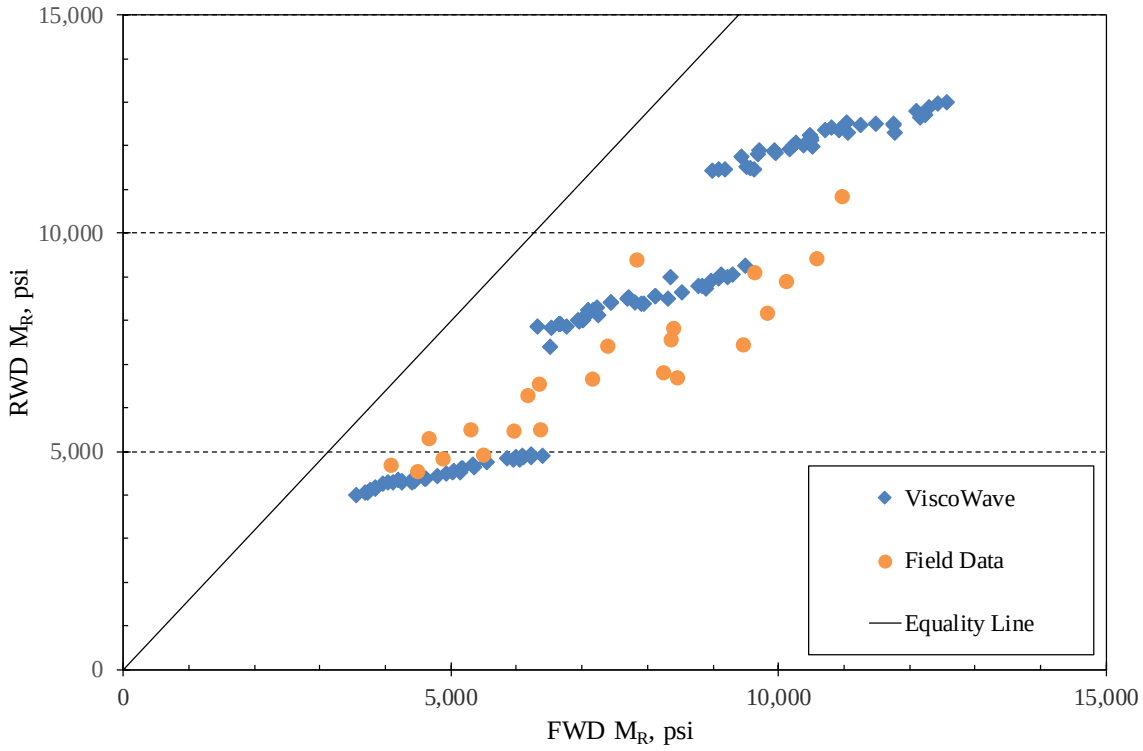


Source: FHWA

**Figure 60. Graph. Field vs. ViscoWave data—FWD vs. RWD $M_R$.**

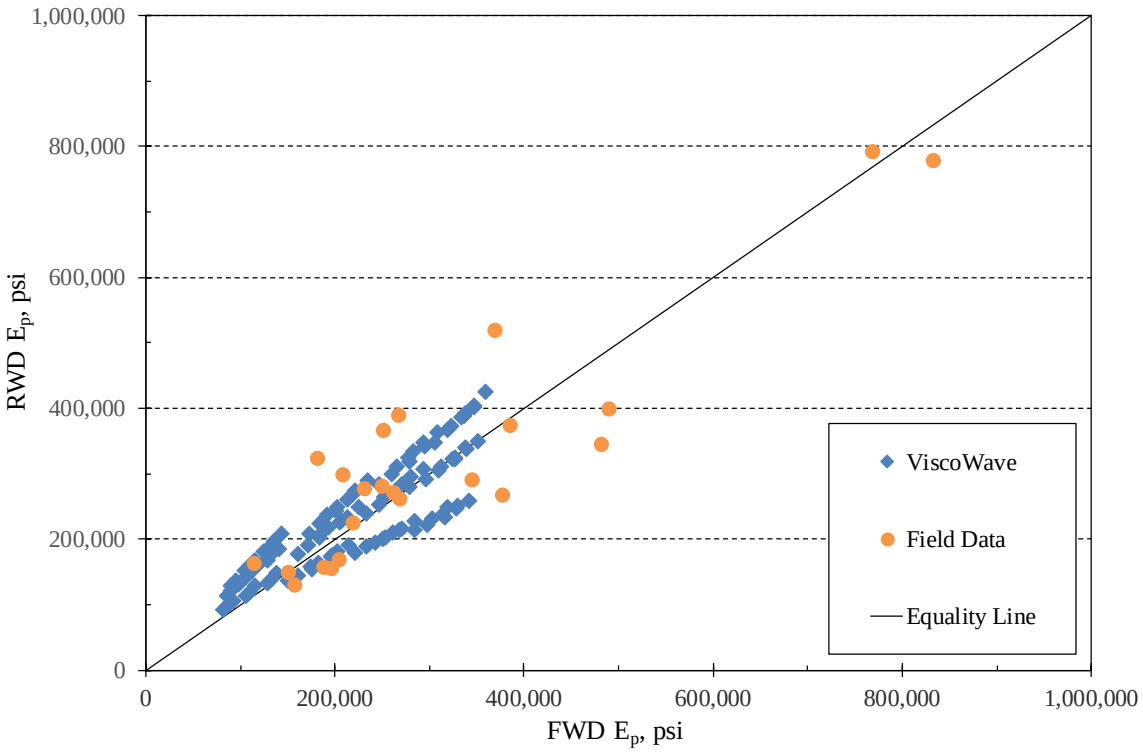


Source: FHWA

**Figure 61. Graph. Field vs. ViscoWave data—FWD vs. RWD $E_p$.**

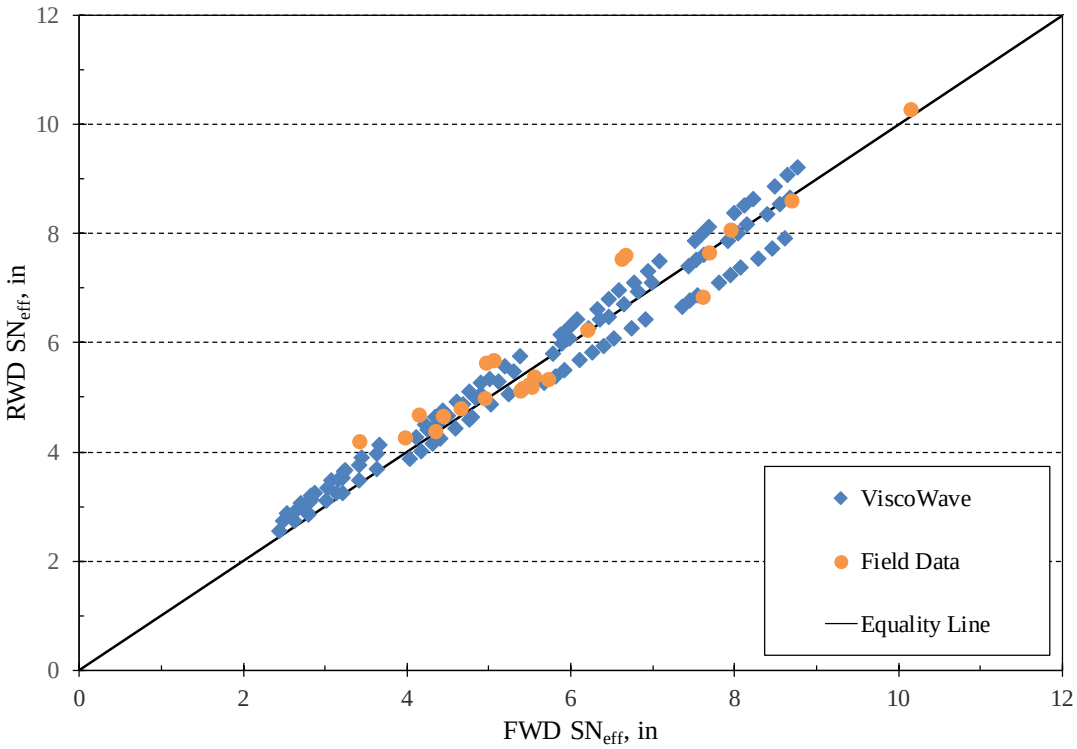


Source: FHWA

**Figure 62. Graph. Field vs. ViscoWave data—FWD vs. RWD $SN_{eff}$.**

- Field data-based $SN_{eff}$ values closely agreed with the theoretical predictions, even though $E_p$ values based on field data did not necessarily agree with theoretical $E_p$ values. This is because pavement thickness is more influential in the $SN_{eff}$ equation than $E_p$.

## CRITICAL AC STRAIN PREDICTIONS

The research team evaluated the six AC strain correlation equations developed in this study to determine the variability between their outputs, based on the field data-determined basin shape factors of SCI, RoC, and AUPP. Table 11 and Table 12 present the results for the FWD- and RWD-based equations, respectively. In addition, the COV between outputs was calculated for each site to evaluate their agreement.

Predicted critical AC strains for the FWD equations ranged from 32 to 251 microstrain, with an average of 133 microstrain. Coefficients of variability ranged from 3.1 to 21.9 percent, with an average of 12 percent, showing good agreement between equations.

**Table 11. Predicted critical AC strains based on three methods for the FWD field data.**

| Section Identifier | SCI, mstrain | RoC, mstrain | AUPP, mstrain | COV, percent |
|---|---|---|---|---|
| 1703 | 218 | 224 | 192 | 7.0 |
| 1797 | 213 | 251 | 178 | 6.3 |
| 1799 | 201 | 227 | 171 | 15.9 |
| 2202 | 155 | 182 | 123 | 10.6 |
| 2824 | 43 | 50 | 38 | 8.8 |
| 2830 | 107 | 129 | 86 | 21.9 |
| 2833 | 87 | 95 | 82 | 10.0 |
| 2851 | 87 | 107 | 71 | 11.3 |
| 4580 | 56 | 64 | 48 | 14.6 |
| 4588 | 77 | 87 | 77 | 7.9 |
| 4742 | 126 | 138 | 122 | 4.4 |
| 4784 | 211 | 227 | 186 | 4.1 |
| 4834 | 125 | 156 | 101 | 17.0 |
| 4889 | 125 | 148 | 108 | 13.9 |
| 4894 | 159 | 181 | 147 | 13.8 |
| 4933 | 37 | 41 | 32 | 17.6 |
| 5105 | 107 | 114 | 105 | 8.0 |
| 5210 | 156 | 158 | 136 | 20.4 |
| 5230 | 168 | 172 | 158 | 20.3 |
| 5506 | 104 | 125 | 88 | 7.5 |
| 5511 | 177 | 194 | 147 | 19.2 |
| 5616 | 113 | 126 | 106 | 3.1 |
| 6015 | 202 | 215 | 207 | 13.2 |

Predicted critical AC strains for the RWD equations ranged from 21 to 177 microstrain, with an average of 83 microstrain. Coefficients of variability ranged from 5.4 to 29.2 percent, with an average of 15.7 percent, showing slightly less agreement between the three methods than the FWD equations.

**Table 12. Predicted critical AC strains based on three methods for the RWD field data.**

| Section Identifier | SCI, mstrain | RoC, mstrain | AUPP, mstrain | COV, percent |
|---|---|---|---|---|
| 1703 | 57 | 43 | 77 | 29.2 |
| 1797 | 105 | 85 | 124 | 19.0 |
| 1799 | 73 | 61 | 83 | 15.0 |
| 2202 | 113 | 96 | 133 | 16.3 |
| 2824 | 52 | 41 | 68 | 25.3 |
| 2830 | 60 | 53 | 65 | 10.3 |
| 2833 | 119 | 105 | 129 | 10.1 |
| 2851 | 23 | 21 | 23 | 5.9 |
| 4580 | 34 | 30 | 37 | 11.1 |
| 4588 | 108 | 94 | 118 | 11.4 |
| 4742 | 107 | 84 | 132 | 22.7 |
| 4784 | 83 | 65 | 110 | 26.4 |
| 4834 | 122 | 107 | 136 | 12.0 |
| 4889 | 124 | 99 | 144 | 18.4 |
| 4894 | 120 | 107 | 122 | 7.2 |
| 4933 | 57 | 44 | 74 | 26.4 |
| 5105 | 135 | 118 | 143 | 9.6 |
| 5210 | 45 | 40 | 53 | 14.6 |
| 5230 | 45 | 40 | 49 | 9.3 |
| 5506 | 59 | 47 | 69 | 19.2 |
| 5511 | 102 | 93 | 103 | 5.4 |
| 5616 | 142 | 115 | 177 | 21.4 |
| 6015 | 30 | 26 | 35 | 14.3 |

# CHAPTER 7. SUMMARY OF FINDINGS AND CONCLUSIONS

This chapter summarizes the main research activities performed, findings, and conclusions.

## INHERENT DIFFERENCES BETWEEN RWD AND FWD DEVICES

The research team identified six inherent differences between RWD and FWD loading characteristics and demonstrated their effect on pavement deflections using thin and thick AC pavement examples. The differences result in the RWD having equal or greater deflections on thick, stiffer pavements that produce low FWD deflections, such as around 5 mils. On thinner, weaker pavements that produce deflections above 10 mils, the RWD produces lower deflections than the FWD. The main factors driving these trends are the slower RWD loading rate and its affect on thick, viscoelastic AC pavements, and the distribution of the RWD's axle load between dual tires, vs. the single plate FWD loading.

## DYNAMIC MODELING OF RWD AND FWD DEFLECTIONS

ViscoWave modeled RWD and FWD loads on 324 AC pavements covering a broad range of layer thicknesses and layer and subgrade moduli to study their deflection differences. The results indicated a linear relationship between RWD and FWD maximum deflections that reinforced the trend seen in the thin and thick AC pavements described above. Comparisons of basin shape factors based on the synthetic RWD and FWD basins also produced good correlations, with the FWD showing higher curvature near the load center due to its single plate loading.

Backcalculating the synthetic deflection basins with the AASHTO flexible pavement procedure showed that $M_R$ values from RWD data were approximately 9 percent higher than those from FWD deflections, due to the predicted slightly lower deflections at the outer sensors. While the relationship between backcalculated $E_p$ values between the two devices was highly variable, the resultant $SN_{eff}$ values were very similar and showed a strong correlation. This shows the greater influence of pavement thickness vs. $E_p$ in the $SN_{eff}$ calculation.

The ViscoWave response data produced good correlations between the three basin shape factors evaluated in this study and the horizontal strain at the bottom of the AC layer. Overall, AUPP and SCI showed very good correlations between basin shape and AC strain. The RoC correlations were also good but correlated less well than the other two.

## FIELD TESTING

Field testing was performed on 23 test sections in Mississippi, for which detailed pavement layer type and thickness data were available. At each site the RWD and FWD tested under similar climatic conditions, and an accelerometer temporarily embedded in the pavement was used to validate RWD data.

The field data for both devices were processed using the same analysis techniques used on the ViscoWave-generated data, including calculation of SCI, RoC, AUPP, and backcalculation of $M_R$, $E_p$, and $SN_{eff}$. The data were compared to the results of the theoretical data set to validate the ViscoWave model.

Overall, the test pavements produced low to medium FWD deflections, with section averages ranging from 3 to 17 mils, consistent with the medium and thick AC pavements tested. Total AC thicknesses (surface, base, and ATB, when present) ranged from 5.8 to 16.8 inches, with a mean of 10.7 inches. Most sections had either a stabilized base or subbase.

## THEORETICAL VS. FIELD DATA COMPARISONS

The RWD and FWD field data from the 23 sites showed very similar deflection trends as the theoretical data generated on 324 pavement structures. The field data supported the theoretical predictions that both devices produce similar deflections in the low deflection range, while the RWD produces smaller maximum deflections in the higher deflection range. Deflections 36 inches from the load center are essentially the same, while the RWD produces slightly lower deflections than the FWD at 60 inches from the load center.

SCI and RoC comparisons for the RWD and FWD based on field data showed only fair agreement with the theoretical predictions. The SCI values from field data tended to bias toward the lower range of the theoretical predictions, with the inverse occurring for the RoC comparisons. AUPP produced agreement between field and theoretical results, with all field data falling within the theoretically predicted range.

$M_R$ values backcalculated from RWD and FWD field data showed similar values, which differed slightly from the theoretically predicted trend, which showed the RWD producing $M_R$ values about 9 percent higher than the FWD.

Backcalculated $E_p$ values showed a similar trend between field and theoretical data, although with more scatter for the field data. Several field values were significantly beyond the theoretical range, likely due to very thick or stiff stabilized bases not considered in the ViscoWave-generated matrix.

Field data-based $SN_{eff}$ values closely agreed with the theoretical predictions, even though $E_p$ values based on field data did not necessarily agree with theoretical $E_p$ values. This is because pavement thickness is more influential in the $SN_{eff}$ equation than $E_p$.

## BASIN SHAPE TO STRAIN CORRELATIONS

Predicted critical AC strains for the three RWD equations (SCI, RoC, and AUPP) ranged from 21 to 177 microstrain, with an average of 83 microstrain. Coefficients of variability ranged from 5.4 to 29.2 percent, with an average of 15.7 percent.

Although field strain measurements were beyond the scope of this study, previous research has shown good results between strains predicted by forward-run pavement response programs and field measurements.

Based on the correlations produced between basin shape factors and AC critical strain produced by theoretical deflections, and the overall agreement between field and theoretical deflections and basin shape factors, the research team concludes that the strain correlation equations produced in this study are feasible tools for predicting strains due to moving wheel loads and are suitable for implementation in network-level pavement analysis. Of the three basin shape factors

evaluated, AUPP produced the best results in terms of strain correlation and also field vs. theoretical RWD to FWD basin comparisons.

## ACKNOWLEDGMENTS

The researchers wish to acknowledge the Mississippi DOT's Research Division staffers for their assistance in the selection of test sites and field data collection. Their efforts were greatly appreciated.

The Mississippi map showing the 23 test site locations in figure 41 was created for this report. The map was printed from ESRI's ArcMap™ program from a SHP file provided by the Mississippi DOT and the pins indicating individual test section locations were added as part of this research using Microsoft® PowerPoint®.

## REFERENCES


1. AASHTO. (1993). *AASHTO Guide for Design of Pavement Structures*. American Association of State Highway and Transportation Officials. Washington, D. C.
2. Asphalt Institute. (1983). *Asphalt Overlays for Highway and Street Rehabilitation*. Manual Series No. 17 (MS-17). Asphalt Institute. Lexington, KY. 1983.
3. Xu, B., Ranjithan, S. R., and Kim Y. R. (2002). *New Relationships between Falling Weight Deflectometer Deflections and Asphalt Pavement Layer Condition Indicators*. Transportation Research Record, No. 1806. TRB, National Research Council, Washington, D.C. pp. 48-56.
4. Kim, Y. R. and Park, H. M. (2002). *Use of FWD Multi-Load Data for Pavement Strength Estimation*. Report No. FHWA/NC/2002-006, Research Project No. HWY-00-4. North Carolina Department of Transportation.
5. Horak, E. (2008). *Benchmarking the Structural Condition of Flexible Pavements with Deflection Bowl Parameters*. Journal of the South African Institution of Civil Engineering, Vol. 50, No. 2, pp. 2-9.
6. Baltzer, S., Ertman-Larson, H.J., Lukanen, E.O., and Stubstad, R.N. (1994). *Prediction of AC Mat Temperature for Routine Load / Deflection Measurements*. Proceedings, Fourth International Conference on the Bearing Capacity of Roads and Airfields, Vol. 1. Minnesota Department of Transportation, pp. 401-412.
7. Lukanen, E. O., Stubstad, R., and Briggs, R. (2000). *Temperature Predictions and Adjustment Factors for Asphalt Pavement*. Report Number FHWA-RD-98-085, Federal Highway Administration.
8. Park, D. Y., Buch, N., and Chatti, K. (2001). *Efffective Layer Temperature Prediction Model and Temperature Correction via Falling Weight Deflectometer Deflections*. Transportation Research Record, No. 1764. TRB, National Research Council, Washington, D.C. pp. 97-111.
9. Chen, D. H., Bilyeu, J., Lin, H. H., and Murphy, M. (2000). *Temperature Correction of Falling Weight Deflectometer Measurements*. Transportation Research Record, No. 1716. TRB, National Research Council, Washington, D.C. pp. 30-39.
10. Kim, Y. R., Hibbs, B. O., Lee, Y. C. (1995). *Temperature Correction of Deflections and Backcalculated Asphalt Concrete Moduli*. Transportation Research Record, No. 1473. TRB, National Research Council, Washington, D.C. pp. 55-62.
11. Flintsch, G., Katcha, S., and Bryce, J. (2013). *Assessment of Continuous Pavement Deflection Measuring Technologies*. SHRP 2 Report S2-R06F-RW-1. TRB, National Research Council, Washington, D.C.
12. Vavrik, W. R., Steele, D. A., and Blue, J. (2008). *Rolling Wheel Deflectometer-Based Pavement Management System Success: Champaign County, IL*. 87th Annual Meeting Compendium of Papers. No. 08-2728. TRB, National Research Council, Washington, D.C.
13. Wilke, P. (2014). *Rolling Wheel Deflectometer for Pavement Evaluation*. 2nd Transportation & Development Congress. ASCE. pp. 259-268.
14. Elseifi, M. A., Dasari, K, Abdel-Khalek, A., Gaspard, K., and Zhang, Z. (2013). *Development of the Triangular Model for Pavement Evaluation Using the Rolling Wheel Deflectometer*. Journal of Transportation Engineering, ASCE, Vol. 139, No. 3, pp. 313-320.

15. Steele, D. A., and Beckemeyer, C. A. (2013). *Using the Rolling Wheel Deflectometer (RWD) to Improve Pavement Management Decisions – Oklahoma DOT Case Study*. Project Report, ARA Project No. 000472, Applied Research Associates, Champaign, IL.
16. Uzan, J. (undated) *JULEA: Jacob Uzan Layered Elastic Analysis*, Technion University, Haifa, Israel.
17. Thyagarajan, S., Sivaneswaran, N., Petros, K., and Muhunthan, B. (2011). *Development of a Simplified Method for Interpreting Surface Deflections for In-Service Flexible Pavement Evaluation*. 8th International Conference on Managing Pavement Assets, IMCPA8, Santiago, Chile.
18. Rada, G. R., Nazarian, S., Visintine, B. A., Siddharthan, R., and Thyagarajan, S. (2016). *Pavement Structural Evaluation at the Network Level*. Final Report No. FHWA-HRT-15-074, Federal Highway Administration.
19. Carvalho, R., Stubstad, R., Briggs, R., Selezneva, O., Mustafa, E., and Ramachandran, A. (2012). *Simplified Techniques for Evaluation and Interpretation of Pavement Deflections for Network-Level Analysis*. Report Number FHWA-HRT-12-023, Federal Highway Administration.
20. Lee, H.S. (2014). *ViscoWave—A New Solution for Viscoelastic Wave Propagation of Layered Structures Subjected to an Impact Load*, International Journal of Pavement Engineering, 15(6), pp. 542–557, Taylor and Francis Group, London, UK.
21. Lee, H.S. Von Quintus, H., and Steele, D. (2018). Effect of Moving Dynamic Loads on Pavement Deflections and Backcalculated Modulus. Paper No. 18-01768. TRB 97th Annual Meeting Compendium of Papers, Transportation Research Board, Washington, D.C.
22. Garg, N., and Thompson, M. R. (1998). *Mechanistic-Empirical Evaluation of the Mn/Road Low Volume Road Test Sections*. Final Report No. FHWA-IL-UI-262, the Illinois Department of Transportation, Springfield, IL.